Temporality of Flower Initiation and Control of Inflorescence Architecture

Anaïs Chaumeret

Numéro National de Thèse : 2017LYSEN059

THESE de DOCTORAT DE L'UNIVERSITE DE LYON
opérée par
L'Ecole Normale Supérieure de Lyon

Ecole Doctorale N° 340
Biologie Moléculaire et Intégrée de la Cellule

Spécialité de doctorat : Biologie du développement, Biologie des plantes

Discipline : Sciences de la vie

Soutenue publiquement le 27/10/2017, par :
Anaïs CHAUMERET

Temporalité de l'initiation des fleurs et contrôle de l'architecture de l'inflorescence

Temporality of flower initiation and control of inflorescence architecture

---

Devant le jury composé de :

FERRANDIZ, Cristina : Lecturer, Maestre ; IBMCP Valencia, Espagne ; Rapporteure
RAMEAU, Catherine : Directeur de recherche ; INRA de Versailles ; Rapporteure
LAUFS, Patrick : Directeur de recherche ; INRA de Versailles ; Examinateur
JAILLAIS, Yvon : Directeur de recherche ; ENS de Lyon ; Examinateur
VERNOUX, Teva : Directrice de recherche ; ENS de Lyon ; Directeur de thèse

TABLE OF CONTENTS

LIST OF MAIN ABBREVIATIONS

GENE NOMENCLATUR

AHP6: HISTIDINE PHOSPHOTRANSFER PROTEIN 6

ATG8E: AUTOPHAGY RELATED PROTEIN 8E

CLV3: CLAVATA

FIL: FILAMENTOUS FLOWER or YABBY1, YAB1

ICU4: INCURVATA4 or ATHB15 or CORONA, CNA

PHB: PHABULOSA

PHV: PHAVOLUTA

REV: REVOLUTA

WUS: WUSHEL

OTHER ABBREVIATIONS

AFM: Atomic Force Microscopy

CRISPR: Clustered Regularly Interspaced Short Palindromic Repeat

CZ: Central Zone

DNA: Desoxyribo Nucleic Acid

NLS: Nuclear Localization Signal

OC: Organizing Centre

PZ: Peripheral Zone

PCR: Polymerase Chain Reaction

QPCR: Quantitative Polymerase Chain Reaction

RNA: Ribo Nucleic Acid

SEM: Scanning Electron Microscopy

SAM: shoot apical meristem

Ws: Wassilewskija ecotype (*Arabidopsis thaliana*)

ABSTRACT OF THE THESIS

Phyllotaxis, the arrangement of botanical elements around plant axis, conforms to a robust spacial-temporal pattern. It is primarily established at the shoot apical meristem (SAM), the post-embryonic aerial stem-cell niche. Local accumulation of the phytohormone auxin locally triggers organ formation at the SAM, while depletion of auxin in the surrounding cells creates an inhibitory field, where no new organ can be initiated. Growth constantly moves older organs away from the SAM, clearing space for new organogenesis. This is a striking example of an iterative and self-organized process driven by inhibitory fields. Molecular and genetic mechanisms regulating phyllotaxis are now being identified, but mostly in the context of the most common Fibonacci spiral. Whether or not the same mechanisms explain other types of phyllotaxis remains to be explored. We identified DRB27, an *Arabidopsis thaliana* mutant with a strong tendency to generate clusters of organs. This is reminiscent of the whorled phyllotaxis, observed in almost all angiosperm flowers and in some shoots of unrelated species. Quantification of DRB27 phyllotaxis and live imaging revealed that clusters are not whorls but correspond to burst of organs initiating in crescent domains at the periphery of the SAM. Conversely, large crescent domains remain devoid of organ initiation. Organogenesis in these clusters violates classical rules of organ spacing in phyllotactic systems. Surprisingly, we identified two candidate mutations affecting the two abaxial regulators *FILAMENTOUS FLOWE*R and *MIR166A,* which likely combines to produce DRB27 peculiar phyllotaxis. Since these genes are expressed in developing organs, it suggests non-cell autonomous feedbacks on phyllotaxis. We identify a series of anomalies in DRB27 SAM, including abnormal patterns of auxin signalling, perturbation of organ boundary formation, modification of *CLV3/WUS* domains and SAM geometry and increase in cell wall stiffness. Taken together our data questions how lateral organ identity and development feedbacks on SAM homeostasis and phyllotaxis patterning.

INTRODUCTION

This introduction is partly based on a revue, published in Wiley:

Galvan-Ampudia, C. S., Chaumeret, A. M., Godin, C. and Vernoux, T. (2016), Phyllotaxis: from patterns of organogenesis at the meristem to shoot architecture. WIREs Dev Biol, 5: 460–473. doi:10.1002/wdev.231

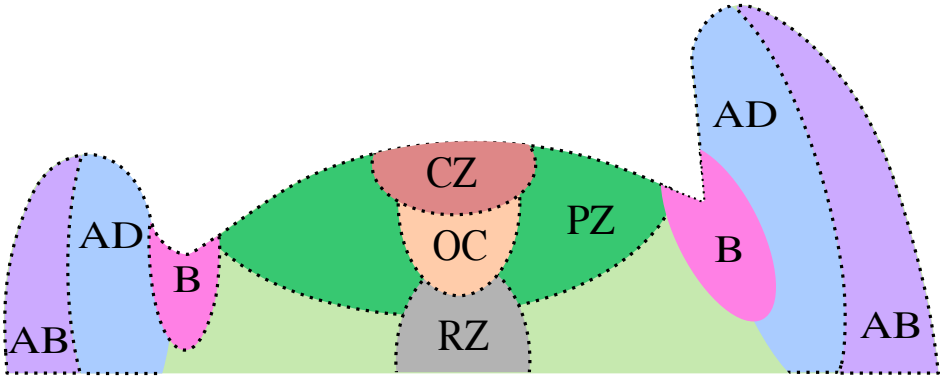

Figure 0.1: Functional subdivision of a SAM. The cartoon represents a longitudinal section of a typical SAM of angiosperm. PZ=Peripheral Zone. CZ = Central Zone. OC = Organizing Centre. RZ = Rib Zone. B = Boundary. AD = ADaxial side. AB = ABaxial side

I – PHYLLOTAXIS, THE ARCHITECTURE OF PLANTS

Higher plants undergo an extensive phase of post-embryonic development during which the plant not only grows but also produces new organs along the apical–basal axis, e.g., the leaves and flowers for the aerial part of plants. This iterative production of new organs is under the influence of both developmental and environmental factors and is controlled by specialized tissues containing stem cell niches called meristems. Two apical meristems, at the shoot and the root tips, are established during embryogenesis at the two ends of the apical–basal axis. Their activity controls growth and development of the shoot and root primary axes, and they are thus called primary meristems. The shoot apical meristem is a highly organized tissue composed of a central zone (CZ) at the very tip of the axis where the stem cells are located, a peripheral zone (PZ) where lateral organs are initiated, and the rib zone (RZ), which is situated beneath the CZ and contains the organizing centre (OC), a group of cells that play a central role in stem cell maintenance (Figure 0.1). In a reference frame centred at the top of the growing meristem, stem cell daughters are progressively displaced away from the CZ through growth (eulerian viewpoint) and become competent to produce new lateral organs when they reach the PZ. In angiosperms, the meristem is, in addition, organized as a multilayered tissue where the outermost L1 and L2 cells proliferate and differentiate in the PZ to produce all epidermal and subepidermal cells, while the L3 underneath provides cells for the less organized inner tissues.

The shoot apical meristem first produces segments of stem that bear lateral leaves (at the axil of which lateral stems can be generated) and can elongate or remain compact depending on the species: during this period, it is called the vegetative meristem. A combination of endogenous and environmental signals, including photoperiod, temperature, and stress (Andres *et al.*, 2012), then triggers a transition from a vegetative meristem to an inflorescence meristem that produces the flowers or, in some cases, a single terminal flower.

The resulting architecture is called phyllotaxis, from ancient Greek *phýllon* "leaf" and *táxis* "arrangement". Literally this means the arrangements of leaves, but can also be applied to branches and flowers.

I.A – PHYLLOTAXIS FOLLOWS STEREOTYPED PATTERNS

Phyllotaxis is characterized by the number of organs inserted on a node (also called jugacy) and by the relative divergence angle between organs. The prevalent phyllotactic patterns in higher plants are the Fibonacci spiral (with a divergence angle of 137,5° between successive organs; Figure 0.2.A & E), distichous (with a divergence angle of 180° between successive organs; Figure 0.2.B & F), opposite-decussate (with successive pairs of opposite organs at 90°; Figure 0.2.C & G) and whorled (with three or more organs at each node; Figure 0.2.D & H).

However, phyllotaxis is not necessarily constant in the plants lifespan, and sometimes undergoes one or more transitions, usually linked to a change of developmental stage. For example the model species *Arabidopsis thaliana* shows spiralled inflorescences, and a single pattern transition when it produces flowers that will be arranged in whorls. Moreover, Kwiatkowska (1995) described more complex phyllotactic transitions with *Anagallis arvensis*. This *Primulaceae* undergoes three phyllotactic transitions in its lifespan, starting with a distichious architecture, then it switches to a Fibonacci spiral before producing three-organs whorls, then eventually a Lucas spiral (with a divergence angle of 99,5°).

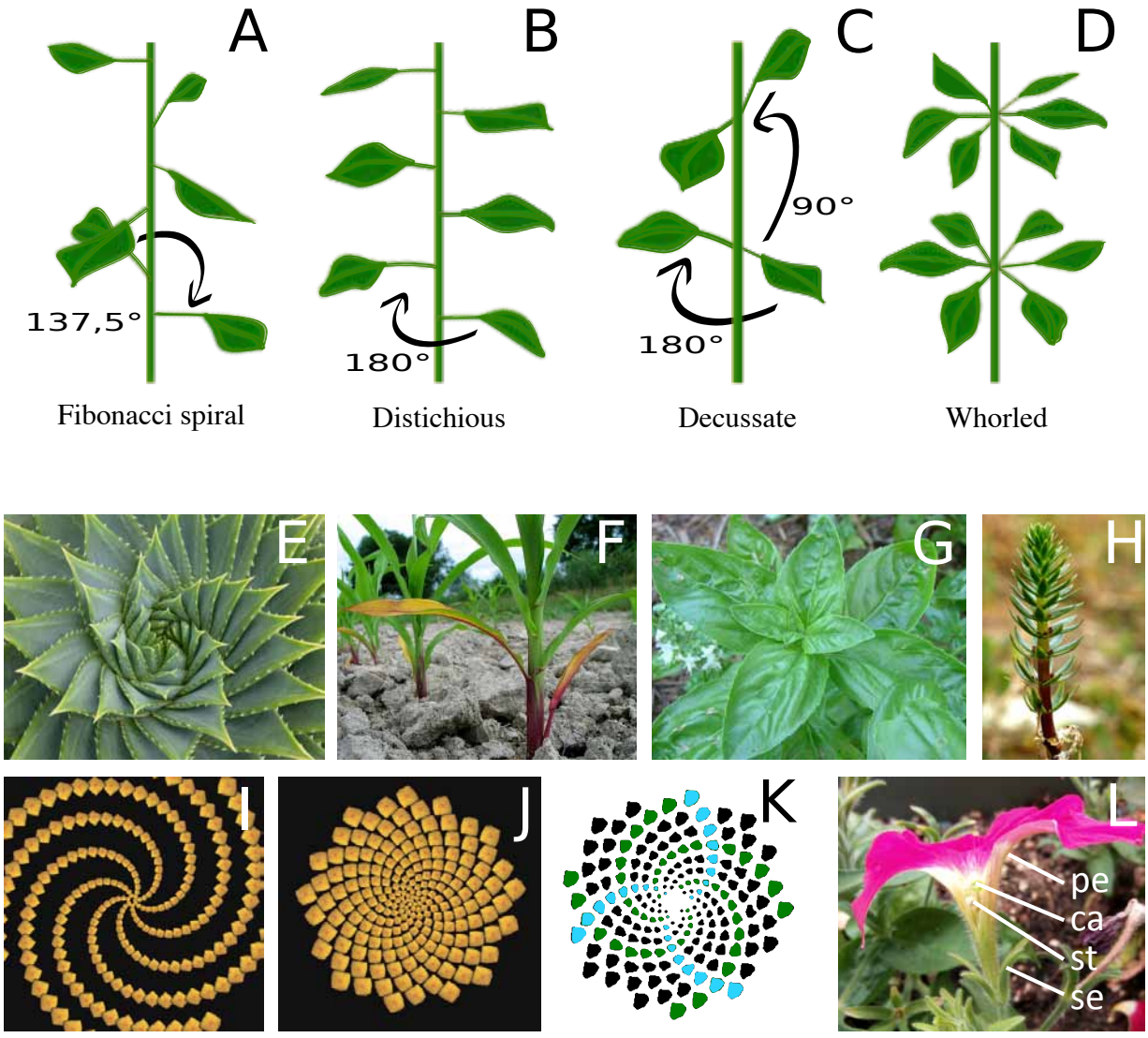

Figure 0.2: Phyllotaxis follows stereotyped patterns. Graphical representations (A-D) and corresponding examples (E-H) of spiral, distichious, decussate and whorled patterns, from left to right. E) *Aloe polyphylla*. F) *Zea mays*. G) *Ocimum basilicum*. H) *Hippuris vulgaris*. I-K) Graphical representations of spirals: spiral pattern with a 51,43° divergence angle shows gaps in the arrangements of organs (I); spiral pattern with an α=137,5° divergence angle shows more compaction (J); From top view of the inflorescence, contact parastichies can be seen clockwise (some are indicated in green) and anticlockwise (blue) (K). L) The four floral whorls in *Petunia hybrida*: sepals (se), petals (pe), stamen (st), carpels (ca). Images sources : see Figures and Tables Inventory.

I.B – FIBONACCI SPIRALLED PHYLLOTAXIS IS THE MOST STUDIED PATTERN

Among phyllotactic patterns, Fibonacci spiral pattern is the most common (see http://www.math.smith.edu/phyllo/About/Classification.html). Fibonacci spiral has intriguing mathematical features in that consecutive primordia are positioned relative to one another with a divergence angle close to α =137.5°, known as the golden angle (Figure 0.2.A & E). This angle is a fraction of the whole circle that follows the golden ratio φ, an irrational number that can't be written as a simple fraction and can only be defined in terms of itself:

$$\varphi = 1 + 1/\varphi$$

In regards of phyllotaxis, an angle that would be defined as a simple fraction of the circle such as 1/7 for example (51.43°), would just divide the circle in 7, and thus create a pattern where organs would stack up in 7 lines around the centre, making gaps between them (Figure 0.2.I). It is the case of some patterns such as opposite (180°, ½ of the circle) or distichious (90°, ¼ of the circle). On the contrary, angles defined by such an irrational number as φ, never complete a full turn that would finish the series of possible positions, and therefore they never stack up in lines (Figure 0.2.J). When viewing the shoot from the top, other spirals, called parastichies, can be defined by connecting organs in contact or in visible proximity either clockwise or anticlockwise (Figure 0.2.K). Interestingly, the numbers of parastichies in each orientation are generally two consecutive numbers of the Fibonacci series.

These mathematical regularities have inspired a long history of multidisciplinary studies (Adler *et al.*, 1997). Indeed, these intriguing features of the Fibonacci spiral can be encountered in many other systems, including development of other living organisms such as the human skull (Bakõrcõ *et al.*, 2016) as well as fluid dynamics (Mokry, 2008), etc. Therefore they have raised curiosity of scientists in many fields and, luckily, they have

brought together mathematicians, physicists and plant scientists for decades. Indeed, phyllotaxis has been a long-term field for interdisciplinarity, without which our present understanding of it would not stand at its current point. Moreover, the most studied species *Arabidopsis thaliana* displays a spiral phyllotaxis, which has allowed investigating the real nature of the mechanisms predicted by mathematical and physical models about this particular pattern.

I.C – WHAT DO WE KNOW ABOUT WHORLS?

Whorls define phyllotactic arrangements where lateral organs are positioned in groups of three or more organs radiating from a single point, thus creating nodes of several axes separated by internodes. True whorls are the result of concomitant formation (generally radially evenly distributed), whereas pseudo-whorls show several organs at the same node that have not been initiated at the same time. Most angiosperm display flowers with organs arranged in four whorls: a calyx of sepals, a corolla of petals, an androecium of stamens, and the gynoecium where the carpels stand (Figure 0.2.L). *A. thaliana* undergoes such a phyllotactic transition during its reproductive phase: a spiralled shoot produces whorled flowers, which development has been extensively described (Smyth *et al.,* 1990). However, *A. thaliana* flowers have not been considered as a model for phyllotaxis so far. This can be explained by practical reasons: only early stages of flower development can be easily observed, because the developing sepals quickly hide the entire floral meristem. Moreover, genetic reporters and anatomical observations on scanning electron microscopy showed that sepals are not established as a true whorl. Indeed, they start growing from the abaxial side inwards (Smyth *et al.,* 1990; Alvarez-Buylla *et al.,* 2010; Chandler *et al.,* 2014), prior to arranging in a pseudo-whorl by absence of internode growth.

Most of our knowledge on phyllotaxis at the meristem is based on the combination of mathematical and physical models (Douady & Couder, 1996a, b, c) with seminal experiments conducted on a few species such as the spiralled *Lupinus albus* and *Dryopteris* (Wardlaw et

al., 1949), or the decussate *Epilobium hirsutum* (Snow & Snow, 1932, 1935; Richards *et al*., 1951). More recently, biological studies on the spiral *A. thaliana* and *Solanum lycopersicum* (tomato), and the alternate *Zea mays* (maize) and *Brachypodium distachyon* (O'Connor *et al*., 2014), brought molecular support to the model predictions. Whorled pattern have been studied in computational science (Kitazawa *et al*., 2015), but no whorled species have been analysed yet, as it is a pattern that is not found in agronomical species and none of them can be explored with classical molecular tools such as genetic fluorescent markers.

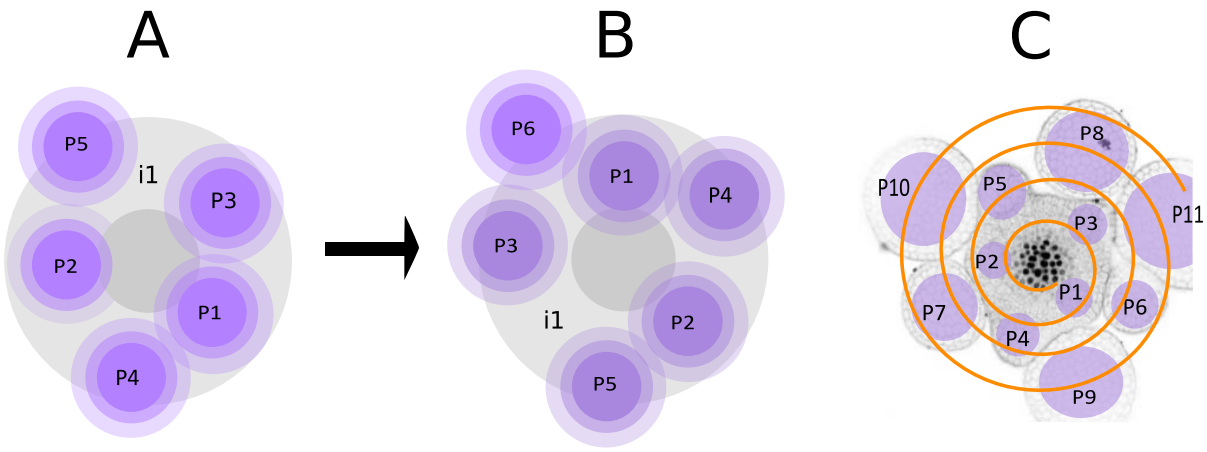

Figure 0.3: Inhibitory fields and growth drive phyllotaxis. Existing primordia (numbered from the youngest, P1, to the oldest, P11) generate inhibitory fields that block organ initiation in their vicinity. In this example (a spiral phyllotaxis), growth moves the existing organs away from the tip of the meristem, thus lowering the inhibition and allowing for the next initiation to occur (i1) (A->B). This process repeats itself as the plant grows, and ultimately successive organs are arranged in a meristem-centred spiral (C).

II – INHIBITORY FIELDS DRIVE PHYLLOTAXIS PATTERNING

II.A – THE INHIBITORY FIELD CONCEPT

As pointed out above, the mathematical regularities observed in shoot phyllotaxis stimulated the development of mathematical, computational, and physical models from the end of the 19th century onwards (Adler *et al.*, 1997). The most widely accepted model for phyllotaxis proposes that spatio-temporal patterns of organ initiation emerge from a self-organizing process. It involves lateral inhibition fields that are generated by organs in the growing shoot apex. Some of the earlier observations supporting the idea that inhibitory fields are involved in controlling phyllotaxis were made by Hofmeister who noticed that primordium initiation is a sequential process that occurs at the meristem periphery, in the largest space left by the existing organs (Hofmeister *et al.*, 1868). This led him to suggest the existence of geometrical constraints that could be interpreted as physical inhibitory fields, and would thus drive phyllotaxis. Experimental disruption of phyllotaxis through surgical incisions near organs in the meristem led to shifts of organ initiation sites that supported Hofmeister's hypothesis (Snow & Snow, 1931). Remarkably, although a regular phyllotactic pattern was quickly recovered in these experiments, this was not obligatorily a restoration of the original pattern. For instance, diagonal dissection of a decussate meristem resulted in recovery on each half of the meristem but with a shift to a spiral phyllotaxis (Snow & Snow, 1935). These pioneering results were later confirmed using local laser ablations in order to minimize secondary effects arising from tissue injuries (Reinhardt *et al.*, 2005). Taken

together, these experiments suggested the existence of a self-organized and self-correcting system robustly driving the spatiotemporal patterning of lateral organ production.

As lateral organs are not always in physical contact, it was proposed early on that the properties of phyllotaxis could rely on chemical inhibition (rather than physical effects) from pre-existing primordia, which influences the positioning of new primordia (Wardlaw *et al*., 1949; Richards *et al*., 1951). This led to the view that inhibitory fields block initiation in the vicinity of existing organs, while growth ultimately allows the initiation of new primordia at spatial positions where the cumulated inhibitory effects are the lowest (Figure 0.3). In the 1990's, Douady and Couder recapitulated these results using both physical and computational models (Douady & Couder 1996,b). They studied the dynamic properties of an inhibitory field-based model in detail, and demonstrated that this provides a simple conceptual framework for understanding phyllotaxis. In particular, they showed that inhibitory fields can drive self-organization of phyllotactic patterns and produce most, if not all phyllotactic patterns observed in nature by varying a single control parameter called Γ. This parameter corresponds to the ratio of the radius of inhibitory fields produced by organs divided by the radius of the generative circle at the centre of the meristem where organs are initiated, thus highlighting the key importance of meristem geometry in determining phyllotactic patterns. It is important to note that postulating a generative circle suggests that another type of inhibitory field ensures that organs can be initiated only at a certain distance from the centre of the meristem. This abstract model and its variants (models with fields of a geometric, physical, or chemical nature have been proposed over the years: see Adler *et al*., 1997 and Shipman *et al*., 2005 for extensive review) thus predict that inhibitory fields generated by organs could lead to the emergence of phyllotactic patterns in the growing meristem.

II.B – THE A CENTRAL ROLE FOR AUXIN SPATIOTEMPORAL DISTRIBUTION IN PHYLLOTAXIS: BIOLOGY AND MODELS

It is only in the past two decades that the molecular mechanisms that generate the inhibitory fields predicted by models have been identified. Starting from the identification of the *PIN-FORMED (PIN1)* gene that encodes an efflux carrier (Galweiler *et al.*, 1998) of the plant hormone auxin, and has emerged as the central regulator of phyllotaxis. The fundamental role of PIN1 as an orchestrator of phyllotaxis is illustrated by the phenotype of the loss-of-function mutant, which produces characteristic needle-like inflorescence stems devoid of organs (Okada *et al.*, 1991). Several studies have shown that auxin is transported directionally toward incipient primordia where it accumulates and activates a transcriptional response, initiating organogenesis upon auxin sensing (Reinhardt *et al.*, 2003, Heisler *et al.*, 2005; Vernoux *et al.*, 2011). A dynamic network of PIN1 auxin efflux carriers, whose cellular polarity determines the direction of the auxin flux (mainly in the L1 layer), regulates the spatiotemporal distribution of auxin in cooperation with influx carriers (Reinhardt *et al.*, 2003, Heisler *et al.*, 2005; Bainbridge *et al.*, 2008). Analysis of the PIN1 auxin efflux carrier network led also to the proposition that auxin transport could not only promote the accumulation of auxin at organ initiation sites but could also deplete auxin levels around organs, thus generating inhibitory fields (Reinhardt *et al.*, 2003). Spatiotemporal analysis of the distribution of the auxin signalling biosensor DII-VENUS, a synthetic protein degraded directly in response to auxin, allowed the direct visualization of the auxin-based inhibitory fields. While DII-VENUS fluorescence is absent from organs due to high auxin levels, the inhibitory fields can be visualized as domains of high fluorescence surrounding primordia and appear to be progressively established (Vernoux *et al.*, 2011; Brunoud *et al.*, 2012). Taken together, these data indicate that it is the depletion of an activator, auxin, rather than the diffusion/movement of a repressor that establishes chemical inhibitory fields. Note however

that the distribution of DII-VENUS fluorescence demonstrates that auxin also accumulates at the centre of the meristem (Vernoux *et al.*, 2011). Thus, auxin distribution does not explain the inhibitory field in the centre of the meristem postulated in models.

As a consequence of the above results, several studies have addressed the question of whether self-organization of the PIN1 network could establish the auxin-based inhibitory fields. While molecular details of the mechanisms controlling PIN1 polarities at the cellular level are well known and involve intracellular trafficking of the protein (for a review, see Friml *et al.*, 2010), how the dynamics of PIN1 polarity are controlled at the tissular level is still largely unknown. Several theoretical models have proposed cell-based hypotheses that can reproduce auxin distribution patterns similar to those observed experimentally (Wabnik *et al.*, 2011). Concentration-based models propose that PIN1 in a given cell is polarized toward the neighbouring cell with the highest concentration of auxin (Smith *et al.*, 2006a, b; Jönsson *et al.*, 2006), while flux-based or canalization models (originally developed to reproduce vascular patterns) propose that a cell senses and enhances its own efflux of auxin, consequently stabilizing auxin flux between cells (Mitchison *et al.*, 1981; Rolland-Lagan *et al.*, 2005; Stoma *et al.*, 2008; Wabnik *et al.*, 2011). A combined model integrating both the concentration-based hypothesis in the L1 layer and the flux-based hypothesis in the vascular tissue was similarly shown to reproduce realistic PIN1 polarization dynamics in different developmental contexts including the meristem (Bayer *et al.*, 2009). This last model recently received experimental support from the analysis of the localization and dynamics of PIN1 homologs in the meristem of *Brachypodium distachyon* (O'Connor *et al.*, 2014). The closest homologs of PIN1, BdPIN1a and BdPIN1b, are found in the developing vasculature of organs while a more distant homolog is found specifically in the L1 layer. These biological observations together with a combined model similar to the one developed by Bayer Bayer *et al.* (2009) support the idea that PIN1 polarities could be controlled by different mechanisms in the epidermis layer and in the developing vasculature. Taken together, the different models indicate that polarization of PIN proteins controlled by a feedback between auxin and its own transport could provide self-organizing properties to the PIN1 auxin efflux carrier network in the meristem, and thus control phyllotaxis. However, the question of which type of feedback mechanism links auxin to its own efflux currently remains unanswered. Indeed, a comparison of the properties of most of the models that have been published suggests that none can fully

explain the dynamics of PIN1 during development (Van Berkel *et al*., 2013) highlighting the need for further knowledge of the molecular mechanisms underlying PIN1 polarization in tissues. Here, modelling is again useful in identifying the molecular mechanisms that could be at play. For example, the work of Wabnik *et al*. (2011) shows, using a detailed molecular model, that the modulation of PIN intracellular trafficking by an extracellular auxin receptor, together with a positive feedback of auxin on PIN transcription, could lead to PIN polarization as seen during vascular tissue development in leaves or during vascular tissue regeneration, two biological contexts that can be explained using the canalization hypothesis (Rolland-Lagan *et al*., 2005; Sauer *et al*., 2006). Consolidating our understanding of auxin signalling mechanisms and of the cellular mechanisms controlling PIN1 polarities in parallel with the development of mechanistic models will thus be instrumental for gaining a full understanding of how the PIN1 network drives phyllotaxis in the meristem.

II.C – GENE REGULATORY NETWORKS CONTROLLING AUXIN HOMEOSTASIS IN THE MERISTEM

Dynamical auxin transport is key to trigger organ initiation and to establish inhibitory sinks that control organ spacing. However, auxin transport is not enough to build such a complex patterning: phyllotaxis is influenced by the tight regulation of auxin homeostasis in the meristem, from biosynthesis to transport and signalling. A complex network of regulatory genes is being discovered and despite the differences in phyllotaxis between species, conserved modules can determine maintenance and patterning of the meristem (Barton *et al*., 2010; Bartlett *et al*., 2014).

As discussed above, production of new organs in the meristem is initiated through accumulation of auxin at specific sites in the PZ. Auxin perception and signalling are controlled by a complex nonlinear pathway, involving nuclear-localized TIR1/ AFB F-box co-receptors that are part of an SCF E3 ubiquitin ligase complex, and Auxin/indole-3-acetic

acid protein (Aux/IAA) transcriptional repressors. Auxin acts as a molecular glue to directly promote the interaction between TIR1/AFBs and Aux/IAAs and thus trigger poly-ubiquitination and degradation of Aux/IAAs (Dharmasiri *et al*., 2005; Kepinski *et al*., 2005). At low auxin concentration, Aux/IAAs interact with the Auxin Response Factors (ARF) transcription factors. Both Aux/IAAs and ARFs are encoded by multigenic families, comprising 29 and 23 members respectively in *A. thaliana*. ARFs can be divided into two classes: either transcriptional activators (ARF5, ARF6, ARF7, ARF8, and ARF19 in *A. thaliana*) or transcriptional repressors (Guilfoyle *et al*., 2007). By promoting Aux/IAA degradation, auxin allows ARFs to modulate target gene transcription. Interactions between Aux/IAAs and ARFs are thus central to the regulation of auxin signalling. A combination of a large-scale analysis of Aux/IAA-ARF interactions, an analysis of the expression patterns of both gene families, and mathematical modelling of the pathway, has suggested that (1) a differential expression of ARFs and Aux/IAAs between the CZ and the PZ creates a differential capacity to sense auxin between the two domains, the CZ being largely insensitive to auxin; (2) co-expression of ARF repressors and activators throughout the meristem gives buffering properties to the auxin signalling pathway and ensures robust transcriptional activation in organs (and thus organogenesis) (Vernoux *et al*., 2011). Experimental support for these two predictions was obtained by comparing the spatial-temporal distribution of the DII-VENUS auxin biosensor to estimate auxin distribution and of the DR5::VENUS auxin-inducible synthetic reporter to monitor auxin-induced transcription. While DII-VENUS indicates that auxin accumulates at the centre of the meristem (as pointed out earlier), this does not induce transcription. In addition, auxin concentrations were found to vary significantly over time, while DR5::VENUS suggests that this does not induce fluctuations in auxin-induced transcription. Importantly, these results also indicate that a spatial regulation of the capacity to respond to auxin provides at least a partial molecular explanation for the absence of organ initiation at the centre of the meristem. This suggests that a regulation of the sensitivity of cells to auxin provides the basis for the inhibitory field at the centre of the meristem proposed in models (Douady & Couder, 1996b).

The AUXIN RESPONSE FACTOR 5/MONOPTEROS (ARF5/MP) is a master regulator of organ formation in the meristem (Zhao *et al*., 2010). Disruption of ARF5 function in the *A. thaliana* meristem leads to the production of needle-like inflorescences similar to

those of *pin1* mutants, a phenotype that illustrates the key role of auxin signalling in the PZ. ARF5 was shown to directly activate the expression of the *LFY, ANT, AINTEGUMENTA-LIKE6/PLETHORA3 (AIL6/PLT3),* and *FILAMENTOUS FLOWER (FIL*) genes that are all essential regulators of flower development (Yamaguchi *et al*., 2012; Wu *et al*., 2015). These studies provide a molecular demonstration that auxin directly activates the transcriptional program leading to organ development (in this case the flower), as was previously indicated by the observation that local application of auxin at the PZ of *pin1* meristems triggers flower initiation (Reinhardt *et al*., 2000) and that LFY expression is downregulated in the *pin1* mutant (Vernoux *et al*., 2000). This further supports an instructive role for auxin accumulation in triggering organogenesis and thus in phyllotaxis. Moreover, *ARF5*-mediated auxin signalling was shown to control the orientation of PIN1 carriers, and therefore phyllotaxis patterning (Bhatia *et al*., 2016).

PLT genes encode members of the AP2-domain transcription factor family and are essential throughout plant development (Prasad *et al*., 2011). In the *A. thaliana* meristem, three members of this family (*PLT3, PLT5*, and *PLT7*) are expressed in the CZ and PZ and are required for spiral phyllotaxis, as double or triple loss-of-function mutants show an increased frequency of distichous phyllotactic patterns (Prasad *et al*., 2011). The expression of two flavin-containing mono-oxygenases, *YUCCA1 (YUC1)* and *YUC4*, which act in a rate-limiting step of auxin biosynthesis (Zhao *et al*., 2001), is reduced in the *plt3plt5plt7* triple mutant. Mutation of both *YUC1* and *YUC4* was also shown to induce strong perturbations in flower development (Cheng *et al*., 2007) and *PIN1* expression is downregulated in the *plt3plt5plt7* mutant. Taken together, these observations suggest that PLTs act in a gene regulatory network that controls the abundance of auxin in the meristem through the regulation of auxin biosynthesis (Pinon *et al*., 2013). These data further point to a potential key role of auxin biosynthesis in phyllotaxis, a role that deserves consideration both in future biological experiments and phyllotaxis models.

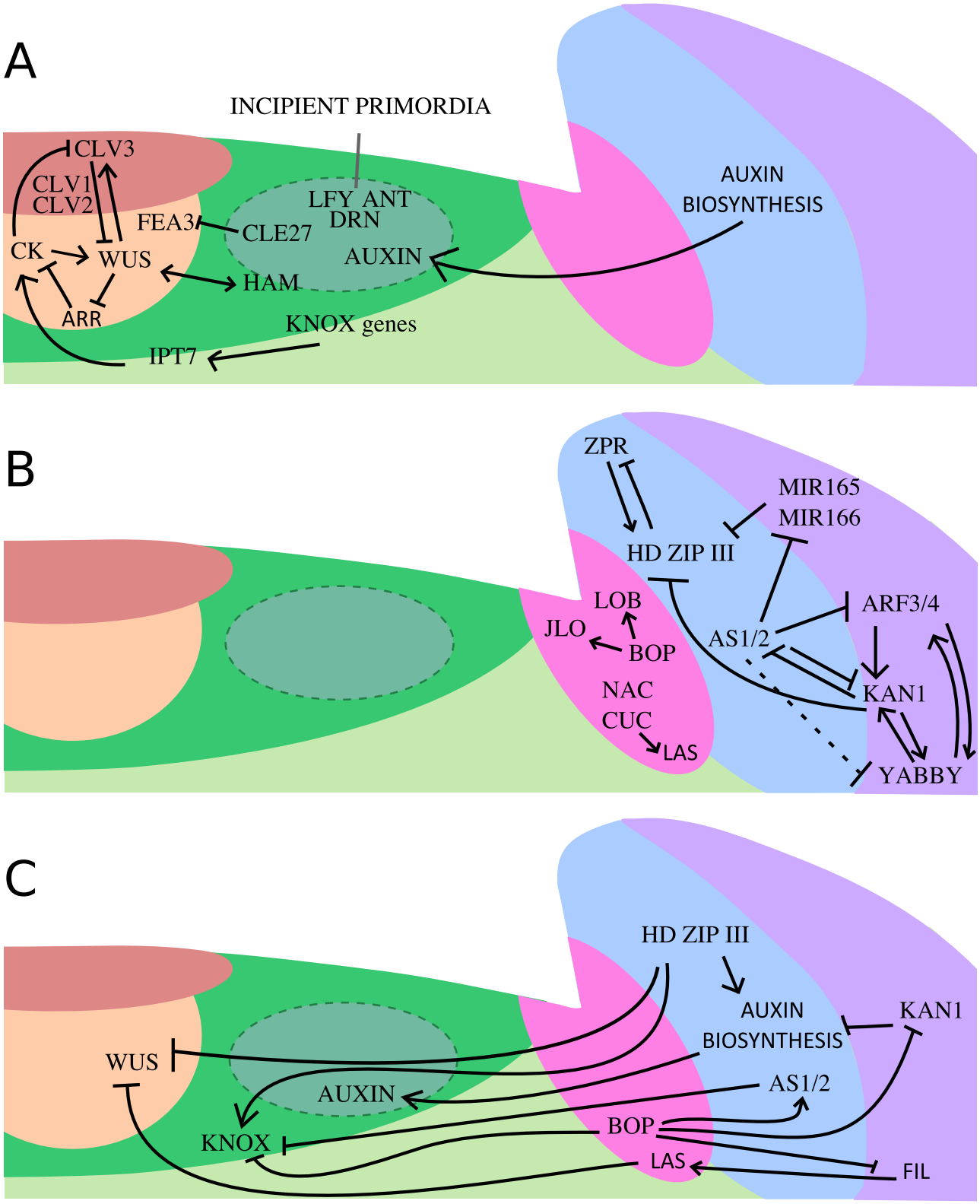

Figure 0.4: Interconnected gene regulation networks pattern the shoot apical meristem and lateral organs. A) Main meristematic gene regulation network controlling geometry. B) Establishment and maintenance of abaxial adaxial polarity requires specific actors. C) Interplay between meristematic zones and lateral organs participate in the meristem homeostasis. Functional zones are schematized with same colours as in Figure 1.

III – FUNCTIONNAL DOMAINS CONTROL PHYLLOTAXIS THROUGH MERISTEM GEOMETRY

Despite their central role, auxin biosynthesis, transport and signalling are not sufficient to explain phyllotaxis. The final phyllotactic pattern is also depending upon the global geometry of the shoot and its growth. Indeed, phyllotactic models predict that the establishment of a specific pattern is controlled by the ratios between the dimensions of organ-centred inhibitory fields and a central non-organogenetic domain (Douady & Couder, 1996b). Such geometry tightly depends on the ability of the cells for specific signal transduction in each zone. Therefore, understanding phyllotaxis requires to explain how the whole shoot is patterned into different functional domains, either competent for organogenesis (at the periphery) or allowing stem-cell renewal and maintenance (in the centre).

Moreover, a key property of meristem patterning is to produce a stable structure despite a constant production of cells and lateral organs (Traas & Vernoux, 2002). Hence, the homeostasis of the meristem is essential for the robustness of phyllotaxis, because it ensures the constancy of growth, geometrical parameters that govern phyllotaxis, and signal transduction activities. In particular, the difference between the CZ where no organogenesis occurs and the PZ from which lateral organs arise is key to phyllotaxis (Bowman *et al*., 2000; Figure 0.1). In this section, I will review the current knowledge on the genetic control of shoot meristem patterning, with a special focus on the possible impact on phyllotaxis (Figure 0.4). Moreover, I will highlight the importance of feedback signals from lateral organs to the

centre, which signal depend on the identity of the emitting cells, and thus on the correct development and patterning of lateral organs.

III.A – THE CENTRAL ZONE FUELS THE PERIPHERY IN COMPETENT CELLS AND CONTRIBUTES TO MERISTEM GEOMETRY

The activity of the meristem requires a variety of transcription factors, and a large number of these regulators have been identified through genetic studies conducted over the last 20 years. The balance between stem-cell maintenance and differentiation in the shoot is under complex genetic control. Many actors have been found, and I will here only outline the major pathways controlling stem cell homeostasis. For extensive review, see Gaillochet *et al.*, 2015. The core module regulating stem cell homeostasis is centred on the *WUSCHEL* (*WUS*) – *CLAVATA3* (*CLV3*) regulatory loop (Brand *et al.*, 2000; Schoof *et al.*, 2000; reviewed by Somssich *et al.*, 2016), which both specifies the OC and stem cell identity, and restricts their abundance (Gordon *et al.*, 2009; Yadav *et al.*, 2011).

WUS is a homeobox gene. Its null mutants have premature consumption of stem cells (Laux *et al.*, 1996), whereas ectopic expression of *WUS* induces *de novo* formation of ectopic meristems (Zuo *et al.*, 2002). In the wild type, *WUS* is also expressed in the organizing centre of flower meristems from late floral stage 2 (one sepal) until the formation of stage 7 (third whorl), concomitantly with *AGAMOUS* (*AG*), another homeotic transcription factor that specifies floral meristem and the two inner floral whorls. After formation of the four floral whorls, meristem termination is achieved through *AGAMOUS*-mediated inhibition of *WUS* (Lenhard *et al.*, 2001; Lohmann *et al.*, 2001).

WUS protein has been shown to move from cell to cell up to the CZ where it activates CLV3 production (Yadav *et al*., 2011). Mutant alleles of *CLV3*, first named after their club-like siliques (Clark *et al*., 1995), show enlarged meristems that are often fasciated and overproduce flowers. *CLV3* is a stem cell-specific protein, and precursor of a 12-amino acid peptide that is secreted from the stem cells (Fletcher *et al*., 1999; Kondo *et al*., 2006) and indirectly represses *WUS* in a dynamic feedback loop. In turn, perception of CLV3 by a receptor complex containing the CLAVATA1 (CLV1) receptor-like kinase and dimers of the *CLV2* pseudo kinases, represses the expression of *WUS* in the L1 and L2 layers of the CZ (Fletcher *et al*., 1999; Bleckmann *et al*., 2010; Yadav *et al*., 2011). However, Nimchuk *et al*. (2017) proposed a divergence between downstream signalling of the *CLV1* and *CLV2* receptors, as the downstream receptor kinase *BARELY ANY MERISTEM* (*BAM*) transcription levels were repressed by *CLV1* but not by other receptors of *CLV3*.

The homeodomain transcription factor *SHOOT MERISTEMLESS (STM)* is expressed in all meristematic cells and required for the specification of meristem identity from embryogenesis onwards. Indeed, its expression recedes during organogenesis initiation around the peripheral zone of the SAM (Long & Barton, 2000; Gordon *et al*., 2009). Mutant alleles of *STM* showed dysfunctional shoot apical meristems, which, when bolting, terminated prematurely as fused flowers (Long *et al*., 1996; Endrizzi *et al*., 1996). Interestingly, *STM* activates the transcription of *ISOPENTENYLTRANSFERASE 7* (*IPT7*) (Jasinski *et al*., 2005; Yanai *et al*., 2005), which product performs an important limiting step of cytokinin biosynthesis, and by this mean promotes the maintenance of the central zone by activating *WUS* expression, and repressing *CLV1* (Gordon *et al*., 2009).

Nevertheless, other players modulate this loop and many molecular actors remain unknown. The question remains of how the *WUS-CLV3* system promotes stem cell identity, which is characterized by undifferentiated state and low mitotic activity (Stewart *et al*., 1970). *WUS* has been shown to repress the expression of several members of the type A *ARABIDOPSIS RESPONSE REGULATOR (ARR)* gene family, which negatively regulate signalling in response to the plant hormone cytokinin. It has been proposed that cytokinin is produced specifically in the L1 and that its distribution in the meristem participates in positioning the *WUS* domain (and thus the OC) in the meristem through a positive feedback

of cytokinin on *WUS* expression (Shani *et al.*, 2006; Chickarmane *et al.*, 2012). More recently, it was shown that ectopic *WUS* expression in roots promotes stem cell activity by reducing auxin response, along with other developmental pathways, and reduces mitotic activity (Negin *et al.*, 2017). Thus, a nonlinear network involving WUS, CLV3, and cytokinins defines the position and size of the stem cell niche in the meristem. Other independent pathways have also been implicated in this process and are reviewed in Heidstra *et al.*, 2014).

As mentioned in the second section of this introduction, inhibitory field models highlight the importance of meristem geometry in setting the phyllotactic pattern (the Γ parameter from the seminal work of Douady & Couder, 1996b). Very few mutants with clear changes in the phyllotactic regime exist, but these can likely be explained by a change in the geometry of the meristem. In maize, mutants impaired in the ABERRANT PHYLLOTAXIS 1 (ABPH1) protein, a two-component response regulator regulating cytokinin signalling, has a decussate rather than alternate phyllotaxis. This phenotype was correlated with a larger meristem while the size of lateral organs (leaves in this case) appeared to be unchanged (Giulini *et al.*, 2004; Lee *et al.*, 2009). This observation is coherent with the well-established function of cytokinin in regulating the size of the stem cell niche (Shani *et al.*, 2006; Chickarmane *et al.*, 2012). As the *abph1* mutation also affects *PIN1* expression, the explanation for the phyllotactic phenotype could however be more complex and not linked solely to the change in the geometry of the meristem (Lee *et al.*, 2009). Another maize mutant, *abph2*, presents the same phenotype as *abph1* and is caused by transposition of the glutaredoxin-encoding *MALE STERILE CONVERTED ANTHER 1 (MSCA1)* gene to a novel genomic location (Yang *et al.*, 2015). This transposition causes ectopic expression of *MSCA1* and an enlargement of the meristem as seen in *abph1*. The MSCA1 protein interacts directly with *FASCIATED EAR4 (FEA4)*, a bZIP transcription factor homologous to *PERIANTHIA* from *A. thaliana* and that has been proposed to act in parallel with the WUS/CLV pathway in the regulation of meristem size (Pautler *et al.*, 2015). This suggests that *MSCA1* could regulate meristem size and in turn phyllotaxis in *abph2* through modulating the activity of *FEA4*. In rice, *decussate (dec)* mutants might also be disturbed in cytokinin signalling, although the molecular basis of this phenomenon remains unclear (Itoh *et al.*, 2012). Again, *dec* mutants show a larger meristem and a decussate instead of an alternate phyllotaxis. The

shared phyllotactic phenotype of the two *abph* mutants and the *dec* mutant further supports the fact that changes in meristem size in the mutants might be the primary trigger for the change in phyllotaxis, although this remains to be directly demonstrated.

Altogether these actors (Figure 0.4.A) contribute in establishing and maintaining the central zone dimensions and homeostasis, thus determining the circumference and the constancy of the central inhibitory domain that was described in models (Douady & Couder 1996,b). Therefore, the balance between renewal and differentiation of meristematic cells achieved through the regulation of the central zone is crucial to establishing the phyllotactic pattern.

III.B – LATERAL ORGANS GIVE FEEDBACKS TO THE CENTRAL ZONE AND CONTRIBUTE TO PHYLLOTAXIS

III.B.1 – EARLY FEEDBACKS FROM INCIPIENT FLOWERS ON THE CENTRAL ZONE

Organogenesis occurs in the peripheral zone of the meristem following auxin concentration peaks in the first layer of the epidermis. Factors regulating the transition from undifferentiated meristematic cells to differentiated cells are still poorly understood, but this process is marked by the fact that lateral organ founder cells in the peripheral zone become transcriptionally different from the PZ meristematic cells, and a release of cell differentiation programs is concomitant to the expression of genetic markers.

Morphogenesis program is launched as founder cells are recruited and start to proliferate and differentiate, a process that is marked by the repression of *STM* concomitantly to the activation of *DORNROSCHEN* (*DRN*) and *DORNROSCHEN-LIKE* (*DRNL*). These two redundant AP2-like transcription factors were shown to be expressed in central zones as well

as founder cells from the stage 1 of *A. thaliana* flower primordia onwards (Kirch *et al*., 2003; Chandler *et al*., 2011; Chandler *et al*., 2014). Single mutants of DRN and DRNL are aphenotypic in *A. thaliana* and the double mutant is embryo lethal, precluding functional analysis. However, the single tomato homologue *LEAFLESS* (*LFS*) was shown to be rapidly induced by auxin application but also to be regulated independently to auxin signalling (Capua & Eshed, 2017). Tomato *lfs* mutants were only able to grow pin-like shoots. A first evidence of feedbacks from developing organs to stem cells in the central zone come from ectopic expression of *DRN*, either under the ubiquitous 35S promoter or under the CLV3 promoter (Kirch *et al*., 2003). This caused enlarged meristem size associated with expanded *WUS/CLV3* domains, early meristem termination, and production of radially symmetrical lateral organs. Altogether these results indicate that *DRN* is linked to primordia formation around the meristem but can impact on WUS/CLV3.

The stability of the central zone WUS/CLV3 system also depends on the GRAS family transcription factor *HAIRY MERISTEM (HAM;* Stuurman et al., 2002). Interestingly, *HAM* is expressed in lateral organs initia and the provasculature, and whereas it is noticeably not detectable in the CZ, its expression pattern overlaps with that of WUS in the rib zone, beneath the central zone. Mutants in *A. thaliana* and *Petunia* undergo expansion and flattening of their shoot apex, early meristem mosaic differentiation and arrest, aberrant phyllotaxis correlated with misregulation of the *WUS* and *CLV3* expression domains (Schulze et al., 2010; Engstrom et al., 2011). Recent studies demonstrated that there was a physical interaction between *HAM* and *WUS*, and that this interaction was necessary to synergistically regulate downstream gene expression and shoot meristem maintenance (Zhou et al., 2015). Moreover, silencing experiments on the tomato homologs of *HAM (SIHAMs)* showed over-proliferation of the PZ cells correlated to misexpression of *WUS*, a phenotype that was suppressed by enzymatic reduction of cytokinin levels (Hendelman et al., 2016).

Functionally opposite to *HAM* is the stem-cell activity repressor FASCIATED EAR 3 (FEA3), a rib zone specific LRR receptor which mutant produced enlarged and fasciated meristems with enlargement of the *WUS* and *CLV3* domains, and aberrant phyllotaxis in maize and *A. thaliana* (Je *et al.,* 2016). In both species, *fea3* mutants were shown to be resistant to treatments with CLV3/EMBRYO-SURROUNDING REGION (CLE) peptides

ZmFCP1 and AtCLE27 respectively. These two CLV3/EMBRYO-SURROUNDING REGION (CLE) peptides were produced in the incipient primordia, and thought to be necessary to control SAM size.

Altogether these regulators guide the development of incipient primordia in the PZ (Figure 0.4.B), and phenotypic analyses have shown their implication in meristem geometrical proportions as well. After specification of organogenesis location, cells begin to proliferate and form new domes at the periphery of the meristem, called primordia. These cells will then start differentiate and form organized structures that develop into leaves, axillary meristems, or flowers in the inflorescence of *A. thaliana*. Each of these lateral organs finally acquires a specific morphology and identity that corresponds to their specific function. At a finer scale, cells integrate of a set of signals that depends on their position in the organ.

III.B.2 – ORGAN POLARITY FEEDBACKS ON THE SAM

Plant lateral organs are polarized along an adaxial/abaxial axis starting from the meristem. These polar identities arise early in developing organs, when they are still in connection with the meristem. Many genetic studies have pointed out the strong effects of polarity mutants on the maintenance of the stem cells and meristem geometry, suggesting an important feedback from organ polarity to the meristem. However, the molecular bases of such a signal are still unknown.

In this section, we will briefly describe the genetic network controlling organ polarity establishment and maintenance (Figure 0.4.B). Then, we will focus on the evidence of feedbacks from organ polarity to the SAM (Figure 0.4.C).

III.B.2.a – THE GENETIC NETWORK OF POLARITY

Adaxial-abaxial polarity is the zonation that specifies the parts of lateral organs closer (adaxial) or further (abaxial) to the meristem (Figure 0.1). The function of such a specification is obvious in the case of leaves, which is a flat shape with distinct functions on the two sides. Indeed, the adaxial (dorsal) side is composed of tightly packed palisade cells enriched in

chloroplasts, and provides the plant with photosynthesis products. On the other hand, the abaxial (ventral) side of leaves is made of more loose spongy cells facilitating gas exchanges. Here obviously, dorso-ventral polarity promotes the establishment of adequate physiological functions that are related to their position in the leaf (Merelo *et al*., 2017). Vascular tissues also are polarized, with the water-transporting xylem lying positioned adaxially to the carbohydrates-containing phloem bundles.

Nevertheless in the inflorescence meristem of *A. thaliana*, dorso-ventral polarity is essential for flower patterning, which starts with the specification of the abaxial sepal, and growth, which is guided by antagonist and coordinated action of polarity players (Takahiro *et al*., 2012; Waites & Hudson, 1995). In the growing primordia, polarity is established through complex signalling networks between players that have polar and complementary expression patterns.

Two major regulators of adaxial fate, the *ASYMETRIC LEAVES* (*AS1* & *AS2*) genes, which first orthologous was discovered in *Antirrhinum majus* (*PHANTASTICA*, *PHAN*; Waites & Hudson, 1995, 1998; Byrne *et al*., 2000; Semiarti *et al*., 2001; Iwakawa *et al*., 2002, Matsumura *et al*., 2009), promote differentiation by physically participating in methylation-mediated repression of meristematic *KNOX* genes (Lodha *et al*., 2013). They also bind to promoters and repress abaxial regulators such as *MIR166A*, *AUXIN RESPONSE FACTOR3* (*ARF3*) and *ARF4* (Iwasaki *et al*., 2013; Husbands *et al*., 2015; Matsumura *et al*., 2016). Mutants of AS1 or AS2 both have adaxial defects that induce the formation of filamentous structures.

Concomitantly and synergistically, a second group of adaxial key regulators, consisting in five transcription activators of *CLASS III HOMEODOMAIN LEUCINE ZIPPER* family (HD ZIP III), is expressed exclusively on the adaxial side and determine adaxial fate (McConnell *et al*., 2001; Emery *et al*., 2003; Prigge *et al*., 2005). This group of genetic regulators is composed of *REVOLUTA (REV)*, *PHAVOLUTA (PHV)*, *PHABULOSA (PHB)*, *ARABIDOPSIS THALIANA HOMEOBOX GENE 8 (ATHB8)* and *ATHB15* (or *INCURVATA4, ICU4,* or *CORONA, CNA*), which are expressed throughout the embryo in early stages of *A. thaliana* development, and become specific to the vasculature and adaxial domains of the

growing organs at the SAM. These five transcription factors hold a leucine zipper domain, which mediates a necessary dimerization prior to DNA binding on specific palindromic DNA sequences (Sessa *et al*., 1998). Besides, this set of transcription factors controls broad range of targets, including auxin biosynthesis genes (Turchi *et al*., 2015), a negative feedback regulator *LITTLE ZIPPER* (*ZPR*) (Wenkel *et al*., 2007; Kim *et al*., 2008; Magnani & Barton, 2011), and up-regulation of STM (Shi *et al*., 2016).

The exclusively adaxial expression pattern of the *HD ZIP III* transcription factors family is achieved through the abaxial repressive gradient two small non-coding RNAs families of *miR165/166* (Emery *et al*., 2003; Mallory *et al*., 2004). The two *MIR165* genes (*A-B*), and the seven *MIR166* genes (*A-G*), respectively display the same mature sequences, but are spatially and temporally differentially regulated, partially by a negative feedback loop with *HD ZIP III* (Jung *et al*., 2007; Zhu *et al*., 2011, 2015; Merelo *et al*., 2016). Interestingly, Singh *et al*. (2017) demonstrated the existence of crosstalk between these regulatory elements and phytohormone signalling in the root (Zhou *et al*., 2015).

On the ventral side of the lateral organ also lays the expression domain of *KAN1* (Kerstetter *et al*., 2001; Eshed *et al*., 2001), a negative transcription factor which expression pattern mirrors that of *HD ZIP III* (Emery *et al*., 2003). Its expression is mediated by other abaxial players such as the auxin signalling intermediates *AUXIN RESPONSE FACTOR 3 (ARF3/ETTIN) & ARF4* (Pekker *et al*., 2005).

Other major roles in abaxial specification in the lateral organs are played by members of the *YABBY* family. The *YABBY* family contains six members *(YAB1, YAB2, YAB3, YAB5, CRABS CLAW/CRC* and *INNER NO OUTER/INO*), four of which are expressed on abaxial domains of lateral organs (*YAB1, YAB2, YAB3, YAB5*). They were shown to act in repressing complexes that promote lamina growth through abaxial/adaxial polarity (Siegfried *et al*., 1999; Kumaran *et al*., 2002; Stahle *et al*., 2009; Sarojam *et al*., 2010). Among these polarity players, *YAB1* also called *FILAMENTOUS FLOWER* (*FIL*) was the first identified (Sawa *et al*., 1999; Siegfried *et al*., 1999). It was shown to be non-mobile, and to have a zinc finger domain that mediates protein interaction on their N-terminus, and a YABBY domain for DNA-binding with a High Mobility Group-like (HMG) helix-loop-helix box on their C-

terminus (Kanaya *et al*., *2001*). Several *fil* mutants were described, displaying a wide range of phenotypes, according to their strength, including the production of filamentous organs with completely radial symmetry, altered phyllotaxis with co-initiations of organs, production of ectopic meristems or meristem arrest (Kumaran *et al*., 2002; Golz *et al*., 2004; Lugassi *et al*., 2010).

Many cross-regulation between the identity genes of the two domains ensure robustness of adaxial/abaxial domains specification and maintenance. All the polarity players described above were widely shown to synergistically contribute to plant development (reviewed by Merelo *et al*., 2017). For instance, the *KAN1* transcription factor directly represses *AS1*/2 in a mutual negative loop (Wu *et al*., 2008), as well as members of the *HD ZIP III* transcription factor group, which expression domains were expanded in *kan1kan2* double mutants (Eshed *et al*., 2001). Moreover, *FIL* targeted *KAN1* and *ARF4* in a positive feedback loop that reinforced their polar pattern (Bonaccorso *et al*. 2012). Conversely, MIR166A and YAB5 were shown to be transcriptionally and epigenetically repressed in an AS1/2-dependant manner (Husbands *et al*., 2015).

III.B.2.b – MANY POLARITY MUTANTS HAVE DEFECTS IN CROSS-REGULATIONS BETWEEN ABAXIAL AND ADAXIAL PLAYERS, AND MERISTEM GEOMETRY, DURING LATERAL ORGAN DEVELOPMENT

Many mutants described for polarity defects also display central zone perturbation. For instance, *ATHB8/15* also were shown to participate in *WUS* downregulation and domain restriction, and consequently in SAM functioning (Green *et al*., 2005). Individually, mutations in any of the five HD ZIP III transcription factors do not induce visible phenotype, but multiple mutants displayed enlarged meristems, adaxialized leaves or pin-like cotyledons (McConnell *et al*., 2001; Prigge *et al*., 2005). Mutants have also been identified for MIR166 genes, such as *men1* and *jabba*, two dominant negative mutants for *MIR166A* and *MIR166G* respectively, which both showed polarity defects in their vascular tissues, associated with enlarged and fasciated meristems with consequently no spiral pattern (Kim *et al*., 2005; Mandel *et al*., 2016). Moreover, mutant lines that were incapable to sequestrate *MIR165/166*

through *AGO10*-binding showed dysfunctionning meristems with pin-like phenotype. Altogether these observations sustain the role of *MIR165/166* and *HD ZIP III* in phyllotaxis.

A feedback of polarity on phyllotaxis could also come directly from a regulation of auxin at the periphery. Indeed, *KAN1* was shown to interfere with auxin biosynthesis. Indeed, *TRYPTOPHANAMINOTRANSFERASE OF ARABIDOPSIS1 (TAA1)* and *YUCCA (YUC)* 2, 5 & 8, which are elements of auxin biosynthesis, were identified as direct negative targets of *KAN1* (Cheng *et al*., 2007; Brandt *et al*., 2012; Huang *et al*., 2014; Xie *et al*., 2015). This decrease of auxin synthesis on the abaxial side, added to an increase of auxin flow towards the CZ (Qi *et al*., 2014), could explain how *DR5* promoter was activated more adaxially than *DRN* in the lateral organs primordia (Chandlers *et al*., 2014), indicating that polarity is set up simultaneously with the positioning and allocation of cells for organogenesis at the shoot apical meristem. Moreover, such regulation of auxin biosynthesis in lateral organs would have an impact on auxin levels at the meristem, and thus on phyllotaxis.

Altogether these polarity players are necessary to normal growth of lateral organs. Mutants in regulators of both adaxial and abaxial identities produced radialized lateral organs and were associated with phyllotaxis defects, such as apparent clustering of organs along the stem (when the plant shoot is described). However few details and quantification were given on the shoot architecture, making unsure to correlate polarity with phyllotaxis. But correlations between gene regulatory networks in the growing lateral organs and the central zone were established, which highlight the role these actors could play on phyllotaxis.

III.C – BOUNDARIES SET THE LIMITS BETWEEN THE MERISTEM AND LATERAL ORGANS

Boundaries are zones of low division rates (Hussey *et al.*, 1971; Reddy *et al.*, 2004; Breuil-Broyer *et al.*, 2004), low differentiation (Ha *et al.*, 2003, 2007) and specific identity (Souer *et al.*, 1996; Aida *et al.*, 1997; Vroemen *et al.*, 2003; Weir *et al.*, 2004; Blein *et al.*, 2008; Berger *et al.*, 2009; Tian *et al.*, 2014) that restricts a given domain from growing when the surrounding ones do. These regions share common regulation pathways in various developmental phenomenons, such as lateral organ outgrowth from the SAM and compound leaves formation (reviewed by Wang *et al.*, 2016; Yu *et al.*, 2016).

In the shoot apical meristem-to-organ boundaries, several actors have been identified, such as the *NAC (NO APICAL MERISTEM (NAM); ARABIDOPSIS TRANSCRIPTION ACTIVATION FACTOR1/2 (ATAF1/2); CUP-SHAPED COTYLEDON2 (CUC2))/CUC* families (Souer *et al.*, 1996; Aida *et al.*, 1997; Breuil-Broyer *et al.*, 2004), which loss-of-function mutants caused fusions of adjacent organs and consequently showed perturbed phyllotaxis. They were proposed to repress growth, notably through a complex interrelation with phytohormone pathways (Gendron *et al.*, 2012; Zhao *et al.*, *2013*). Interestingly, *CUC2* was shown to enhance the expression of *LATERAL SUPRESSOR* (*LAS*), a GRAS (GA INSENSITIVE, REPRESSOR OF GA1-3, SCARECROW) protein identified in several species including *A. thaliana* for its role in organ separation (Schumacher *et al.*, 1999; Greb *et al.*, 2003; Goldshmidt *et al.*, 2008; Busch *et al.*, 2011). *LAS* was also shown to mediate a non-cell autonomous action of *FIL* to the central zone of the inflorescence meristem (Goldshmidt *et al.*, 2008), thus connecting lateral organ polarity and boundary players to meristem geometry, and thus phyllotaxis.

Similarly, members of the *LATERAL ORGAN BOUNDARIES DOMAIN (LBD)* family were identified in the SAM to organ boundary, such as *JAGGED LATERAL ORGANS (JLO)*

(Borghi *et al.*, 2007; Bureau *et al.*, 2010; Rast & Simon, 2012) *and LATERAL ORGAN BOUNDARY (LOB;* Shuai *et al.*, 2002; Matsumura et al., 2009*)*. They were shown to be locally activated by *BLADE ON PETIOLE (BOP) 1* and *2* (Ha *et al.*, 2003, 2004, 2007; Norberg *et al.*, 2005), which single mutants *bop1* and *bop2* generated clusters of flowers along their stem from fused inflorescence (Hepworth *et al.*, 2005; Ha *et al.*, 2007). *BOP* genes were found to interact with abaxial-adaxial polarity through activation of and overlapping functions with AS1/2, such as negative regulation of *KNOX* genes and spatial regulation of *FIL* and *KAN1* abaxial regulators (Ha *et al.*, 2007).

Altogether these regulators participate in meristem homeostasis, as the correct separation of lateral organs from the meristem guaranties its integrity and preserve it from the influence of developmental programs (Figure 0.4.B).

III.D – A ROLE FOR MECHANICAL FORCES IN PATTERNING THE MERISTEM SURFACE

Until now, we have addressed only chemical and molecular players involved in phyllotaxis. However, a role for mechanical signals in phyllotaxis has also been proposed. Plant cells are under turgor pressure and are physically attached to their neighbours by cell walls. Geometry, together with growth, can create dynamic fields of mechanical forces in the meristem that can be either tensile or compressive (Newell *et al.*, 2008; Robinson *et al.*, 2013). Such forces could act downstream of chemical signals and control morphogenesis, but could also be instructive for developmental patterning in the meristem and thus act in parallel with chemical signals such as auxin. To correlate mechanical forces and meristem function, Paul Green *et al.* (1999) developed a biophysical model in which primordium initiation was considered to be the result of compressive forces in the epidermis, a view fuelled by a large body of previous modelling work (more discussion can be found in Newell *et al.*, 2008). Differential growth between internal tissues and the epidermis was proposed to generate

compressive stresses in the epidermis resulting from pushing forces. These lead to deformation of the epidermis, a phenomenon called buckling, and to outgrowth of the organs (Green *et al.*, 1999). However, while compressive forces can be observed in the concave meristems of certain species such as the sunflower (Green *et al.*, 1999), meristematic tissues are generally convex and likely to be under tension (i.e., exposed to pulling forces). The actual contribution of buckling in organ initiation thus remains to be demonstrated, although it could in theory act cooperatively with auxin-based mechanisms to drive phyllotaxis (Newell *et al.*, 2008).

More recently, a collection of studies has revealed that local changes in mechanical properties are intrinsically associated with organ outgrowth and suggested ways in which this might impact meristem activity and phyllotaxis. Auxin has long been known to induce a reduction in apoplastic pH, which in turn causes cell wall softening (Jacobs et al., 1976), supporting the idea that auxin could trigger changes in the mechanical properties of tissues. Changes in tissues mechanical properties could also be mediated by pectin methyl-esterases (PMEs), which target the major cell wall component pectin, and have been shown to be necessary for cell wall loosening during organ initiation and for subsequent organ outgrowth (Peaucelle *et al.*, 2008; Peaucelle *et al.*, 2011a; Braybrook *et al.*, 2013). The expression of PME5 is controlled by the homeodomain transcription factor *BELLRINGER* (*BLR*; Peaucelle *et al.*, 2011b) mutations in which induce important defects in phyllotaxis. The phyllotactic defects of blr mutants are in part due to defects in internode elongation, thus providing another example of the importance of post-meristematic growth in phyllotaxis (next section). However, BLR also acts to exclude PME5 from the meristem proper, thus restricting the expression of PME5 and rapid growth to organs (Peaucelle *et al.*, 2011b). Conversely, inhibition of pectin methyl-esterification due to overexpression of the PME Inhibitor PMEI3 leads to the production of pin-shaped meristems, while ectopic application of PME to the meristem leads to perturbations in phyllotactic patterning (Peaucelle *et al.*, 2008). In addition, immuno-labelling experiments have confirmed that pectins are de-methyl-esterified during organ initiation (Peaucelle *et al.*, 2008). Taken together, these studies demonstrate that a dynamic regulation of cell wall composition likely plays an important role not only during postmeristematic growth but also at the meristem where it might be essential in establishing patterns of organogenesis. This view is further supported by several independent approaches

using modelling and direct measurements of the mechanical properties of the meristem that demonstrate that the CZ is stiffer than the PZ (Milani *et al.*, 2011; Kierzkowski *et al.*, 2012). These differential mechanical properties, which closely match the differential sensitivity of cells to auxin (Vernoux *et al.*, 2011), could thus restrict growth in the centre of the meristem and allow for organ outgrowth at the periphery.

It has also recently been demonstrated that microtubules align preferentially with the main direction of mechanical stress in the meristem. This observation led to the proposal that microtubules might sense mechanical stress (through an unknown mechanism) and guide anisotropic deposition of cellulose, thus counteracting the mechanical stress (Hamant *et al.*, 2008; Nakayama *et al.*, 2012). Mechanical stress could also have a direct impact on auxin distribution as PIN1 efflux transporters have been shown to localize preferentially to membranes that are oriented tangentially to the direction of growth imposed by microtubule orientation (Heisler *et al.*, 2010). A partial coupling between PIN1 localization and microtubule orientation could then create a feedback from growth-driven mechanical forces on auxin fluxes, contributing to the robustness of phyllotaxis. The extensive interplay between auxin and mechanics in the meristem is further illustrated by a recent study that demonstrated, using both biological experiments and modelling, that auxin accumulation triggers a shift from an anisotropic to an isotropic distribution of microtubules in cells at sites of organ initiation (Sassi *et al., 2014*). Together with cell wall softening mediated by cell wall modifying enzymes, this is thought to permit local changes in growth orientation allowing organ emergence in response to auxin. Taken together, these different studies support a scenario in which phyllotaxis is driven by auxin through the coordinated action of both genetic and biochemical pathways and of mechanical forces at the meristem. These factors feedback, in turn, onto auxin distribution dynamics.

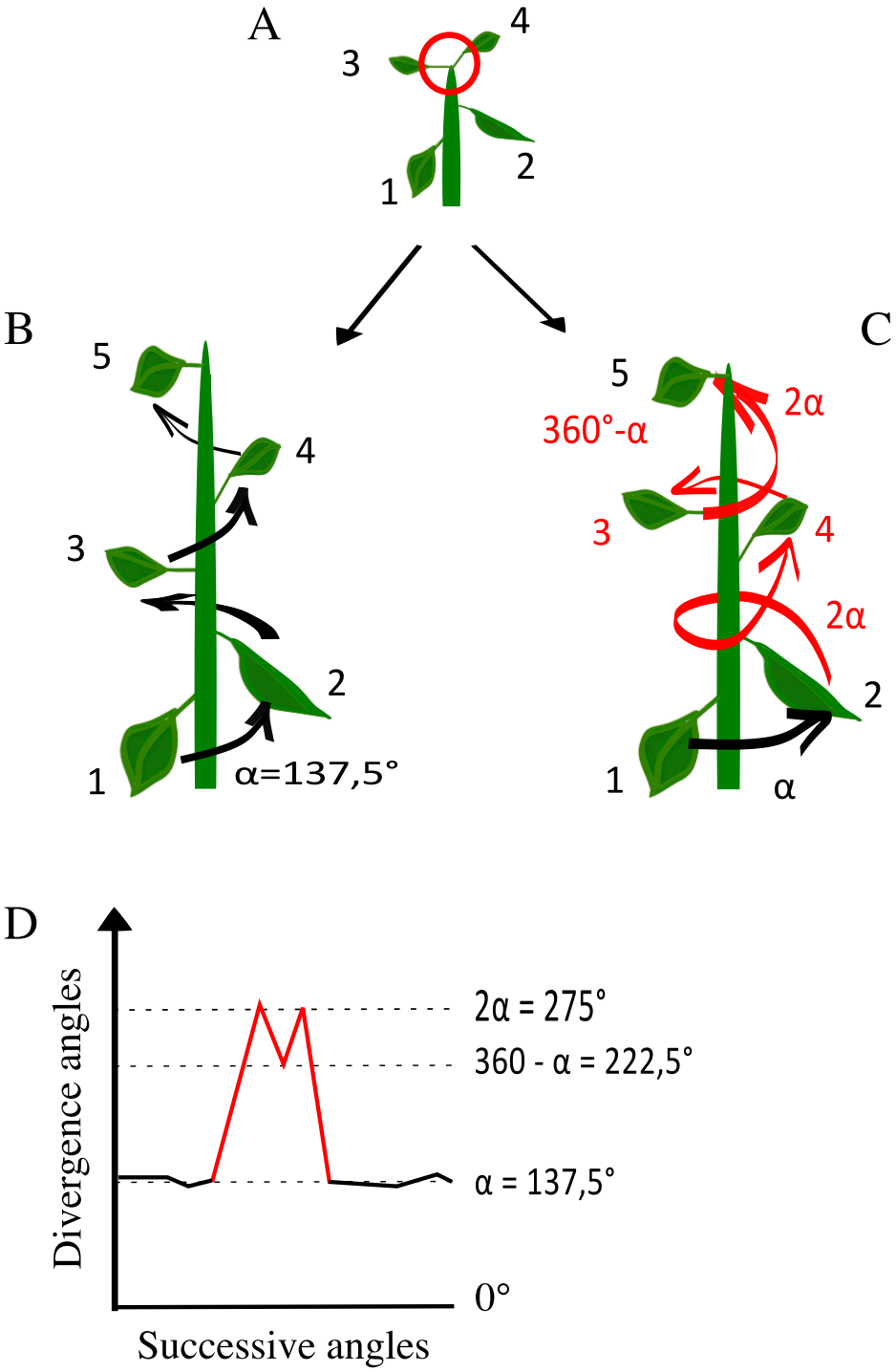

Figure 0.5: Permutations in spiral phyllotaxis. Two organs that are initiated simultaneously at the meristem (A) can lead either to a canonical sequence of divergence angles along a stem with a spiral phyllotaxis (B) or to a permutation of the order of organs along the stem (C), depending on which organ is positioned above the other after the development of the internode. D) A single permutation gives rise to a new angle sequence: 2α, 360-α, 2α (with α = 137.5°).

IV – TEMPORAL PRECISIONS ON PHYLLOTAXIS

Shoot phyllotaxis is often considered to provide a direct readout of spatiotemporal patterning at the shoot apical meristem. In addition, the inhibitory field models we have discussed have contributed to a very regular and deterministic view of phyllotaxis, with organ initiations occurring sequentially at specific spatial positions. If this simplistic view were correct, the determination of the relative angles between organs in the meristem would indeed directly explain the relative angles found between fully developed organs on the stem. However, recent work shows that the situation is more complex at least for spiral phyllotaxis.

IV.A – A TIMING - RELATED INHIBITORY FIELD

A. thaliana mutants in the gene encoding the cytokinin signalling inhibitor *ARABIDOPSIS HISTIDINE PHOSPHOTRANSFER PROTEIN 6 (AHP6)* were found to have characteristic defects in shoot phyllotaxis that motivated a careful analysis of the dynamics of organ initiation at the shoot apical meristem using live-imaging (Besnard *et al.*, 2014). This demonstrated that while relative angle specification in wild-type meristems is extremely robust, the plastochron is on the contrary variable, resulting frequently in very short or null plastochrons and thus to organ co-initiations. The frequency of organ co-initiations was significantly increased in *ahp6* mutant meristems without any detectable effects on the spatial positioning of organs, thus identifying *AHP6* as a specific regulator of the robustness of the plastochron at the meristem. AHP6 was, in addition, shown to act as a moving signal in the meristem (Besnard *et al.*, 2014a, b). *AHP6* is expressed specifically in organs early after their

initiation. The expression of *AHP6* is regulated by auxin and the AHP6 proteins moves to create inhibitory fields of cytokinin signalling. The movement of AHP6 creates a differential in AHP6 levels and in cytokinin signalling activity between the site where the new organ is being produced and that where the next organ initiation event is expected. The differential in AHP6 concentration provides positional cues that promote sequential initiation of organs, explaining the plastochron noise-filtering function of *AHP6*. As mentioned above, shoot phyllotaxis of the *ahp6* mutant clearly deviates from that of wild-type plants (when analysing the inflorescence), due to an increase in the frequency of defects that are nonetheless also observed, albeit at lower frequencies, in wild-type plants (Guedon *et al*., 2013; Besnard *et al*., 2014) Indeed, an analysis of both wild-type and *ahp6* shoot phyllotaxis demonstrated deviations from the canonical Fibonacci spiral that can be explained if the position of several consecutive organs along the stem is permuted (in comparison with the canonical distribution) without affecting the angular positioning of organs (Figure 0.5). These deviations were thus called permutations. The frequency of permutations is significantly increased in *ahp6* mutants, suggesting that co-initiations of organs at the meristem result in the permutations observed on the inflorescence shoot axis. A plausible interpretation of this phenomenon, supported by an extensive statistical analysis of shoot phyllotaxis (Guedon *et al*., 2013) and a theoretical analysis of the effect of noise on inhibitory fields models (Mirabet *et al*., 2012), is that internodes are established even when organs are co-initiated. However, the development of the internode distributes co-initiated organs along the stem randomly. This idea is supported by the fact that (1) the size of internodes is significantly smaller when organs are permuted and that, (2) the frequency of organ co-initiation events in the meristem is twice the frequency of permutations observed on the inflorescence stem (Guedon *et al*., 2013; Besnard *et al*., 2014). These studies thus identify noise on the plastochron as a genetically controlled phenomenon that, combined with postmeristematic growth (internode development), directly affects the robustness of shoot phyllotaxis by causing deviations of the relative angle between organs from the expected golden angle. Of course this work also highlights a key role for cytokinin in regulating phyllotaxis downstream of auxin.

Interestingly, the occurrence of co-initiations and permutations was also found to change in different *A. thaliana* accessions or mutants and with environmental conditions (when testing different light regimes, Landrein *et al*., 2015). This revealed a correlation

between meristem size and shoot phyllotaxis robustness. Indeed, the conditions and genotypes tested showed variations in meristem sizes indicating that lower levels of organ permutations and co-initiations might result from a decrease in meristem size (without apparent changes in organ size). These results highlight the importance of meristem geometry for phyllotaxis, but in this case, the change in geometry is not sufficient to significantly modify the phyllotactic pattern. Instead, it appears to affect the coupling between the spatial positioning of organs and the timing of their initiation. These observations also indicate that the noise in the plastochron is sensitive to environmental conditions. Finally, it has been proposed that the abnormal phyllotaxis of the *cuc2cuc3* mutant that we discuss in the next section also contributes to shoot phyllotaxis, despite being largely due to postmeristematic growth defects, could also result in part from an increase in organ permutations (Burian *et al.*, 2015). This suggests that organ co-initiation at the meristem could be buffered by complex gene networks implicating *AHP6* as well as the *CUC* genes.

IV.B – POST-MERISTEMATIC GROWTH CONTRIBUTION IN PHYLLOTAXIS

While the spatiotemporal pattern of organ initiation in the meristem is the primary level of control of shoot phyllotaxis, lateral organs produced at the meristem are then distributed along the stem axis through growth. Indeed, postmeristematic growth also makes an important contribution to phyllotaxis, and several transgenic plants and mutants illustrate this. Ectopic expression of the boundary gene *CUC* was shown to have no effect on phyllotaxis in the meristem while inducing drastic changes in shoot phyllotaxis resulting in whorls of organ on the inflorescence stem (Peaucelle *et al.*, 2007; Sieber *et al.*, 2007). The *cuc2cuc3* double mutant also has an altered shoot phyllotaxis without major defects in the meristem. In these plants, growth and cell divisions patterns are modified in the internode on the stem, suggesting that an altered internode development could be the primary explanation for the shoot phyllotaxis phenotype in the *cuc2cuc3* mutant (Burian *et al.*, 2015). Similarly,

the *bellringer* mutation leads to reduced cell expansion in internodes due to defective pectin methyl esterification (Peaucelle *et al.*, 2011) and to alterations of the shoot phyllotactic pattern, with a clear tendency to form organ clusters on the stem. Taken together, these studies identify internode specification and elongation as a key developmental step in establishing a given shoot phyllotaxis.

A striking example of the contribution of postmeristematic growth to shoot phyllotaxis was also recently provided by the analysis of the *cesa interactive protein 1 (csi1)* mutant (Landrein *et al.*, 2015). CSI1 acts in the regulation of growth by directly connecting the cortical microtubules to cellulose synthase complexes (CESA). The *csi1* mutant presents a novel bimodal shoot phyllotaxis that is not seen in nature, in which plants have either a dominant phyllotactic angle of 90° or of 180° on the inflorescence stem. While phyllotaxis at the meristem is unchanged in the mutant, the mutation results in a slight torsion of the inflorescence stem. The authors demonstrated using a simple mathematical model that this torsion, combined with the fact that the ratio of internode length over stem diameter is rather invariant along the inflorescence axis, leads to one or the other dominant angles depending on whether the spiral at the meristem is left- or right-handed (which happens in equal proportions). The *csi1* phyllotaxis phenotype thus demonstrates that postmeristematic growth can produce completely novel shoot phyllotaxis patterns, further highlighting the importance of postmeristematic growth regulation in shoot phyllotaxis.

Likewise, the sepals of *A. thaliana* flowers were shown to be formed separately, with the abaxial side growing first. However their whorled final arrangement was engendered by differential growth of the four sepals (see section I.C).

Altogether these phenomenons highlight the importance of postmeristematic growth in setting the final architecture, sometimes differently than the primary meristematic pattern. Moreover, mathematical and physical models predict that the dynamics of the phyllotaxis is controlled by the receding of organs away from the centre, i.e. growth, and the rhythm of organogenesis, i.e. plastochron. It is then not surprising that the relation between the two is determinant for the arrangement of lateral organs around the shoot.

V – CONCLUSIONS AND RATIONALE OF THE THESIS

While our understanding of phyllotaxis still remains partial, notably due to the fact that few phyllotactic mutants have been thoroughly characterized, recent years have seen tremendous advances that have identified the plant hormone auxin as the major regulator of phyllotaxis. A role for mechanical feedbacks in phyllotaxis is also emerging, providing an interesting model system to analyse how chemical and mechanical signal cooperate to control morphogenesis. Modelling has been crucial in these advances and provides a rich toolbox for understanding how the mechanisms identified could explain the self-organizing properties of this unique developmental system. The emergence of powerful live-imaging approaches has also been instrumental in the analysis of the dynamic properties of the phyllotactic system, revealing the importance of the timing of organ initiation in controlling shoot phyllotaxis. The development of an auxin biosensor has also allowed the visualization of the auxin-based inhibitory fields, and opened the possibility of further analysing how these fields are formed. Modelling has also suggested that temporal variations in the strength of the fields might be important for the stability of phyllotaxis (Smith *et al.*, 2006a, b). Combining such quantitative approaches with molecular genetics by identifying new players for meristem patterning may provide key experimental data that, coupled with further refinement of the existing models, should push forward our understanding of phyllotaxis. Finally, it will also be important to question whether current knowledge of mechanisms regulating spiral phyllotaxis is fully relevant to all types of phyllotaxis including whorled and multijugate modes, or whether other mechanisms are involved.

In my thesis, we relied on a T-DNA mutant collection to select plants with impaired phyllotaxis. I chose a mutant among a pre-selected panel of insertion mutants showing phyllotactic irregularities, in a forward genetic approach. This mutant showed clustered arrangement of lateral organs that were reminiscent of whorled patterns observed in unrelated

species. I proceeded through phenotypic analysis and sequenced its genome to select candidate genes. I used genetic markers to investigate the mutant meristem's behaviour, in order to: 1) understand how the mutant's particular phyllotaxis was set up, and 2) try and understand the molecular cause of such a divergence from the canonical spiral.

REFERENCE LIST

Adler, I., D. Barabe, and R. V. Jean. 1997. "A History of the Study of Phyllotaxis." *Annals of Botany* 80(3): 231–44. http://aob.oxfordjournals.org/content/80/3/231\nhttp://aob.oxfordjournals.org/content/80/3/231.full.pdf.

Aida, Mitsuhiro et al. 1997. "Genes Lnvolved in Organ Separation in Arabidopsis: . An Analysis of the Cup-Shaped Cotyledon Mutant." *The Plant Cell American Society of Plant Physiologists* 9(June): 841–57.

Alvarez-Buylla Elena, R et al. 2010. "Flower Development." *The Arabidopsis Book* 8(1): 1–57. http://dx.doi.org/10.1199/tab.0127.

Andrés, Fernando, and George Coupland. 2012. "The Genetic Basis of Flowering Responses to Seasonal Cues." *Nature reviews. Genetics* 13(9): 627–39. http://www.nature.com/doifinder/10.1038/nrg3291\nhttp://www.ncbi.nlm.nih.gov/pubmed/22898651\nhttp://dx.doi.org/10.1038/nrg3291\nhttp://dx.doi.org/10.1038/nrg3291

Bainbridge, Katherine et al. 2008. "Auxin Influx Carriers Stabilize Phyllotactic Patterning." *Genes and Development* 22(6): 810–23.

Bakõrcõ, S. et al. 2016. "A Comparison of Anatomical Measurements of the Infraorbital Foramen of Skulls of the Modern and Late Byzantine Periods and the Golden Ratio." *International Journal of Morphology* 34(2).

Bartlett, Madelaine E, and Beth Thompson. 2014. "Meristem Identity and Phyllotaxis in Inflorescence Development." *Frontiers in plant science* 5(October): 1–11.

Barton, M K. 2010. "Twenty Years on: The Inner Workings of the Shoot Apical Meristem, a Developmental Dynamo." *Developmental biology* 341(1): 95–113. http://www.ncbi.nlm.nih.gov/pubmed/19961843 (December 12, 2013).

Bayer, Emmanuelle M. et al. 2009. "Integration of Transport-Based Models for Phyllotaxis and Midvein Formation." *Genes and Development* 23(3): 373–84.

Berger, Yael et al. 2009. “The NAC-Domain Transcription Factor GOBLET Specifies Leaflet Boundaries in Compound Tomato Leaves.” *Development (Cambridge, England)* 136(5): 823–32.

Van Berkel, Klaartje, Rob J de Boer, Ben Scheres, and Kirsten ten Tusscher. 2013. “Polar Auxin Transport: Models and Mechanisms.” *Development (Cambridge, England)* 140(11): 2253–68. http://dev.biologists.org/content/140/11/2253.long.

Besnard, Fabrice, Frédérique Rozier, and Teva Vernoux. 2014. “The AHP6 Cytokinin Signaling Inhibitor Mediates an Auxin-Cytokinin Crosstalk That Regulates the Timing of Organ Initiation at the Shoot Apical Meristem.” *Plant Signaling & Behavior*: 4–7.

Besnard, Y Refahi, V Morin, B Marteaux, G Brunoud, P Chambrier, F Rozier1, V Mirabet, J Legrand, S Laine, E Thevenon, Et Farcot, C Cellier, P Das, A Bishopp, R Dumas, F Parcy, Y Helariutta, A Boudaoud, Y Guedon & C Godin, J Traas, and T Vernoux. 2014. “Cytokinin Signalling Inhibitory Fields Provide Robustness to Phyllotaxis ´.” *Nature*: 2–9.

Bleckmann, a., S. Weidtkamp-Peters, C. a.M. Seidel, and R. Simon. 2010. “Stem Cell Signaling in Arabidopsis Requires CRN to Localize CLV2 to the Plasma Membrane.” *Plant Physiology* 152(1): 166–76. http://www.plantphysiol.org/cgi/doi/10.1104/pp.109.149930.

Blein, T et al. 2008. “A Conserved Molecular Framework for Compound Leaf Development .” *Science* 322(December): 1835–39.

Bonaccorso, Oliver et al. 2012. “FILAMENTOUS FLOWER Controls Lateral Organ Development by Acting as Both an Activator and a Repressor.” *BMC Plant Biology* 12(1): 176. BMC Plant Biology.

Borghi, Lorenzo, Marina Bureau, and Rüdiger Simon. 2007. “*Arabidopsis JAGGED LATERAL ORGANS* Is Expressed in Boundaries and Coordinates *KNOX* and *PIN* Activity.” *The Plant Cell* 19(6): 1795–1808. http://www.plantcell.org/lookup/doi/10.1105/tpc.106.047159.

Bowman, John L., Yuval Eshed, and Stuart F. Baum. 2002. “Establishment of Polarity in Angiosperm Lateral Organs.” *Trends in Genetics* 18(3): 134–41.

Brand, U et al. 2000. “Dependence of Stem Cell Fate in Arabidopsis on a Feedback Loop Regulated by CLV3 Activity.” *Science (New York, N.Y.)* 289(5479): 617–19.

Brandt, Ronny et al. 2012. "Genome-Wide Binding-Site Analysis of REVOLUTA Reveals a Link between Leaf Patterning and Light-Mediated Growth Responses." *Plant Journal* 72(1): 31–42.

Braybrook, Siobhan a., and Alexis Peaucelle. 2013. "Mechano-Chemical Aspects of Organ Formation in Arabidopsis Thaliana: The Relationship between Auxin and Pectin." *PLoS ONE* 8(3).

Breuil-Broyer, Stephanie et al. 2004. "High-Resolution Boundary Analysis during Arabidopsis Thaliana Flower Development." *Plant Journal* 38(1): 182–92.

Brunoud, Géraldine et al. 2012. "A Novel Sensor to Map Auxin Response and Distribution at High Spatio-Temporal Resolution." *Nature* 482(7383): 103–6. http://www.nature.com/doifinder/10.1038/nature10791.

Bureau, Marina, Madlen I. Rast, Jasmin Illmer, and Rüdiger Simon. 2010. "JAGGED LATERAL ORGAN (JLO) Controls Auxin Dependent Patterning during Development of the Arabidopsis Embryo and Root." *Plant Molecular Biology* 74(4): 479–91.

Burian, a. et al. 2015. "The CUP-SHAPED COTYLEDON2 and 3 Genes Have a Post-Meristematic Effect on Arabidopsis Thaliana Phyllotaxis." *Annals of Botany*: 807–20. http://aob.oxfordjournals.org/cgi/doi/10.1093/aob/mcv013.

Busch, B. L. et al. 2011. "Shoot Branching and Leaf Dissection in Tomato Are Regulated by Homologous Gene Modules." *The Plant Cell* 23(10): 3595–3609.

Byrne, M E et al. 2000. "Asymmetric leaves1 Mediates Leaf Patterning and Stem Cell Function in Arabidopsis." *Nature* 408(6815): 967–71.

Capua, Yossi, and Yuval Eshed. 2017. "Coordination of Auxin-Triggered Leaf Initiation by Tomato *LEAFLESS*." *Proceedings of the National Academy of Sciences*: 201617146. http://www.pnas.org/lookup/doi/10.1073/pnas.1617146114.

Chandler, J. W., and W. Werr. 2014. "Arabidopsis Floral Phytomer Development: Auxin Response Relative to Biphasic Modes of Organ Initiation." *Journal of Experimental Botany* 65(12): 3097–3110.

Chandler, John William et al. 2011. "DORNRÖSCHEN-LIKE Expression Marks Arabidopsis Floral Organ Founder Cells and Precedes Auxin Response Maxima." *Plant Molecular Biology* 76(1-2): 171–85.

Cheng, Youfa, Xinhua Dai, and Yunde Zhao. 2007. "Auxin Synthesized by the YUCCA Flavin Monooxygenases Is Essential for Embryogenesis and Leaf Formation in Arabidopsis." *The Plant cell* 19(8): 2430–39. http://www.pubmedcentral.nih.gov/articlerender.fcgi?artid=2002601&tool=pmcentrez&rendertype=abstract.

Chickarmane, Vijay S et al. 2012. "Cytokinin Signaling as a Positional Cue for Patterning the Apical-Basal Axis of the Growing Arabidopsis Shoot Meristem." *Proceedings of the National Academy of Sciences of the United States of America* 109(10): 4002–7. http://www.pnas.org/content/109/10/4002.full.

Clark, Se, Mp Running, and Em Meyerowitz. 1995. "*CLAVATA3* Is a Specific Regulator of Shoot and Floral Meristem Development Affecting the Same Processes as *CLAVATA1*." *Development* 121: 2057–67. http://dev.biologists.org/content/121/7/2057.short.

Clymo, Rs. 1984. "The Royal Society Is Collaborating with JSTOR to Digitize, Preserve, and Extend Access to Philosophical Transactions of the Royal Society of London. Series B, Biological Sciences. ® Www.jstor.org." *Philosophical Transactions of the Royal Society of London* 303: 605–54.

Dharmasiri, Nihal, Sunethra Dharmasiri, and Mark Estelle. 2005. "The F-Box Protein TIR1 Is an Auxin Receptor." *Nature* 435(7041): 441–45. http://www.ncbi.nlm.nih.gov/pubmed/15917797.

Douady, S. 1996a. "Phyllotaxis as a Dynamical Self Organizing Process Part I: The Spiral Modes Resulting from Time-Periodic Iterations." *Journal of Theoretical Biology* 178: 275–94. http://linkinghub.elsevier.com/retrieve/pii/S0022519396900259.

———. 1996b. "Phyllotaxis as a Dynamical Self Organizing Process Part II: The Spontaneous Formation of a Periodicity and the Coexistence of Spiral and Whorled Patterns." *Journal of Theoretical Biology* 178(3): 275–94. http://linkinghub.elsevier.com/retrieve/pii/S0022519396900259.

Emery, John F. et al. 2003. "Radial Patterning of Arabidopsis Shoots by Class III HD-ZIP and KANADI Genes." *Current Biology* 13(20): 1768–74.

Endrizzi, Karin et al. 1996. "The SHOOT MERISTEMLESS Gene Is Required for Maintenance of Undifferentiated Cells in Arabidopsis Shoot and Floral Meristems and Acts at a Different Regulatory Level than the Meristem Genes WUSCHEL and

ZWILLE." *The Plant Journal* 10(6): 967–79. http://doi.wiley.com/10.1046/j.1365-313X.1996.10060967.x.

Engstrom, E. M. et al. 2011. "Arabidopsis Homologs of the Petunia HAIRY MERISTEM Gene Are Required for Maintenance of Shoot and Root Indeterminacy." *Plant Physiology* 155(2): 735–50. http://www.plantphysiol.org/cgi/doi/10.1104/pp.110.168757.

Fletcher, J. C. et al. 1999. "Signaling of Cell Fate Decisions by \emph{CLAVATA3} in \emph{Arabidopsis} Shoot Meristems." *Science* 19(5409): 1911–14. http://www.sciencemag.org/cgi/doi/10.1126/science.283.5409.1911.

Friml, Jiří. 2010. "Subcellular Trafficking of PIN Auxin Efflux Carriers in Auxin Transport." *European Journal of Cell Biology* 89(2-3): 231–35. http://linkinghub.elsevier.com/retrieve/pii/S017193350900332X.

Galvan-Ampudia, C. S., Chaumeret, A. M., Godin, C. and Vernoux, T. (2016), Phyllotaxis: from patterns of organogenesis at the meristem to shoot architecture. WIREs Dev Biol, 5: 460–473. doi:10.1002/wdev.231

Gälweiler, L. et al. 1998. "Regulation of Polar Auxin Transport by AtPIN1 in Arabidopsis Vascular Tissue." *Science* 282(5397): 2226–30. <Go to ISI>://WOS:000077645800037\nhttp://apps.webofknowledge.com.proxy-remote.galib.uga.edu/full_record.do?product=UA&search_mode=GeneralSearch&qid=12&SID=4FE4hO2CCZpSMvOLXvR&page=1&doc=1.

Gendron, Joshua M et al. 2012. "Brassinosteroids Regulate Organ Boundary Formation in the Shoot Apical Meristem of Arabidopsis." *Proceedings of the National Academy of Sciences of the United States of America* 109(51): 21152–57. http://www.pubmedcentral.nih.gov/articlerender.fcgi?artid=3529081&tool=pmcentrez&rendertype=abstract.

Giulini, Anna, Jing Wang, and David Jackson. 2004. "Control of Phyllotaxy by the Cytokinin-Inducible Response Regulator Homologue ABPHYL1." *Nature* 430: 1031–34.

Goldshmidt, Alexander, John Paul Alvarez, John L Bowman, and Yuval Eshed. 2008. "Signals Derived from YABBY Gene Activities in Organ Primordia Regulate Growth and Partitioning of Arabidopsis Shoot Apical Meristems." *The Plant cell* 20(5): 1217–30.

http://www.pubmedcentral.nih.gov/articlerender.fcgi?artid=2438466&tool=pmcentrez&rendertype=abstract (December 19, 2013).

Golz, John F, Mario Roccaro, Robert Kuzoff, and Andrew Hudson. 2004. "GRAMINIFOLIA Promotes Growth and Polarity of Antirrhinum Leaves." *Development (Cambridge, England)* 131(15): 3661–70.

Gordon, Sean P, Vijay S Chickarmane, Carolyn Ohno, and Elliot M Meyerowitz. 2009. "Multiple Feedback Loops through Cytokinin Signaling Control Stem Cell Number within the Arabidopsis Shoot Meristem." *Proceedings of the National Academy of Sciences of the United States of America* 106(16): 16529–34.

Green, Kirsten a, Michael J Prigge, Rebecca B Katzman, and Steven E Clark. 2005. "CORONA, a Member of the Class III Homeodomain Leucine Zipper Gene Family in Arabidopsis, Regulates Stem Cell Specification and Organogenesis." *The Plant cell* 17(3): 691–704. papers3://publication/doi/10.1105/tpc.104.026179.

Green, Paul B. 1999. "Expression of Pattern in Plants: Combining Molecular and Calculus-Based Biophysical Paradigms." *American Journal of Botany* 86(8): 1059–76.

Guédon, Yann et al. 2013. "Pattern Identification and Characterization Reveal Permutations of Organs as a Key Genetically Controlled Property of Post-Meristematic Phyllotaxis." *Journal of Theoretical Biology* 338: 94–110. http://dx.doi.org/10.1016/j.jtbi.2013.07.026.

Guilfoyle, Tom J., and Gretchen Hagen. 2007. "Auxin Response Factors." *Current Opinion in Plant Biology* 10(5): 453–60.

Ha, Chan Man et al. 2003. "The BLADE-ON-PETIOLE 1 Gene Controls Leaf Pattern Formation through the Modulation of Meristematic Activity in Arabidopsis." *Development (Cambridge, England)* 130(1): 161–72.

Ha, Chan Man, Ji Hyung Jun, Hong Gil Nam, and Jennifer C Fletcher. 2004. "BLADE-ON-PETIOLE1 Encodes a BTB/POZ Domain Protein Required for Leaf Morphogenesis in Arabidopsis Thaliana." *Plant & cell physiology* 45(10): 1361–70.

———. 2007. "BLADE-ON-PETIOLE 1 and 2 Control Arabidopsis Lateral Organ Fate through Regulation of LOB Domain and Adaxial-Abaxial Polarity Genes." *The Plant cell* 19(6): 1809–25. http://www.pubmedcentral.nih.gov/articlerender.fcgi?artid=1955725&tool=pmcentrez&rendertype=abstract.

Hamant, O. et al. 2008. “Developmental Patterning by Mechanical Signals in Arabidopsis.” *Science* 322(5908): 1650–55. http://www.sciencemag.org/cgi/doi/10.1126/science.1165594.

Heidstra, Renze, and Sabrina Sabatini. 2014. “Plant and Animal Stem Cells: Similar yet Different.” *Nature reviews. Molecular cell biology* 15(5): 301–12. http://www.ncbi.nlm.nih.gov/pubmed/24755933.

Heisler, Marcus G. et al. 2005. “Patterns of Auxin Transport and Gene Expression during Primordium Development Revealed by Live Imaging of the Arabidopsis Inflorescence Meristem.” *Current Biology* 15: 1899–1911.

Hendelman, Anat et al. 2016. “Tomato HAIRY MERISTEM Genes Are Involved in Meristem Maintenance and Compound Leaf Morphogenesis.” *Journal of Experimental Botany* 67(21): 6187–6200.

Hepworth, Shelley R et al. 2005. “BLADE-ON-PETIOLE-Dependent Signaling Controls Leaf and Floral Patterning in Arabidopsis.” *The Plant cell* 17(5): 1434–48. http://www.plantcell.org/cgi/doi/10.1105/tpc.104.030536\nhttp://www.ncbi.nlm.nih.gov/pubmed/15805484\nhttp://www.pubmedcentral.nih.gov/articlerender.fcgi?artid=PMC1091766.

Hofmeister Allgemeine HW, der Gewächse M. Handbuch Der Physiologischen Botanik I-2. Leipzig: W. Engelmann; 1868

Huang, Tengbo et al. 2014. “Arabidopsis KANADI1 Acts as a Transcriptional Repressor by Interacting with a Specific Cis-Element and Regulates Auxin Biosynthesis, Transport, and Signaling in Opposition to HD-ZIPIII Factors.” *The Plant cell* 26(1): 246–62. http://www.ncbi.nlm.nih.gov/pubmed/24464295.

Husbands, Aman Y. et al. 2015. “The ASYMMETRIC LEAVES Complex Employs Multiple Modes of Regulation to Affect Adaxial-Abaxial Patterning and Leaf Complexity.” *The Plant Cell* 7(December): tpc.15.00454. http://www.plantcell.org/lookup/doi/10.1105/tpc.15.00454.

Hussey, G. 1970. “Vitro Growth of Vegetative Tomato Shoot Apices.” *Journal of Experimental Botany* 22(72).

Itoh, Jun Ichi et al. 2012. “Rice DECUSSATE Controls Phyllotaxy by Affecting the Cytokinin Signaling Pathway.” *Plant Journal* 72: 869–81.

Iwakawa, Hidekazu et al. 2002. “The ASYMMETRIC LEAVES2 Gene of Arabidopsis Thaliana, Required for Formation of a Symmetric Flat Leaf Lamina, Encodes a Member of a Novel Family of Proteins Characterized by Cysteine Repeats and a Leucine Zipper.” *Plant & cell physiology* 43(5): 467–78.

Iwasaki, Mayumi et al. 2013. “Dual Regulation of ETTIN (ARF3) Gene Expression by AS1-AS2, Which Maintains the DNA Methylation Level, Is Involved in Stabilization of Leaf Adaxial-Abaxial Partitioning in Arabidopsis.” *Development* 140(9): 1958–69. http://dev.biologists.org/content/develop/140/9/1958.

Jacobs, M, and P M Ray. 1976. “Rapid Auxin-Induced Decrease in Free Space pH and Its Relationship to Auxin-Induced Growth in Maize and Pea.” *Plant physiology* 58: 203–9.

Jasinski, Sophie et al. 2005. “KNOX Action in Arabidopsis Is Mediated by Coordinate Regulation of Cytokinin and Gibberellin Activities.” *Current Biology* 15(17): 1560–65.

Je, Byoung Il and Gruel, Jeremy and Lee, Young Koung and Bommert, Peter and Arevalo, Edgar Demesa and Eveland, Andrea L and Wu, Qingyu and Goldshmidt, Alexander and Meeley, Robert and Bartlett, Madelaine and Others. 2016. “Signaling from Maize Organ Primordial via FASCIATED EAR3 Regulates Stem Cell Proliferation and Yield Traits.” *Nature Genetics* 48(7): 785–91. http://dx.doi.org/10.1038/ng.3567.

Jönsson, Henrik et al. 2006. “An Auxin-Driven Polarized Transport Model for Phyllotaxis.” *Proceedings of the National Academy of Sciences of the United States of America* 103(5): 1633–38.

———. 2010. “Alignment between PIN1 Polarity and Microtubule Orientation in the Shoot Apical Meristem Reveals a Tight Coupling between Morphogenesis and Auxin Transport.” *PLoS Biology* 8(10).

Jung, Jae-hoon Park, Chung-mo. 2007. “MIR166 / 165 Genes Exhibit Dynamic Expression Patterns in Regulating Shoot Apical Meristem and Floral Development in Arabidopsis.” *Planta*: 1327–38.

Kanaya, Eiko et al. 2001. “Zinc Release from the CH2C6 Zinc Finger Domain of FILAMENTOUS FLOWER Protein from Arabidopsis Thaliana Induces Self-Assembly.” *Journal of Biological Chemistry* 276(10): 7383–90.

Kepinski, S, and O. Leyser. 2005. “The F-Box Protein TIR1 Is an Auxin Receptor.” *Nature* 435(7041): 441–45. http://www.ncbi.nlm.nih.gov/pubmed/15917797.

Kerstetter, R a et al. 2001. “KANADI Regulates Organ Polarity in Arabidopsis.” *Nature* 411(June): 706–9.

Kierzkowski, Daniel et al. 2012. “Elastic Domains Regulate Growth and Organogenesis in the Plant Shoot Apical Meristem.” *Science* 335(6072): 1096–99. http://www.ncbi.nlm.nih.gov/pubmed/22383847.

Kim, Joonki et al. 2005. “microRNA-Directed Cleavage of ATHB15 mRNA Regulates Vascular Development in Arabidopsis Inflorescence Stems.” *Plant Journal* 42(1): 84–94.

Kim, Y.-S. et al. 2008. “HD-ZIP III Activity Is Modulated by Competitive Inhibitors via a Feedback Loop in Arabidopsis Shoot Apical Meristem Development.” *the Plant Cell Online* 20(4): 920–33. http://www.plantcell.org/cgi/doi/10.1105/tpc.107.057448.

Kirch, Thomas, and Wolfgang Werr. 2003. “The DORNRÖSCHEN/ENHANCER OF SHOOT REGENERATION1 Gene of Arabidopsis Acts in the Control of Meristem Cell Fate and Lateral Organ Development.” *Society* 15(March): 694–705.

Kitazawa, Miho S., and Koichi Fujimoto. 2015. “A Dynamical Phyllotaxis Model to Determine Floral Organ Number.” *PLOS Computational Biology* 11: e1004145. http://dx.plos.org/10.1371/journal.pcbi.1004145.

Kumaran, Mande K, John L Bowman, and Venkatesan Sundaresan. 2002. “YABBY Polarity Genes Mediate the Repression of KNOX Homeobox Genes in Arabidopsis.” *The Plant cell* 14(11): 2761–70.

Kwiatkowska, Dorota. 1995. “Changes of Phyllotaxis in Anagallis Arvensis L.” *Acta Societatis Botanicorum Poloniae* 64(4): 319–25.

———. 2006. “Flower Primordium Formation at the Arabidopsis Shoot Apex: Quantitative Analysis of Surface Geometry and Growth.” *Journal of Experimental Botany* 57(3): 571–80.

Landrein, Benoit et al. 2015. “Meristem Size Contributes to the Robustness of Phyllotaxis in Arabidopsis.” *Journal of Experimental Botany* 66(5): 1317–24.

Landrein, Benoît et al. 2013. “Impaired Cellulose Synthase Guidance Leads to Stem Torsion and Twists Phyllotactic Patterns in Arabidopsis.” *Current Biology* 23(10): 895–900.

Laux, T, K F Mayer, J Berger, and G Jürgens. 1996. "The WUSCHEL Gene Is Required for Shoot and Floral Meristem Integrity in Arabidopsis." *Development* 122: 87–96.

Lee, Byeong-ha et al. 2009. "Studies of Aberrant phyllotaxy1 Mutants of Maize Indicate Complex Interactions between Auxin and Cytokinin Signaling in the Shoot Apical Meristem." *Plant physiology* 150(1): 205–16. http://www.ncbi.nlm.nih.gov/pubmed/19321707\nhttp://www.pubmedcentral.nih.gov/articlerender.fcgi?artid=PMC2675719.

Lenhard, Michael, Andrea Bohnert, Gerd J??rgens, and Thomas Laux. 2001. "Termination of Stem Cell Maintenance in Arabidopsis Floral Meristems by Interactions between Wuschel and Agamous." *Cell* 105(6): 805–14.

Lodha, Mukesh, Cristina F. Marco, and Marja C P Timmermans. 2013. "The ASYMMETRIC LEAVES Complex Maintains Repression of KNOX Homeobox Genes via Direct Recruitment of Polycomb-Repressive complex2." *Genes and Development* 27(6): 596–601.

Lohmann, Jan U. et al. 2001. "A Molecular Link between Stem Cell Regulation and Floral Patterning in Arabidopsis." *Cell* 105(6): 793–803.

Long, J, and M K Barton. 2000. "Initiation of Axillary and Floral Meristems in Arabidopsis." *Developmental biology* 218(2): 341–53.

Long, Jeff a, E. I. Moan, J. I. Medford, and M. Kathryn Barton. 1996. "A Member of the KNOTTED Class of Homeodomain Proteins Encoded by the STM Gene of Arabidopsis." *Nature*.

Lugassi, Nitsan, Naomi Nakayama, Rachel Bochnik, and Moriyah Zik. 2010. "A Novel Allele of FILAMENTOUS FLOWER Reveals New Insights on the Link between Inflorescence and Floral Meristem Organization and Flower Morphogenesis." *BMC plant biology* 10: 131. http://www.pubmedcentral.nih.gov/articlerender.fcgi?artid=3017777&tool=pmcentrez&rendertype=abstract.

Magnani, Enrico, and M. Kathryn Barton. 2011. "A Per-ARNT-Sim-Like Sensor Domain Uniquely Regulates the Activity of the Homeodomain Leucine Zipper Transcription Factor REVOLUTA in *Arabidopsis*." *The Plant Cell* 23(2): 567–82. http://www.plantcell.org/lookup/doi/10.1105/tpc.110.080754.

Mallory, Allison C et al. 2004. "MicroRNA Control of PHABULOSA in Leaf Development: Importance of Pairing to the microRNA 5′ Region." *The EMBO Journal* 23(16): 3356–64. http://emboj.embopress.org/cgi/doi/10.1038/sj.emboj.7600340.

Mandel, Tali et al. 2016. "Differential Regulation of Meristem Size, Morphology and Organization by the ERECTA, CLAVATA and Class III HD-ZIP Pathways." *Development* 143(9): 259–64. http://www.ncbi.nlm.nih.gov/pubmed/26989178.

Matsumura, Yoko et al. 2016. "A Genetic Link between Epigenetic Repressor AS1-AS2 and a Putative Small Subunit Processome in Leaf Polarity Establishment of *Arabidopsis*." *Biology Open* 5(7): 942–54. http://bio.biologists.org/lookup/doi/10.1242/bio.019109.

Matsumura, Yoko, Hidekazu Iwakawa, Yasunori MacHida, and Chiyoko MacHida. 2009. "Characterization of Genes in the ASYMMETRIC LEAVES2-LATERAL ORGAN BOUNDARIES (AS2-LOB) Family in Arabidopsis Thaliana, and Functional and Molecular Comparisons between AS2 and Other Family Members." *Plant Journal* 58(3): 525–37.

Mcconnell, Jane R et al. 2001. "Role of PHABULOSA and PHAVOLUTA in Determining Radial Patterning in Shoots." *Nature* 411(June): 709–13.

Merelo, Paz et al. 2013. "Genome-Wide Identification of KANADI1 Target Genes." *PLoS ONE* 8(10): 1–14.

———. 2016. "Regulation of MIR165 / 166 by Class II and Class III Homeodomain Leucine Zipper Proteins Establishes Leaf Polarity." *Proceedings of the National Academy of Sciences* 166: 3–8.

Merelo, Paz, Esther Botterweg Paredes, Marcus G Heisler, and Stephan Wenkel. 2017. "The Shady Side of Leaf Development: The Role of the REVOLUTA/KANADI1 Module in Leaf Patterning and Auxin-Mediated Growth Promotion." *Current Opinion in Plant Biology* 35: 111–16. http://linkinghub.elsevier.com/retrieve/pii/S1369526616302114.

Milani, Pascale et al. 2011. "In Vivo Analysis of Local Wall Stiffness at the Shoot Apical Meristem in Arabidopsis Using Atomic Force Microscopy." *Plant Journal* 67: 1116–23.

Mirabet, Vincent, Fabrice Besnard, Teva Vernoux, and Arezki Boudaoud. 2012. "Noise and Robustness in Phyllotaxis." *PLoS computational biology* 8(2).

Mitchison, G. J., D. E. Hanke, and a. R. Sheldrake. 1981. "The Polar Transport of Auxin and Vein Patterns in Plants [and Discussion]." *Philosophical Transactions of the Royal*

Society B: Biological Sciences 295(1078): 461–71. http://rspb.royalsocietypublishing.org/cgi/doi/10.1098/rspb.1980.0015\nhttp://rstb.royalsocietypublishing.org/cgi/doi/10.1098/rstb.1981.0154.

Mizukami, Y, and R L Fischer. 2000. "Plant Organ Size Control: AINTEGUMENTA Regulates Growth and Cell Numbers during Organogenesis." *Proceedings of the National Academy of Sciences of the United States of America* 97(2): 942–47.

Mokry, M. 2008. "Encounters with the Golden Ratio in Fluid Dynamics." *Design and Nature IV* I(1): 119–28. http://library.witpress.com/viewpaper.asp?pcode=DN08-013-1.

Nakayama, Naomi et al. 2012. "Mechanical Regulation of Auxin-Mediated Growth." *Current Biology* 22: 1468–76.

Negin, Boaz, Or Shemer, Yonatan Sorek, and Leor Eshed Williams. 2017. "Shoot Stem Cell Specification in Roots by the WUSCHEL Transcription Factor." *Plos One* 12(4): e0176093. http://dx.plos.org/10.1371/journal.pone.0176093.

Newell, Alan C, Patrick D Shipman, and Zhiying Sun. 2008. "Phyllotaxis as an Example of the Symbiosis of Mechanical Forces and Biochemical Processes in Living Tissue." *Plant signaling & behavior* 3(May 2015): 586–89.

Nimchuk, Zachary L. 2017. "CLAVATA1 Controls Distinct Signaling Outputs That Buffer Shoot Stem Cell Proliferation through a Two-Step Transcriptional Compensation Loop." *PLoS Genetics* 13(3).

Norberg, Mikael, Mattias Holmlund, and Ove Nilsson. 2005. "The BLADE ON PETIOLE Genes Act Redundantly to Control the Growth and Development of Lateral Organs." *Development (Cambridge, England)* 132(9): 2203–13. http://www.ncbi.nlm.nih.gov/pubmed/15800002.

O'Connor, Devin L. et al. 2014. "A Division in PIN-Mediated Auxin Patterning during Organ Initiation in Grasses." *PLoS Computational Biology* 10(1): 21–24.

Okada, K et al. 1991. "Requirement of the Auxin Polar Transport System in Early Stages of Arabidopsis Floral Bud Formation." *The Plant cell* 3(July): 677–84.

Parcy, Francis et al. 1998. "A Genetic Framework for Floral Patterning." *Nature* 395(6702): 561–66.

Pautler, Michael et al. 2015. "FASCIATED EAR4 Encodes a bZIP Transcription Factor That Regulates Shoot Meristem Size in Maize." *The Plant Cell Online* 2(January): tpc.114.132506. http://www.plantcell.org/lookup/doi/10.1105/tpc.114.132506.

Peaucelle, Alexis et al. 2008. “Arabidopsis Phyllotaxis Is Controlled by the Methyl-Esterification Status of Cell-Wall Pectins.” *Current Biology* 18: 1943–48.

Peaucelle, Alexis, Siobhan a. Braybrook, et al. 2011. “Pectin-Induced Changes in Cell Wall Mechanics Underlie Organ Initiation in Arabidopsis.” *Current Biology* 21: 1720–26.

Peaucelle, Alexis, Romain Louvet, et al. 2011. “The Transcription Factor BELLRINGER Modulates Phyllotaxis by Regulating the Expression of a Pectin Methylesterase in Arabidopsis.” *Development* 4741: 4733–41.

Peaucelle, Alexis, and Patrick Laufs. 2007. “Phyllotaxy: Beyond the Meristem and Auxin Comes the miRNA.” *Plant signaling & behavior* 2(May 2015): 293–95.

Pekker, I. 2005. “Auxin Response Factors Mediate Arabidopsis Organ Asymmetry via Modulation of KANADI Activity.” *the Plant Cell Online* 17(11): 2899–2910. http://www.plantcell.org/cgi/doi/10.1105/tpc.105.034876.

Pinon, Violaine et al. 2013. “Local Auxin Biosynthesis Regulation by PLETHORA Transcription Factors Controls Phyllotaxis in Arabidopsis.” *Proceedings of the National Academy of Sciences of the United States of America* 110(24): 1107–12. http://www.pubmedcentral.nih.gov/articlerender.fcgi?artid=3549086&tool=pmcentrez&rendertype=abstract.

Prigge, Michael J et al. 2005. “Class III Homeodomain-Leucine Zipper Gene Family Members Have Overlapping, Antagonistic, and Distinct Roles in Arabidopsis Development.” *The Plant cell* 17(1): 61–76. http://www.pubmedcentral.nih.gov/articlerender.fcgi?artid=544490&tool=pmcentrez&rendertype=abstract.

Qi, Jiyan et al. 2014. “Auxin Depletion from Leaf Primordia Contributes to Organ Patterning.” *Proceedings of the National Academy of Sciences* 111(52): 18769–74. http://www.pnas.org/content/111/52/18769.full\nhttp://www.pnas.org/lookup/doi/10.1073/pnas.1421878112.

Rast, M I, and R Simon. 2012. “Arabidopsis JAGGED LATERAL ORGANS Acts with ASYMMETRIC LEAVES2 to Coordinate KNOX and PIN Expression in Shoot and Root Meristems.” *Plant Cell* 24(7): 2917–33. http://www.ncbi.nlm.nih.gov/pubmed/22822207\nhttp://www.ncbi.nlm.nih.gov/pmc/articles/PMC3426123/pdf/2917.pdf.

Rayburn, a. Lane, and B. S. Gill. 1987. "Molecular Analysis of the D-Genome of the *Triticeae*." *Theoretical and applied genetics* 73: 385–88.

Reddy, G Venugopala, Marcus G Heisler, David W Ehrhardt, and Elliot M Meyerowitz. 2004. "Real-Time Lineage Analysis Reveals Oriented Cell Divisions Associated with Morphogenesis at the Shoot Apex of Arabidopsis Thaliana." *Development (Cambridge, England)* 131(17): 4225–37. http://www.ncbi.nlm.nih.gov/pubmed/15280208 (December 12, 2013).

Reinhardt, D, T Mandel, and C Kuhlemeier. 2000. "Auxin Regulates the Initiation and Radial Position of Plant Lateral Organs." *The Plant cell* 12(April): 507–18.

Reinhardt, Didier et al. 2003. "Regulation of Phyllotaxis by Polar Auxin Transport." *Nature* 426: 255–60.

Reinhardt, Didier, Martin Frenz, Therese Mandel, and Cris Kuhlemeier. 2005. "Microsurgical and Laser Ablation Analysis of Leaf Positioning and Dorsoventral Patterning in Tomato." *Development (Cambridge, England)* 132(1): 15–26.

Reinhart, Brenda J et al. 2013. "Establishing a Framework for the Ad/abaxial Regulatory Network of Arabidopsis: Ascertaining Targets of Class III Homeodomain Leucine Zipper and KANADI Regulation." *The Plant cell* 25(9): 3228–49. http://www.plantcell.org/content/25/9/3228/F7.expansion.html.

Richards, F. J. 1951. "Phyllotaxis: Its Quantitative Expression and Relation to Growth in the Apex." *Philosophical Transactions of the Royal Society of London. Series B, Biological Sciences* 235(629): 509–64. http://dx.doi.org/10.1098/rstb.1951.0007\nhttp://rstb.royalsocietypublishing.org/content/235/629/509.abstract\nhttp://rstb.royalsocietypublishing.org/content/235/629/509.full.pdf.

Robinson, Sarah et al. 2013. "Mechanical Control of Morphogenesis at the Shoot Apex." *Journal of Experimental Botany* 64(15): 4729–44.

Rolland-Lagan, a. G., and Przemyslaw Prusinkiewicz. 2005. "Reviewing Models of Auxin Canalization in the Context of Leaf Vein Pattern Formation in Arabidopsis." *Plant Journal* 44(5): 854–65.

Sarojam, Rajani et al. 2010. "Differentiating Arabidopsis Shoots from Leaves by Combined YABBY Activities." *The Plant cell* 22(July): 2113–30.

Sassi, Massimiliano et al. 2014. "An Auxin-Mediated Shift toward Growth Isotropy Promotes Organ Formation at the Shoot Meristem in Arabidopsis." *Current Biology* 24: 2335–42. http://linkinghub.elsevier.com/retrieve/pii/S0960982214010495.

Sauer, Michael et al. 2006. "Canalization of Auxin Flow by Aux / IAA-ARF-Dependent Feedback Regulation of PIN Polarity." *Genes & Development*: 2902–11.

Sawa, Shinichiro et al. 1999. "Filamentous Flower, a Meristem and Organ Identity Gene of Arabidopsis, Encodes a Protein with a Zinc Finger and HMG-Related Domains." *Genes and Development* 13(9): 1079–88.

Schoof, Heiko et al. 2000. "The Stem Cell Population of Arabidopsis Shoot Meristems Is Maintained by a Regulatory Loop between the CLAVATA and WUSCHEL Genes." *Cell* 100(6): 635–44.

Schulze, Silke et al. 2010. "LOST MERISTEMS Genes Regulate Cell Differentiation of Central Zone Descendants in Arabidopsis Shoot Meristems." *Plant Journal* 64(4): 668–78.

Schumacher, K et al. 1999. "The Lateral Suppressor (Ls) Gene of Tomato Encodes a New Member of the VHIID Protein Family." *Proc Natl Acad Sci U S A* 96(1): 290–95. http://www.ncbi.nlm.nih.gov/pubmed/9874811\nhttp://www.ncbi.nlm.nih.gov/pmc/articles/PMC15132/pdf/pq000290.pdf.

Semiarti, E et al. 2001. "The ASYMMETRIC LEAVES2 Gene of Arabidopsis Thaliana Regulates Formation of a Symmetric Lamina, Establishment of Venation and Repression of Meristem-Related Homeobox Genes in Leaves." *Development* 128(10): 1771–83.

Sessa, Giovanna, Corinna Steindler, Giorgio Morelli, and Ida Ruberti. 1998. "The Arabidopsis Athb-8, -9 and -14 Genes Are Members of a Small Gene Family Coding for Highly Related HD-ZIP Proteins." *Plant Molecular Biology* 38(4): 609–22.

Shani, Eilon, Osnat Yanai, and Naomi Ori. 2006. "The Role of Hormones in Shoot Apical Meristem Function." *Current Opinion in Plant Biology* 9(5): 484–89.

Shipman, P. D., and a. C. Newell. 2005. "Polygonal Planforms and Phyllotaxis on Plants." *Journal of Theoretical Biology* 236: 154–97.

Shuai, Bin, Cristina G Reynaga-pen, and Patricia S Springer. 2002. "Lateral Organ Boundaries." *Plant Physiology* 129(June): 747–61.

Sieber, Patrick et al. 2007. "Redundancy and Specialization among Plant microRNAs: Role of the MIR164 Family in Developmental Robustness." *Development (Cambridge, England)* 134(6): 1051–60.

Siegfried, K R et al. 1999. "Members of the YABBY Gene Family Specify Abaxial Cell Fate in Arabidopsis." *Development* 126(18): 4117–28.

Singh, Archita et al. 2017. "Phytohormonal Crosstalk Modulates the Expression of miR166/165s, Target Class III HD-ZIPs, and KANADI Genes during Root Growth in Arabidopsis Thaliana." *Scientific Reports* 7(1): 3408. http://www.nature.com/articles/s41598-017-03632-w.

Smith, Richard S et al. 2006. "A Plausible Model of Phyllotaxis." *Proceedings of the National Academy of Sciences of the United States of America* 103(5): 1301–6.

Smith, Richard S., Cris Kuhlemeier, and Przemyslaw Prusinkiewicz. 2006. "Inhibition Fields for Phyllotactic Pattern Formation: A Simulation studyThis Article Is One of a Selection of Papers Published on the Special Theme of Shoot Apical Meristems." *Canadian Journal of Botany* 84(11): 1635–49.

Smyth, D R, J L Bowman, and E M Meyerowitz. 1990. "Early Flower Development in Arabidopsis." *Plant Cell* 2(8): 755–67. http://www.ncbi.nlm.nih.gov/pubmed/2152125.

Snow, M, and R Snow. 1935. "II-Experiments on Phyllotaxis Part III-Diagonal Splits through Decussate Apices." *Philosophical Transactions of the Royal Society of London* 225(519): 63–94.

Snow, M Snow, R. 1931. "Experiments on Phyllotaxis. 1.-The Elfect of Lsolating a Prirnordiu." *Philosophical Transactions of the Royal Society of London* 221(May): 1–43.

Somssich, Marc, Byoung Il Je, Rüdiger Simon, and David Jackson. 2016. "CLAVATA-WUSCHEL Signaling in the Shoot Meristem." *Development* 143(18): 3238–48. http://dev.biologists.org/lookup/doi/10.1242/dev.133645%5Cnhttp://www.ncbi.nlm.nih.gov/pubmed/27624829.

Souer, Erik et al. 1996. "The No Apical Meristem Gene of Petunia Is Required for Pattern Formation in Embryos and Flowers and Is Expressed at Meristem and Primordia Boundaries." *Cell* 85(2): 159–70.

Stahle, Melissa I et al. 2009. "YABBYs and the Transcriptional Corepressors LEUNIG and LEUNIG_HOMOLOG Maintain Leaf Polarity and Meristem Activity in Arabidopsis." *The Plant cell* 21(10): 3105–18.

Stewart, R N, and Haig Dermen. 1970. "Determination of Number and Mitotic Activity of Shoot Apical Initial Cells by Analysis of Mericlinal Chimeras." *American Journal of Botany* 57(7): 816–26.

Stoma, Szymon et al. 2008. "Flux-Based Transport Enhancement as a Plausible Unifying Mechanism for Auxin Transport in Meristem Development." *PLoS Computational Biology* 4(10): e1000207. http://www.pubmedcentral.nih.gov/articlerender.fcgi?artid=2565506&tool=pmcentrez&rendertype=abstract.

Stuurman, Jeroen, Fabienne Jäggi, and Cris Kuhlemeier. 2002. "Shoot Meristem Maintenance Is Controlled by a GRAS -Gene Mediated Signal from Differentiating Cells Service Shoot Meristem Maintenance Is Controlled by a GRAS -Gene Mediated Signal from Differentiating Cells." *Genes and Development*: 2213–18.

Tian, Caihuan et al. 2014. "An Organ Boundary-Enriched Gene Regulatory Network Uncovers Regulatory Hierarchies Underlying Axillary Meristem Initiation." *Molecular Systems Biology* 10: 755. http://www.pubmedcentral.nih.gov/articlerender.fcgi?artid=4299377&tool=pmcentrez&rendertype=abstract.

Traas, Jan, and Teva Vernoux. 2002. "The Shoot Apical Meristem: The Dynamics of a Stable Structure." *Philosophical transactions of the Royal Society of London. Series B, Biological sciences* 357(1422): 737–47. http://www.pubmedcentral.nih.gov/articlerender.fcgi?artid=1692983&tool=pmcentrez&rendertype=abstract.

Turchi, L., S. Baima, G. Morelli, and I. Ruberti. 2015. "Interplay of HD-Zip II and III Transcription Factors in Auxin-Regulated Plant Development." *Journal of Experimental Botany*. http://jxb.oxfordjournals.org/lookup/doi/10.1093/jxb/erv174.

Vernoux, T et al. 2000. "PIN-FORMED 1 Regulates Cell Fate at the Perifery of the Shoot Apical Meristem." *Development* 127(23): 5157–65.

Vernoux, T. et al. 2014. “The Auxin Signalling Network Translates Dynamic Input into Robust Patterning at the Shoot Apex.” *Molecular Systems Biology* 7(1): 508–508. http://msb.embopress.org/cgi/doi/10.1038/msb.2011.39.

Vroemen, Casper W et al. 2003. “The CUP-SHAPED COTYLEDON3 Gene Is Required for Boundary and Shoot Meristem Formation in Arabidopsis.” *The Plant cell* 15(7): 1563–77. http://www.pubmedcentral.nih.gov/articlerender.fcgi?artid=165401&tool=pmcentrez&rendertype=abstract.

Wabnik, K et al. 2010. “Emergence of Tissue Polarization from Synergy of Intracellular and Extracellular Auxin Signaling.” *Mol Syst Biol* 6(447): 447. http://www.ncbi.nlm.nih.gov/entrez/query.fcgi?cmd=Retrieve&db=PubMed&dopt=Citation&list_uids=21179019.

Wabnik, Krzysztof, Jürgen Kleine-Vehn, Willy Govaerts, and Jiří Friml. 2011. “Prototype Cell-to-Cell Auxin Transport Mechanism by Intracellular Auxin Compartmentalization.” *Trends in Plant Science* 16(9): 468–75. http://linkinghub.elsevier.com/retrieve/pii/S1360138511001002.

Waites, R, and a Hudson. 1995. “*phantastica*: A Gene Required for Dorsoventrality of Leaves in *Antirrhinum Majus*.” *Development* 121(7): 2143–54. http://dev.biologists.org/content/121/7/2143.abstract.

Waites, Richard, Harinee R N Selvadurai, Ian R. Oliver, and Andrew Hudson. 1998. “The PHANTASTICA Gene Encodes a MYB Transcription Factor Involved in Growth and Dorsoventrality of Lateral Organs in Antirrhinum.” *Cell* 93(5): 779–89.

Wang, Quan, Alice Hasson, Susanne Rossmann, and Klaus Theres. 2016. “Divide et Impera: Boundaries Shape the Plant Body and Initiate New Meristems.” *New Phytologist* 209(2): 485–98.

Weir, Irene et al. 2004. “CUPULIFORMIS Establishes Lateral Organ Boundaries in Antirrhinum.” *Development* 131(4): 915–22. http://eutils.ncbi.nlm.nih.gov/entrez/eutils/elink.fcgi?dbfrom=pubmed&id=14757643&retmode=ref&cmd=prlinks\npapers3://publication/doi/10.1242/dev.00993.

Wenkel, S. et al. 2007. “A Feedback Regulatory Module Formed by LITTLE ZIPPER and HD-ZIPIII Genes.” *the Plant Cell Online* 19(11): 3379–90. http://www.plantcell.org/cgi/doi/10.1105/tpc.107.055772.

Wu, Miin Feng et al. 2015. "Auxin-Regulated Chromatin Switch Directs Acquisition of Flower Primordium Founder Fate." *eLife* 4(OCTOBER2015): 1–20.

Xie, Yakun et al. 2015. "Meta-Analysis of Arabidopsis KANADI1 Direct Target Genes Identifies a Basic Growth-Promoting Module Acting Upstream of Hormonal Signaling Pathways." *Plant Physiology* 169(2): 1240–53. http://www.plantphysiol.org/lookup/doi/10.1104/pp.15.00764.

Yadav, Ram Kishor et al. 2011. "WUSCHEL Protein Movement Mediates Stem Cell Homeostasis in the Arabidopsis Shoot Apex." *Genes & Development*: 2025–30.

Yamaguchi, Nobutoshi et al. 2012. "LEAFY Controls Arabidopsis Pedicel Length and Orientation by Affecting Adaxial-Abaxial Cell Fate." *Plant Journal* 69: 844–56.

Yamaguchi, Takahiro, Akira Nukazuka, and Hirokazu Tsukaya. 2012. "Leaf Adaxial-Abaxial Polarity Specification and Lamina Outgrowth: Evolution and Development." *Plant and Cell Physiology* 53(7): 1180–94.

Yanai, Osnat et al. 2005. "Arabidopsis KNOXI Proteins Activate Cytokinin Biosynthesis." *Current Biology* 15(17): 1566–71.

Yang, F et al. 2015. "A Maize Glutaredoxin Gene , Abphyl2 , Regulates Shoot Meristem Size and Phyllotaxy." *The Plant cell*: 1–12. http://www.ncbi.nlm.nih.gov/pubmed/25616873.

Yu, Hongyang, and Tengbo Huang. 2016. "Molecular Mechanisms of Floral Boundary Formation in Arabidopsis." *International Journal of Molecular Sciences* 17(3): 317. http://www.mdpi.com/1422-0067/17/3/317.

Zhao, Hongtao et al. 2013. "The ATP-Binding Cassette Transporter ABCB19 Regulates Postembryonic Organ Separation in Arabidopsis." *PLoS ONE* 8(4).

Zhao, Y et al. 2001. "A Role for Flavin Monooxygenase-like Enzymes in Auxin Biosynthesis." *Science* 291(5502): 306–9. http://www.ncbi.nlm.nih.gov/pubmed/11209081.

Zhao, Zhong et al. 2010. "Hormonal Control of the Shoot Stem-Cell Niche." *Nature* 465(7301): 1089–92. http://www.nature.com/doifinder/10.1038/nature09126.

Zhou, Yuyi et al. 2015. "Spatiotemporal Sequestration of miR165/166 by Arabidopsis Argonaute10 Promotes Shoot Apical Meristem Maintenance." *Cell Reports* 10(11): 1819–27. http://linkinghub.elsevier.com/retrieve/pii/S2211124715002053.

Zhu, Hongliang et al. 2011. "Arabidopsis argonaute10 Specifically Sequesters miR166/165 to Regulate Shoot Apical Meristem Development." *Cell* 145(2): 242–56. http://dx.doi.org/10.1016/j.cell.2011.03.024.

Zuo, Jianru, Qi Wen Niu, Giovanna Frugis, and Nam Hai Chua. 2002. "The WUSCHEL Gene Promotes Vegetative-to-Embryonic Transition in Arabidopsis." *Plant Journal* 30(3): 349–59.

RESULTS

PREAMBLE: SEVERAL WAYS TO MAKE WHORLS, CLUES FROM OTHER SPECIES

One goal of my Ph.D. was to explore the dynamics of phyllotaxis in other patterns than the extensively studied Fibonacci spirals, and notably the whorled arrangements. In the model species *A. thaliana*, the formation of floral whorls is hidden by sepal tissues, preventing easy imaging. Moreover, only 5 whorls are produced in a flower (sepal, petal, 2 whorls of stamens and carpels) before floral termination. However, some species display very accessible whorls, produced by indeterminate vegetative or inflorescence shoots. This indeterminacy allows observing several whorls iteration in a single snapshot, which gives an insight on the dynamics even on static images from fixed specimens. I thus selected a few species with such accessible whorled phyllotaxis from plants available at the botanical garden of Lyon and observe their shoot apical meristem under Scanning Electron Microscopy. All collected species were angiosperms displaying whorls of four or more leaves:

- *Villiantia muralis*, a member of the *cruciata* genus (eudicotyledons from the *rubiaceae* family, the *asterid* clade, and the *gentianales* order) commonly known as "Crosswort", bears whorls of four leaves sometimes additionned with flowers (Preamble figure A-D).

- *Peperonia rubella*: a *magnoliid* endemic from Jamaica, of the *piperales* order and the *piperaceae* family, displays whorls of four elliptical leaves (Preamble figure E-F).

- *Hippuris vulgaris*: a semi-aquatic plant commonly known as "mare's tail" grows aerial shoots above underwater rhizomes. It belongs to the *asterid* clade and the *lamiales* order, and displays unbranched shoots with whorls composed of six to twelve needle-shaped leaves (Preamble figure G-H).

- *Elodea species*: an entirely underwater monocotyledon of the *alismatales* clade and the *hydrocharitaceae* family, which shoot is arranged in whorls of up to seven oblong leaves (Preamble figure I-K).

These four species displayed apparent whorled phyllotaxis. However, observation of their meristem showed that these whorls were not necessarily assembled at the meristem, but later thanks to the absence of internode development. In *Villiantia muralis* indeed (Preamble figure A-D), the meristematic pattern was that of a decussate phyllotaxis, where organs arise from the meristem two by two and opposite to each other, at 90° divergence angle from the preceding pair (Preamble figure C-D). Indeed, we could observe lateral organs with equal size to the ones in front of them across the meristem only, forming a pair of presumably co-initiated organs, which pattern was visible on the next row with a divergence angle of 90°. Although this was a surprising observation with no more support than the size of the lateral organs at the meristem, and considering the aspect of the whorl shown in Preamble figure B where it is not possible to distinguish the decussate pattern, it was nevertheless consistent with a description of the *cruciata* genus made by Hutchinson (1955), who described these whorls as sets of two real leaves accompanied by two laminar stipules. Similarly, other species such as *Peperonia rubella* displayed a whorled phyllotaxis despite a decussate meristematic pattern. In fact, this can be sometimes visible at the tip of the shoot as shown in the Preamble figure E where the last two leaves produced are smaller in size, whereas older leaves stack up in whorls. Conversely, some species establish true whorls right at the meristem, such as *Hippuris vulagaris* or *Elodea species* (Preamble figure G-K), two aquatic plants, which collected samples displayed whorls of ten and three leaves respectively.

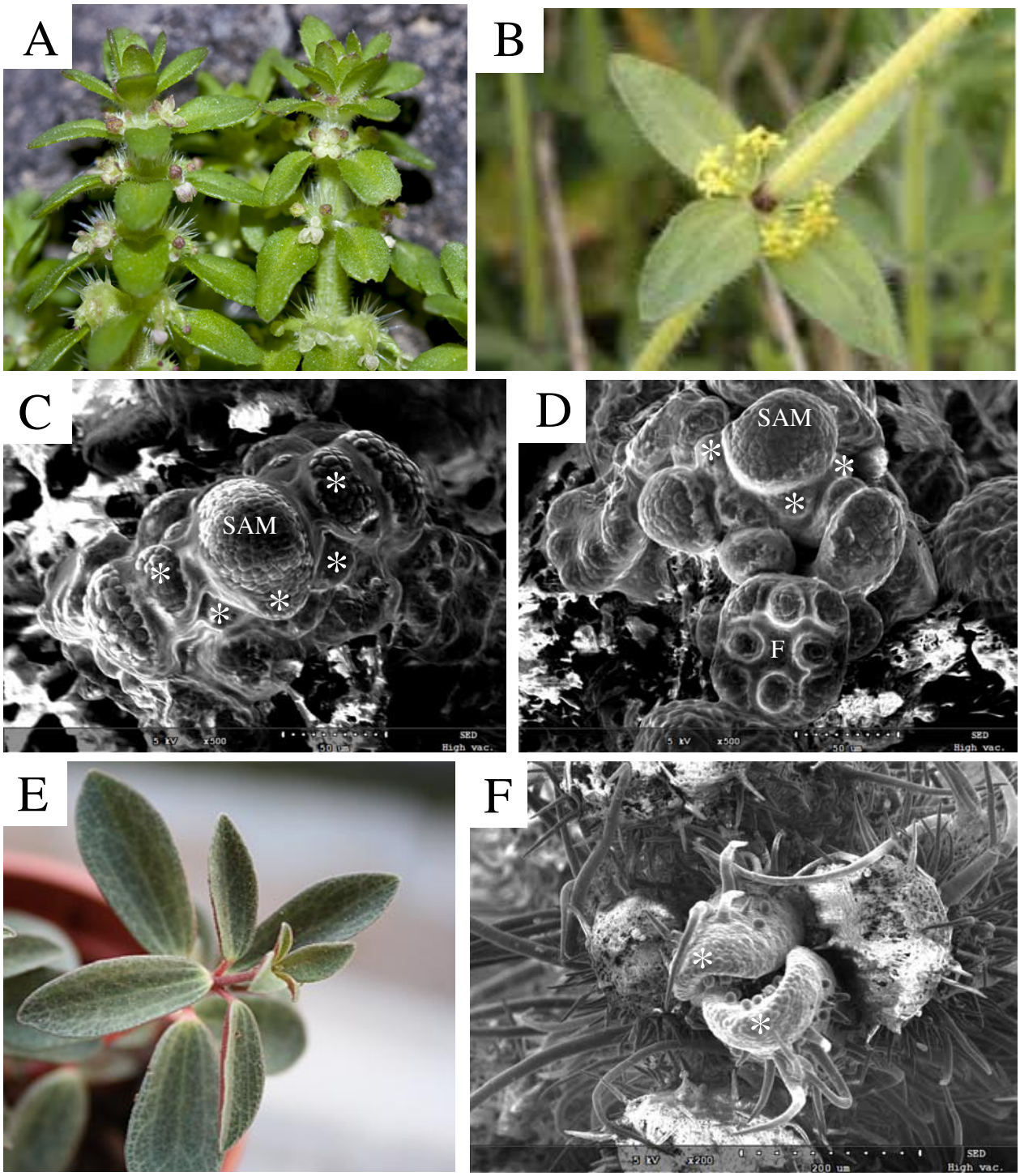
A
B
C
SAM
D
SAM
F
E
F

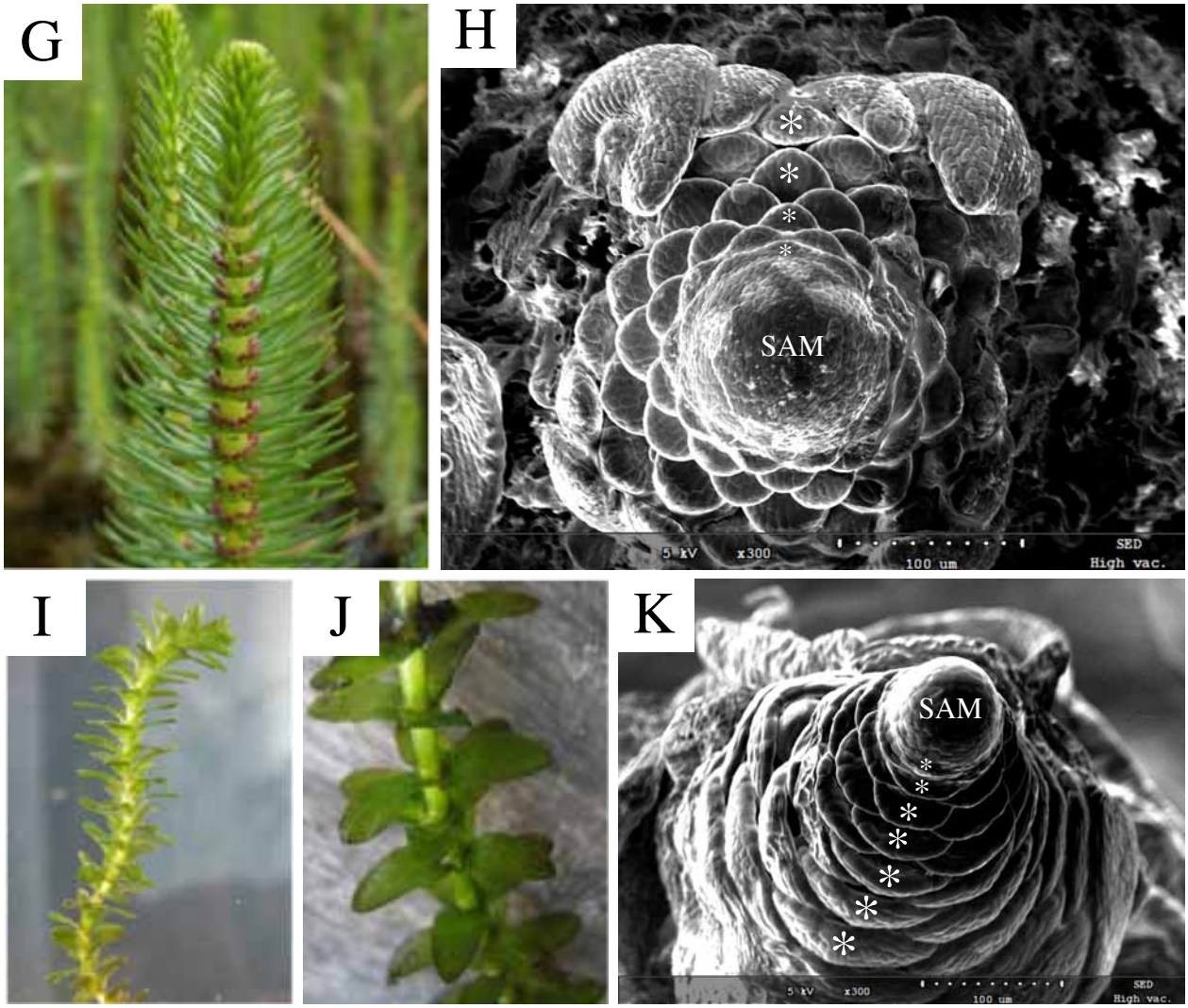

Preamble figure: Species establish whorled phyllotaxis in different ways. A-D) *Villantia muralis* displays whorls on their inflorescence shoot (A) with four leaves in each (B). C-D) Shoot apical meristems. E-F) *Peperonia rubella* displays a four-leaves whorled phyllotaxis on the shoot (E) that is established as distichious at the meristem (F). *Hippuris vulgaris* (G-H) and *Elodea species* (I-K) are two aquatic species with fully whorled shoots (G, I, J) and shoot apical meristems (H, K). White stars indicate growing leaves. SAM = Shoot Apical Meristem. F = Flower.

Some striking observations of these last two meristems were first that their domes were extremely convex. The organogenesis zones were positioned at the basis of the domes far from the climax, leaving possibly more free space for the central zone. Second, the Preamble figure C shows a *Peperonia rubella* meristem that is approximately 45 µm wide with a primordium deforming the meristem surface on a proportionally large width (≈ 35 µm). This corresponds to approximately 45 xπ=110 µm circumference, and a circumference occupancy by the primordia of 32%. On the contrary, *Hippuris vulgaris* (Preamble figure H, G) and *Elodea species* (Preamble figure H, K) displayed wider circumferences (349 µm and 283 µm respectively) and proportionally thinner deformation of the meristem surfaces at the site of the smallest primordia development (35 µm and 45 µm, i.e. 10% and 16% respectively). In all these species, lateral organs equitably shared the space around the peripheral zone, which might indicate that Hofmeister's rule for organogenesis (it occurs in the largest available gap) also fit here. Although these observations could not be statistically validated due to the small amount of available samples, nevertheless they remained consistent with the mathematical models that predict that lateral organs will be arranged in whorls as the ratio between organ size and meristem size decreases (Douady & Couder, 1996).

These exploratory results show that whorled species have several ways to assemble clusters either they produce more than two organs at the same time, to post-meristematic growth.

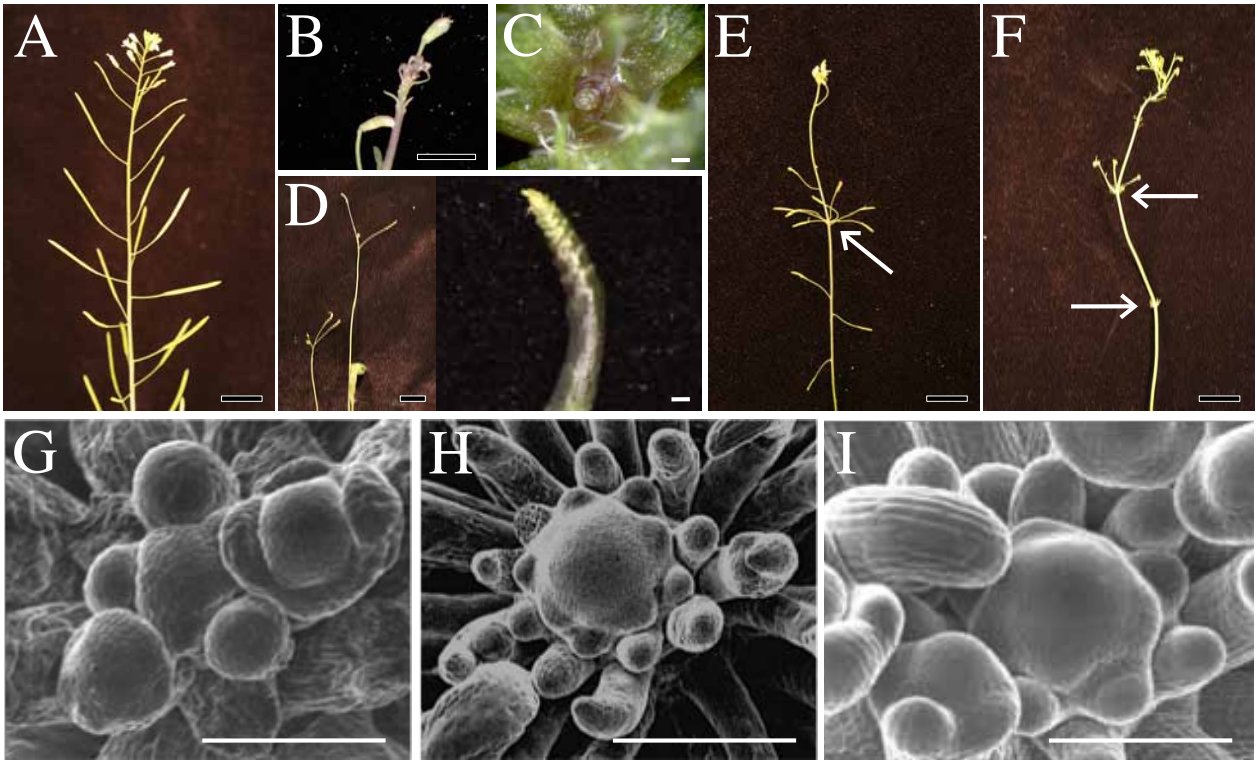

Figure I.1: T-DNA mutants showing phyllotaxis defects.
A) *Ws-4* wild type shoot. B-F) T-DNA mutants from Versailles Arabidopsis Stock Centre. B) Inflorescence of EAT101. C) Top view of the shoot apical meristem of EAV83 shows pin-like apex. D) shoot (left panel) and shoot apical meristem (right panel) of EAT197 shows pin-like apex. E) DZP10 shoot. F) DRB27 shoot. White arrows show lateral organ clusters along the inflorescence shoot. G-I) Shoot apical meristems of wild type (G) DZP10 (H) and DRB27 (I) in scanning electron microscopy. Black scale bars = 1cm. White scale bars = 100 μm

I – ISOLATION AND CHARACTERISATION OF A MUTANT WITH STRONG PHYLLOTAXIS DEFECTS

I.A – THE ORIGIN OF DRB27: A FORWARD GENETIC SCREEN FOR ALTERED PHYLLOTAXIS

To find new molecular regulators of phyllotaxis, we followed a forward genetic approach by looking at random insertion mutants from the Versailles Arabidopsis Stock Centre (http://publiclines.versailles.inra.fr/). Initiated in 1992, this collection was generated by *agrobacterium*-mediated insertion of the binary pGKB5 vector in the wild-type *Wassilevskija*-4 (*Ws-4*) *Arabidopsis thaliana* accession. The pGKB5 construct contains a *GUS* promoter trap and *NPT2* and *BAR*, two resistance genes allowing selection of transformants on kanamycin and glufosinate (phosphinothricin) respectively, thanks to a constitutive expression (driven by the agrobacterium *NOS* and the cauliflower *35S* promoters respectively, see methods).

From this mutant collection, an initial screen was performed to isolate mutants affected inflorescence architecture and organogenesis, and 5 lines were selected: EAT101, EAV83, EAT197, DZP10 and DRB27 (Figure I.1). Among other phenotypic features, none of

them were able to form the regular canonical Fibonacci spiral observed in wild type *Arabidopsis thaliana*.

EAV83, EAT101 and EAT197 lines showed naked stems with scarce lateral organs, suggesting strong defects in early organogenesis. As a consequence, their phyllotaxis patterns could not be easily analysed, similarly to auxin defective mutants. Indeed, if their inhibitory fields are obviously perturbed, so is organogenesis. Therefore they do not allow studying how the pattern is tuned and how parameters such as inhibitory fields, organ-organ interaction, and geometry are controlled.

On the other hand, the two other mutants, DZP10 and DRB27, produced many lateral outgrowths and never displayed naked shoots, although the morphology and identity of the organ produced could be dramatically affected. The persistence of organ production allows to observe and quantify many alterations of the phyllotaxis, notably clusters of numerous lateral organs along the stem (Figure I.1.E-F), interspaced by irregular distances. To eliminate possible post-meristematic controls of phyllotaxis (Peaucelle *et al.*, 2007; Landrein *et al.*, 2013; Burian *et al.*, 2015), the inflorescence meristems of these two lines were scanned by electron microscopy, revealing that the regular spiral of organogenesis never formed (Figure I.1.G-I). Other defects were obvious at this scale, like the altered geometry of the meristem, the increase in the number of organs in the peripheral zone compared to wild type and production of filamentous organs. As our current understanding of phyllotaxis places meristem geometry and interactions between organs as major contributors for plants architecture (see introduction), we focused on these two phenotypes.

	F1	F2 + antibiotics	F2
nb of plants	87	64	90
[WT]	87	42	68
[DRB27]	0	22	22
% [DRB27]	0	34,375	24,44

Table I.A: Segregation of the DRB27 phenotype. F1, F2 and Kanamycin and Phosphinothrycin resistant F2 plants were observed, and qualified as Wild Type ([WT]) or mutant ([DRB27]) based on their phenotype.

I chose to study further DRB27 and DZP10 because these mutants partially uncoupled organogenesis from phyllotaxis, which allows studying the robustness of phyllotaxis. In particular, new questions arose from preliminary observations, such as 1) Are these phyllotaxis defects related to alteration of meristem size and geometry? 2) Are they related to alterations of organ shape and identity? 3) Are organ clusters observed along the stem related to modifications of the plastochron or to problems in post-meristematic growth?

The phenotype of DRB27 was strong and fully penetrant, whereas DZP10 plants showed a range of expressivity and partial penetrance of architecture defects, and was not always distinguishable from the wild type. Several progeny batches had milder phenotypes compared to the original seeds. The DRB27 line was thus chosen for further investigations.

Segregation of T-DNA lines on kanamycin resistance was pre-estimated at 3:1 prior to our selection of the mutant, on about 100 seedlings. Verification on bulk segregating T3 lines showed that DRB27 was also sterile (no seeds were obtained from plants showing the mutant phenotype), monolocus, and linked to a T-DNA insertion (Table I.A). Indeed, both direction crossings from DRB27 heterozygous plants with wild type phenotypes produced 100% wild type F1, which progeny was either 100% wild type or ¼ mutant if sewed on soil. On basta-kanamycin, these very same F2 batches were either 100% non resistant, or 2/3 resistant, with 1/3 of the growing seedlings showing the mutant phenotype when planted in soil. This genetic analysis suggested that the phenotype of DRB27 is a recessive mutation caused by a single insertion.

I.B – PHYLLOTAXIS DEFECTS IN DRB27 MUTANTS RESULT IN THE FORMATION OF CRESCENT CLUSTERS

I.B.1 – DRB27 IS NOT IMPAIRED IN LATERAL ORGAN FORMATION

Considering the importance of organ initiation in the current model of phyllotaxis, we first quantified whether DRB27 mutants could have reduced organogenesis potential, as in auxin-related defective mutants. Indeed, long stretches of naked stem could indicate that there were fewer organs produced (Figure I.1.F).

The aerial architecture of fully-grown mutants and wild types were quantified. The height of DRB27 mutant plants were highly variable, but not significantly different as the wild types (47.6 cm for DRB27 and 50.58 cm for the wild type, Figure I.2.A). Nevertheless, measuring the ratio between the number of organs per plants and the shoot height showed that there was a significantly higher density of lateral organs along the DRB27 shoot (1.38 per cm), compared to the wild types (1.00 per cm, Figure I.2.B). It should be noted that in the DRB27 mutant, the identity of lateral organs produced along the stem were not clearly defined since siliques, leaves, lateral secondary meristems and filaments grew in mixed arrangements along the stem. All lateral structures were then counted in this assay. This result confirms the qualitative observation of DRB27 inflorescence meristems by scanning electron microscopy: organ outgrowth seemed to accumulate in the peripheral zone in a more crowded manner as usually seen in the wild type (Figure I.1.I). It was thus possible to conclude that organ formation was not limited in DRB27 mutants, and that we were observing a genetic situation where phyllotaxis defects are not the result of a significant defect in organogenesis potential.

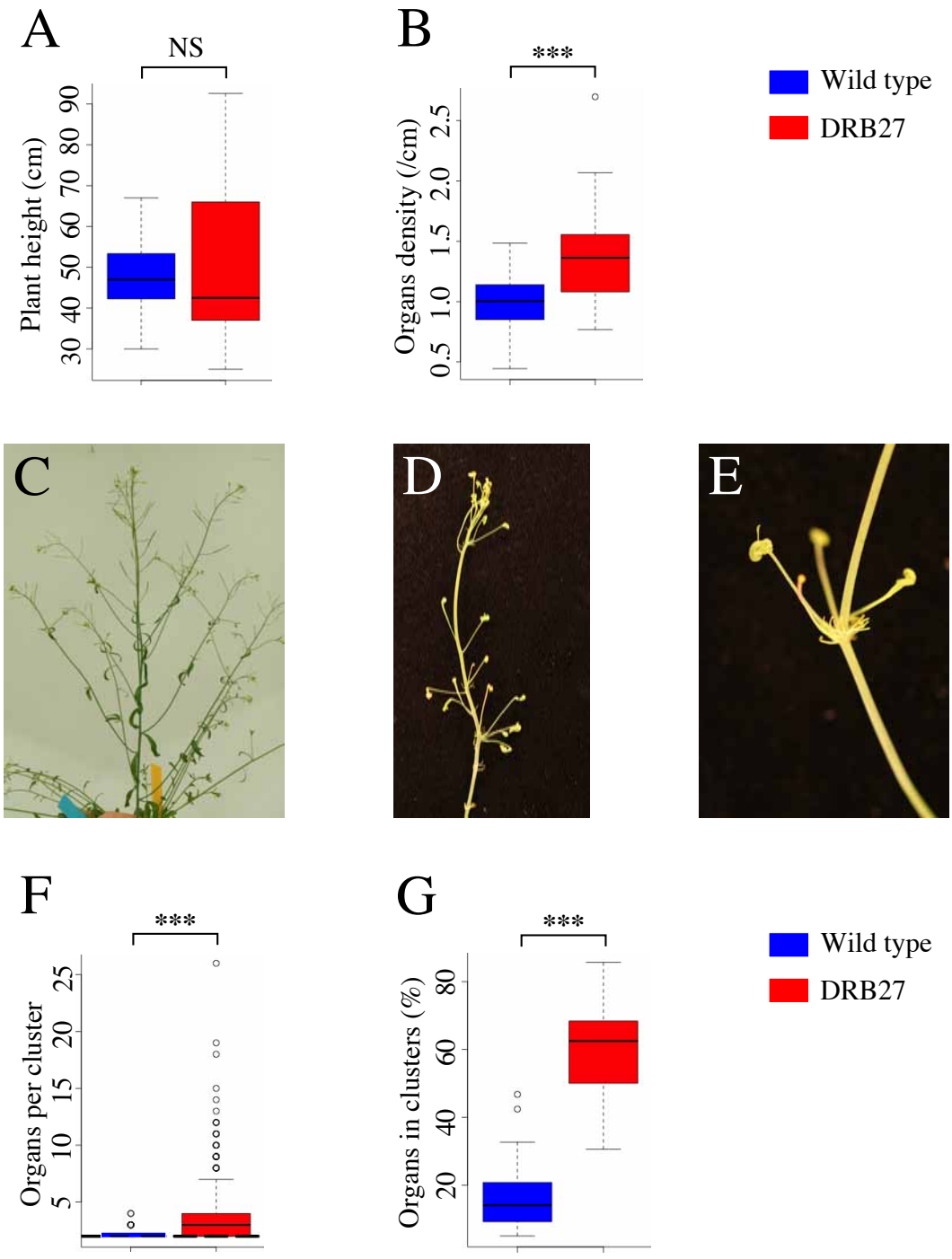

Figure I.2: DRB27 shoot apical meristems produce many lateral structures that cluster irregularly along the stem. A) Plant height variations; p-value=0.4576. B) density of lateral organs per shoot; p-value=$9.66.10^{-6}$. C-E) Wild type (C) and DRB27 (D) shoot inflorescences with close-up on DRB27 cluster (E). F) Number of organs per cluster; p-value<$2.2.10^{-16}$. G) Proportions of lateral organs in clusters; p-value=$1.079.10^{-12}$. n= 39 plants and 1870 organs for wild type; n= 32 plants and 2281 organs for DRB27. NS=Not Significant. ***: p-value<0,0005

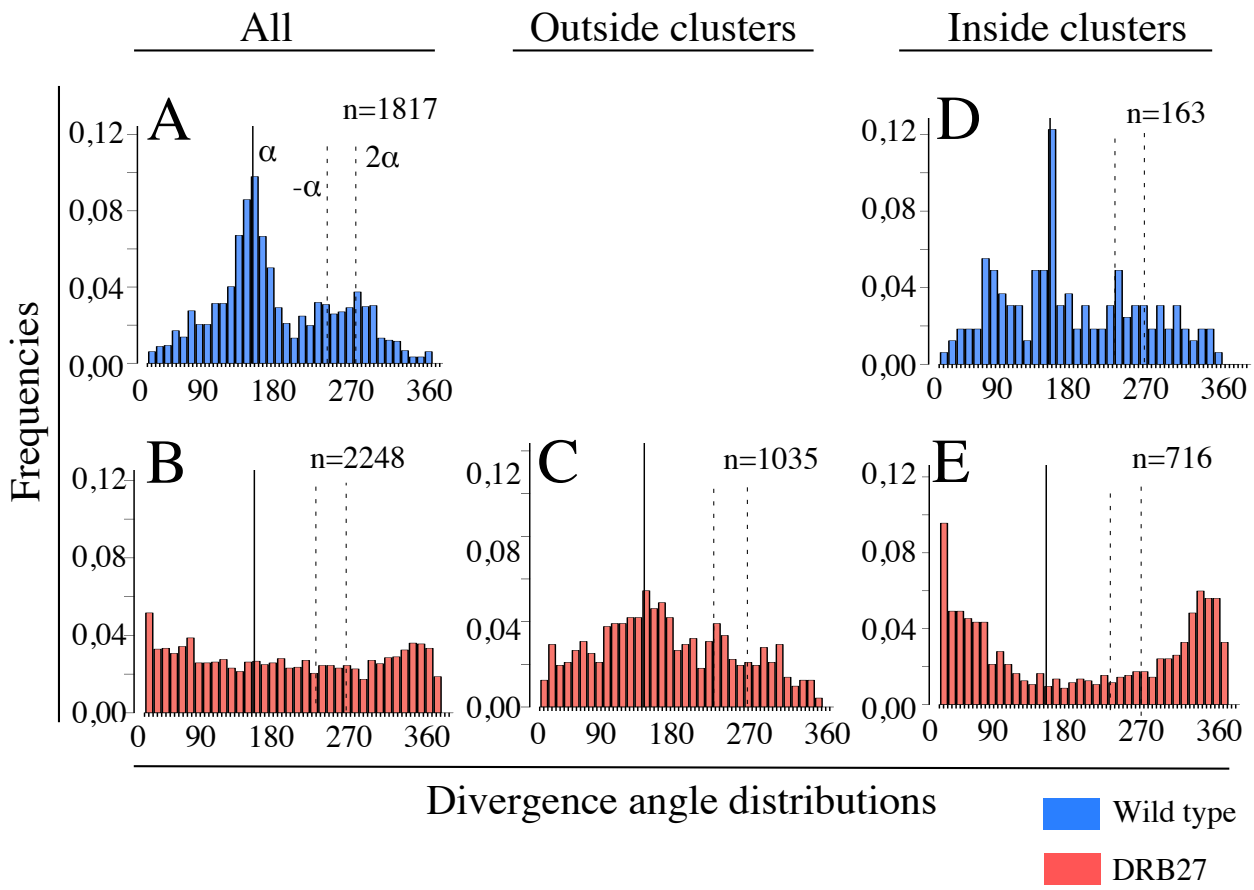

Figure I.3: Distribution of divergence angles in DRB27. The distribution of the divergence angles in the wild type (A) and DRB27 are different with (B) or without (C) clusters. Over representation of small angles inside clusters of DRB27 (E) is not observed in wild type clusters (D). n on the figures = nb of angles; nb of plants = 39 wild types and 33 DRB27.

I.B.2 – THE MAJORITY OF LATERAL ORGANS IRREGULARLY CLUSTER ALONG THE DRB27 MUTANT STEM

Unlike the regularly interspaced organ distribution along the stem observed in wild type inflorescences (Figure I.2.C), the DRB27 mutant produced aggregations of lateral organs in clusters (Figure I.2.D), characterized by small or inexistent internodes (Figure I.2.E). These lateral organs were composed of filaments and more complex flower-like structures that will be described later (section I.C.1). For quantification purpose, we defined as cluster a group of organs separated by internodes equal or smaller to 1 mm. In such clusters, the high local density prevents to distinguish the order along the stem. Clusters also exist in wild-type plants but they are generally made of only 2 siliques (Figure I.2.F) and involve a minority of organs along the stem (Figure I.2.G). By contrast, DRB27 clusters were much larger and variable, reaching up to 26 organs in a single cluster (Figure I.2.F). Furthermore, clusters represented 61.06% of total organ production of mutant inflorescences in DRB27, versus 16.88% in wild types (Figure I.2.G).

I.B.3 – PERTURBATIONS OF DIVERGENCE ANGLES IN DRB27 ARE OBSERVED OUTSIDE AND INSIDE CLUSTERS AND PRODUCE CRESCENT-LIKE DISTRIBUTIONS OF ORGANS

We then investigated the radial distribution of organs by measuring divergence angles between successive organs along the stem. Because of the abnormal identity of lateral organs in DRB27 mutants, I adapted previous well-tested methods (Peaucelle *et al.*, 2007; Ragni *et al.*, 2008; Prasad *et al.*, 2011; Pinon *et al.*, 2013; Landrein *et al.*, 2013; Guédon *et al.*, 2013; Besnard *et al.*, 2014a; Landrein *et al.*, 2015) which consisted in measuring only siliques, by including any lateral organs or axes grown out of the principal inflorescence in the measurements (see Methods). Wild-type *A. thaliana* plants show a classical distribution of divergence angles composed of a majority of angles close to the canonical angle (α = 137.5) and additional angles close to $-\alpha$, 2α and other multiples of α. This typical distribution has been described for wild-type plants (Peaucelle *et al.*, 2007; Guédon *et al.*, 2013; Besnard *et al.*, 2014; Landrein *et al.*, 2015) and can be explained by permutations of the order of organs along the stem, as a consequence of co-initiations at the meristem followed by differential post-meristematic growth (Figure I.3.A; Guédon *et al.*, 2013; Besnard *et al.*, 2014). In our culture condition, the wild-type accession *Ws-4* has been showed to produce a higher proportion of such permutations, compared to other accessions like the popular lab accession *Col-0* (Landrein *et al.*, 2015).

Strikingly, the distribution of divergence angles in DRB27 was completely random (Figure I.3.B). However, given that more than 60% of DRB27 lateral organs were distributed in clusters in which the sequence of organ is not distinguishable, this distribution could be an artefact due to randomization of organ order along the stem. We thus analysed separately the divergence angles inside and outside clusters. Outside clusters, the distribution got closer to a wild type pattern with a main peak around 137.5 (Figure I.3.C), but the variance was larger. This distribution could come: either from more permutations increasing $-\alpha$, 2α, 3α at the expense of the main α peak; or from random variation of the divergence angle at each organ formation. This suggests that destabilization of phyllotaxis is not necessarily correlated to cluster formation in DRB27 mutants.

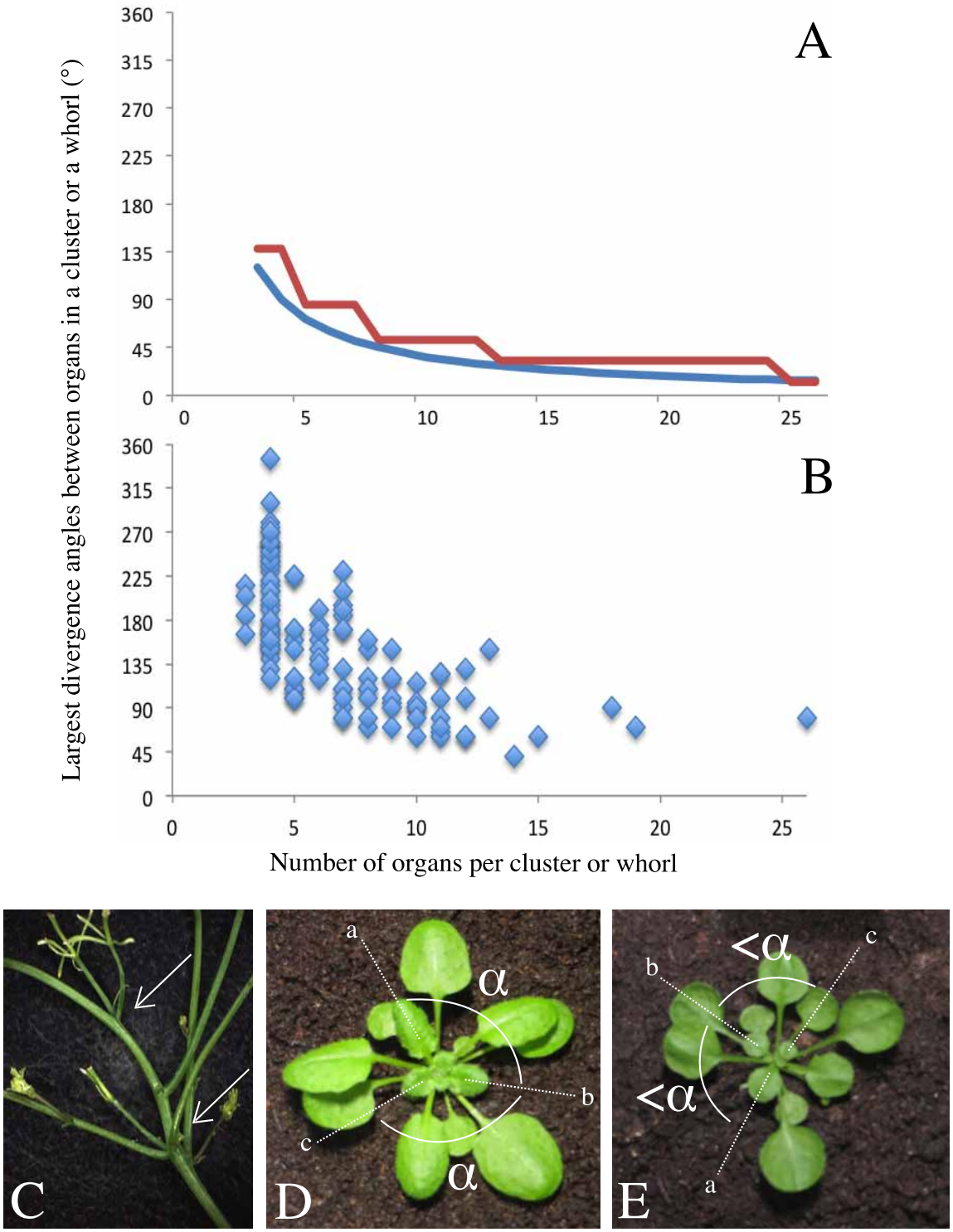

Figure I.4: Perturbations of divergence angles in DRB27. A) Theorical largest divergence angles between equidistant organs within whorls (in blue) or between organs of a spiral with no post-meristematic growth (red). B) Largest divergence angle between organs of single clusters in DRB27 (n=126) are wider than theorical divergence angle for a same number of organs in the cluster. C) Orientated clusters observed in DRB27 shoot (white arrows). Wild type (D) and DRB27 (E) rosette; successive leaves (a, b, c) diverge by golden angle (α) in the wild type whereas divergence angle seems smaller in DRB27. Wild type (F) and DRB27 (G) lateral organs of a sinle plant are represented by numbered coloured circles. Numbers correspond to the order of measurements from the bottom upwards, organs within clusters beare the same number. Co-initiations are circled in the corresponding colour and some divergence angle are highlighted. We do not consider co-initiations too close to the SAM (red).

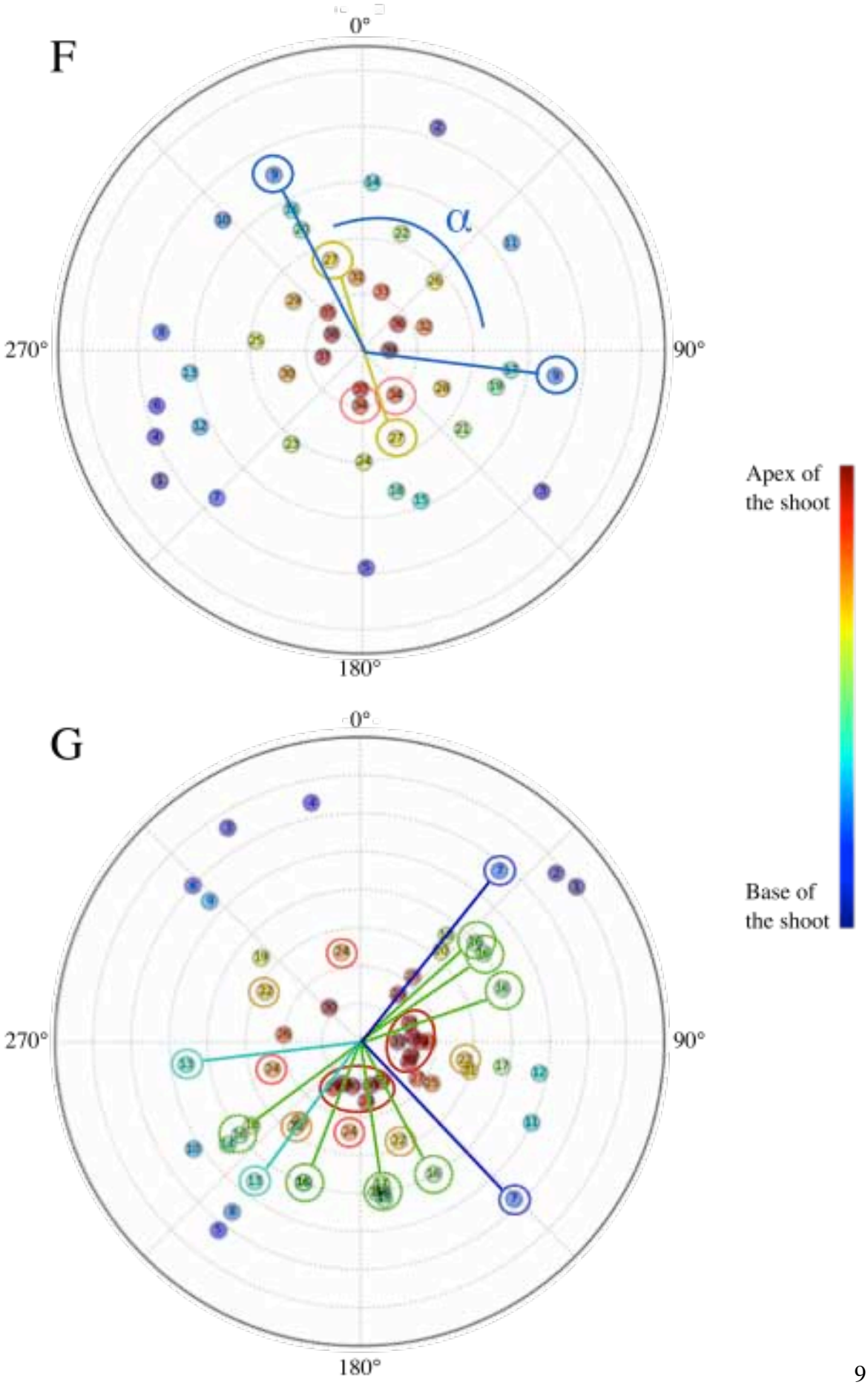
F
0°
270°
90°
180°
α
G
0°
270°
90°
180°
Apex of the shoot
Base of the shoot

Inside clusters, wild types still exhibited a large preference for the canonical α=137.5° and an under-representation of small divergence angles between organs (Figure I.3.D). The distribution was more variable than the distribution of all pooled angles, most likely because of the small number of angles considered (n=163) in groups of organs that show probably more permutations. Indeed, Guédon et al. (2013) showed that there was a positive correlation between short internodes and permutations. Inside DRB27 clusters, divergence angles (n=1035) were surprisingly small: the distribution was depleted in the canonical α=137,5, and enriched in divergence angles close to 0°/360°, indicating that clustered organs in DRB27 mutants were preferentially close to each other (Figure I.3.E; Figure I.4). Therefore, phyllotaxis of the DRB27 clusters was completely different from the phyllotaxis of WT clusters (which is likely just a wild-type situation with more permutations). Moreover, phyllotaxis of the DRB27 clusters was unusual. The production of organs close to each others suggested that phyllotaxis in DRB27 did not follow the phenomenological rule of Hofmeister (1868) saying that organogenesis occurs in the largest gap available left by the other growing organs.

The distributions discussed so far pool all angles from different plants, from different stem positions and from different clusters. To quantify these observations at the level of a given cluster, we calculated the largest angle between azimuths for each cluster of four or more organs. In theory, true whorls would produce organs equidistantly around the meristem (Douady et Couder, 1996; Preamble figure G-K), i.e. at a divergence angle of 360/n, with n = the number of organs in the whorl, as illustrated in Figure I.4.A. However in DRB27, this relation between the number of organs, and the largest space left around the stem was not consistent with a true whorled pattern, and shifted instead towards an increase of this largest space between organs in a single cluster (Figure I.4.B), meaning that the other organs are more closely packed around the stem. This was consistent with our observations of oriented clusters on the DRB27 shoot (Figure I.4.C). In the rosette, phyllotaxis seemed to undergo the same perturbations as well (Figure I.4.D-E), although we did not quantify them.

To illustrate the production of oriented clusters in the DRB27 inflorescence shoot, we used radial plots reproducing a top view of an inflorescence: organs were plotted as small discs in a larger target-like disc representing the stem. They were numbered from the bottom

upwards, and corresponding organ-discs were laid from periphery to centre with this number and a blue-to-red colour gradient. Distances from centre to periphery are arbitrary, while azimuths correspond to real measurements. In a typical wild type (Figure I.4.F), a two-organs cluster (n°9, circled in blue) usually shows a normal α divergence angle, or a large angle (n°27 in yellow). It is important to note that we do not consider the organs too close to the shoot apical meristem (in red) because measures can be confused due to low post-meristematic growth. In DRB27 (Figure I.4.G), clustered organs preferentially aggregated on one side of the plant, forming crescents of organs (for examples the n°7 circled in blue, 13 in light blue, 16 in pointy green). We could define a crescent as a cluster of more than three organs inserted at the same node along the stem, and which sum of azimuths does not cover a full turn, as would do Fibonacci spirals and whorls.

To conclude, the phyllotactic pattern of DRB27 is highly disrupted in comparison to the wild type, and shows many differences with the regular wild-type arrangement. Vertically, the production of organs, normally occurring one by one, creates clusters of highly variable size. Radially, the regular Fibonacci spiral, composed mainly of α (golden) angles and permutation angles in the wild type, changes drastically in DRB27. Outside clusters, the distribution suggests a destabilization of this Fibonacci spiral. Inside clusters, a completely new pattern arises: organs are inserted preferentially at small divergence angles, which creates a crescent-shape stretch in one side of the stem. Crescents in DRB27 are an intriguing mode of organ production because 1) Hofmeister's rule no longer holds; 2) they are partially penetrant as they only occur by burst along the stem whereas each plant show the same phenotype; 3) in these clusters, there is no internode elongation.

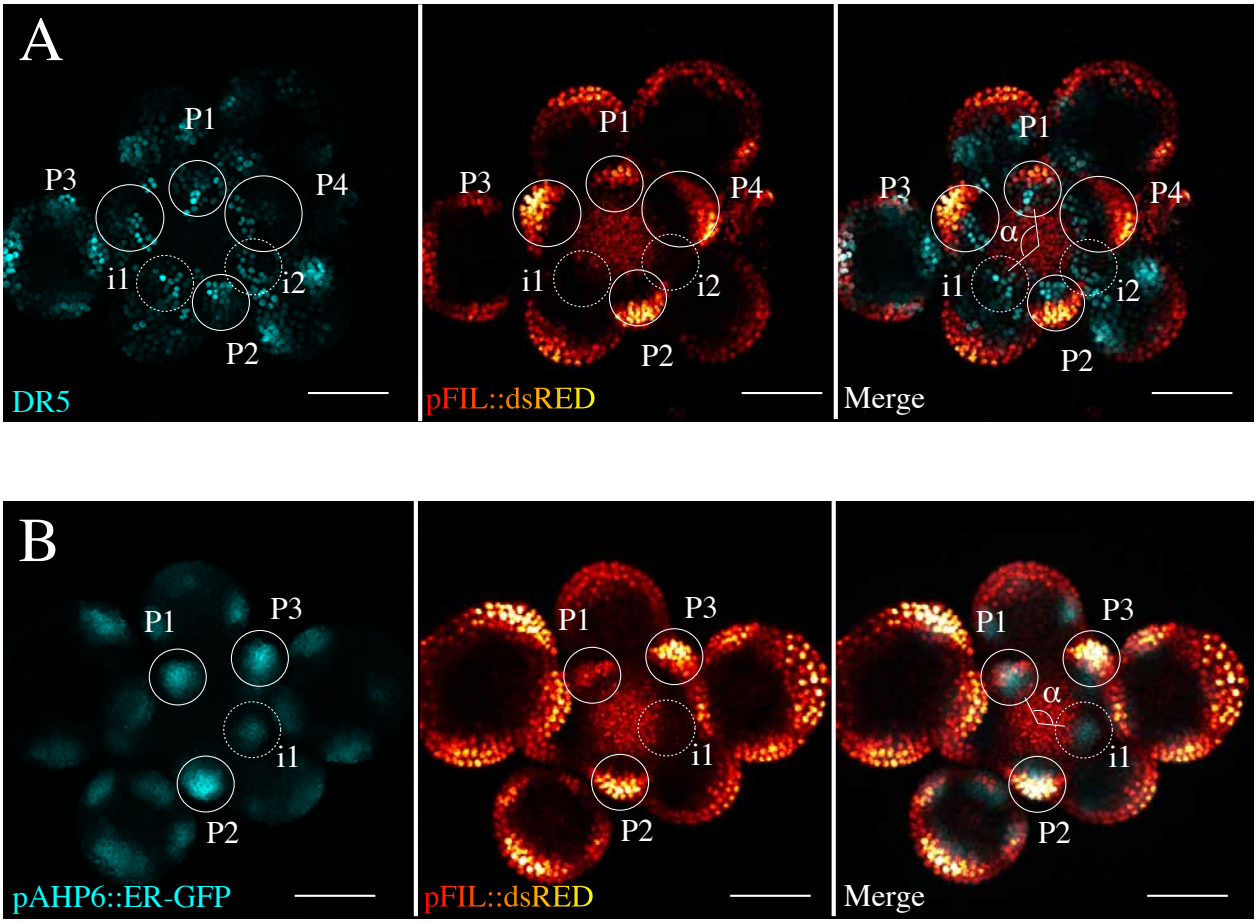

Figure I.5: *DR5, AHP6* and *FIL* transcriptional reporters activate sequencialy in wild type SAM. Confocal microscopy of wild type plants bearing the synthetic *pDR5* and the *pFIL* reporters (A) or *pAHP6* and *pFIL* reporters (B). White circles mark primordia, labelled P1, P2 onwards, according to their age from the youngest to elders. Dotted circles show initia, which are not marked by pFIL reporter. Classical 137.5° divergence angles separate two successive organogenesis, indicated here between P1 and i1. Images: Fabrice Besnard, unpublished. Scale bars=50µm.

I.B.4 – CRESCENT CLUSTERS ORIGINATE IN THE MERISTEM FOLLOWING ATYPICAL PATTERN OF ORGAN INITIATION

DRB27 initial screen with SEM identified problems in the meristem that were not likely to be post-meristematic. However, it was necessary to determine the precise timing of the formation of crescents. Indeed, either such formation followed the expected Fibonacci spiral and was modified afterwards by preferential outgrowth or development of organs in crescent-like domain; either the pattern of organ formation was modified from the beginning. To discriminate these two hypotheses, we investigated the dynamics of organogenesis at the DRB27 meristem by live-confocal microscopy with different genetic markers. *In-vitro* cultured inflorescence meristems (see methods) were imaged several times for up to 48 hours in order to observe several events of new organogenesis. To track organ formation at different stages, we introduced different genetic markers in the DRB27 strain, expressed sequentially during organogenesis.

The synthetic auxin reporter *DR5* is the earliest known marker of organ initiation and labels the site of organogenesis at the initium stage (i1), when no deformation is visible (Heisler *et al.*, 2005). One plastochron after DR5 starts the expression of *AHP6* (Besnard *et al.*, 2014). One to two plastochrons after *AHP6* starts the expression of *FIL*, localized at the abaxial side of growing primordia from P1-P2 onwards (Figure I.5; also Heisler *et al.*, 2005). A *DR5::3xVENUS-N7* reporter line and two lines bearing transcriptional reporters *promAHP6::GFP* and *promFIL::dsRED-N7*, respectively, were crossed with DRB27. To control for the differences in the genetic background between the reporter lines (all in *Col-0*) and DRB27 (in *Ws-4*), wild-type controls were taken from segregating F2 plants in each cross.

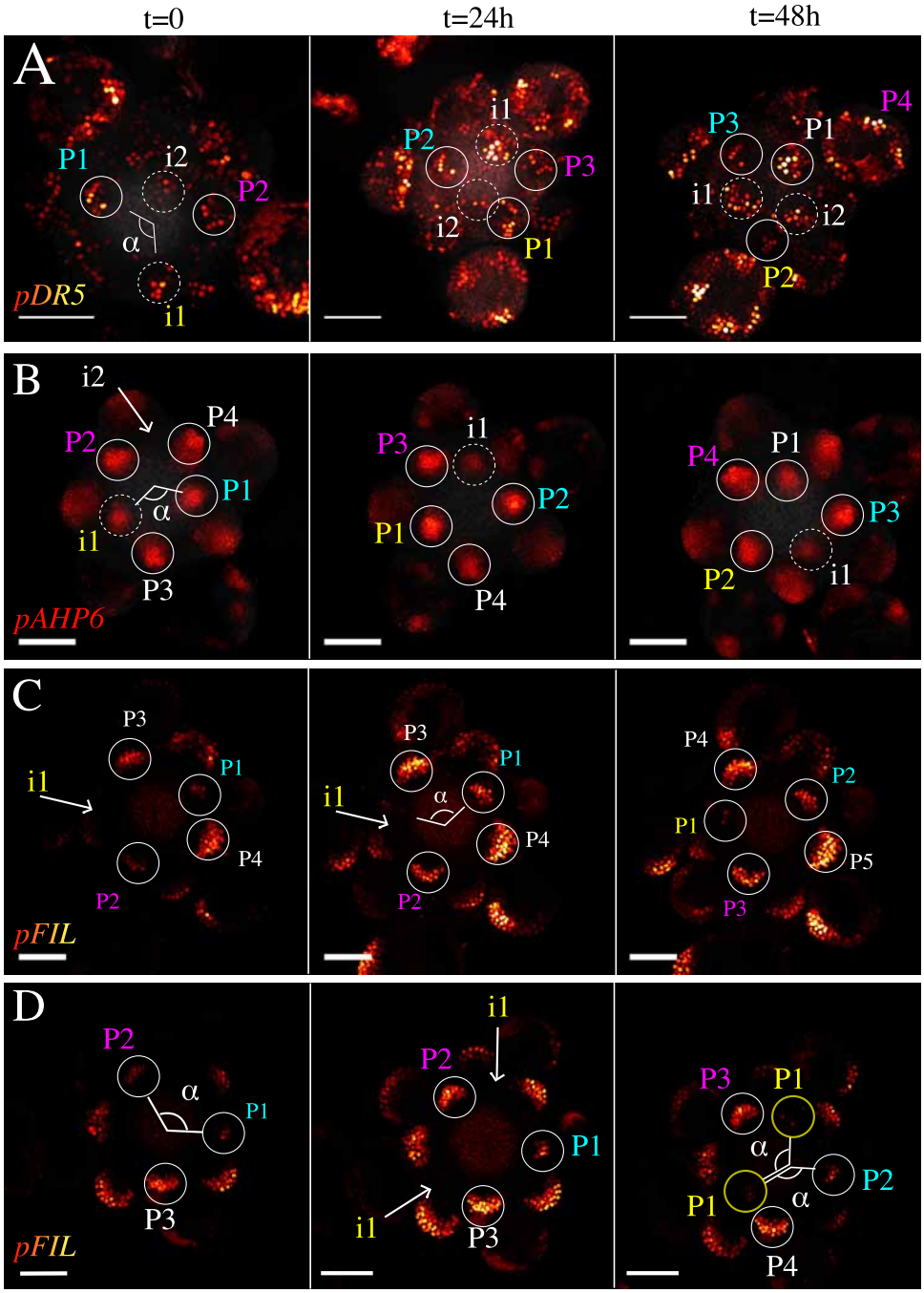

Figure I.6: Time course imaging of wild type meristems baring DR5 (A), AHP6 (B) and FIL (C-D) transcriptionnal reporters at t=0, 24h, 48h. White circles mark primordia, labelled P1, P2 onwards, according to their age from the youngest to elders. Dotted circles show initia, which are not marked by pFIL reporter, a white arrow marks the probable i1 position instead. At t=0, i1 to P2 are coloured in yellow, blue and pink respectively; organs keep their assigned colour as they shift to the next stage in the following time point. Canonical α≈137,5° divergence angles separate two successive organogenesis, indicated here between P1 and i1. Occasionaly, possible co-initiations occur (D). Scale bars=50µm.

In wild type plants, each marker activates sequentially in the peripheral zone, describing a Fibonacci spiral. As early as i2, the new initium is positioned at an angle of 137.5° from the previous organ formed, as revealed by *DR5* activation (Figure I.6.A). Organ azimuths are maintained when they grow and move centrifugally, as indicated by *de novo* activation of *prom*AHP6 (Figure I.6.B) and *prom*FIL (Figure I.6.C) at stage i1 and P1-P2, respectively. A new initium was visible approximately every 24 hours close to the centre and in the largest gap available around the peripheral zone, i.e. at approximately 137° of divergence angle, as older ones grew away from the centre. It is interesting to note that images of Figure I.5 are taken with plants of *Col-0* background whereas those of Figure I.6 are taken with segregating plants from crossings between DRB27 (*Ws-4*) and marker lines (*Col-0*). The fact that we observe very similar patterns in the two lines indicates that they are not modified between these two genetic backgrounds.

Occasionally in the wild type, two-organs formation could be observed at a given time point and following the canonical pattern with the *pFIL* marker (Figure I.6.D). We could not tell whether it was true co-initiations, or whether the time intervals were too large to temporally separate these events. However, the similar sizes of the *pFIL* domains suggest that the two primordia were of similar sizes and hence of probably the same age too. Such co-initiations of two organs have been observed and described previously in wild type plants (Besnard *et al*., 2014).

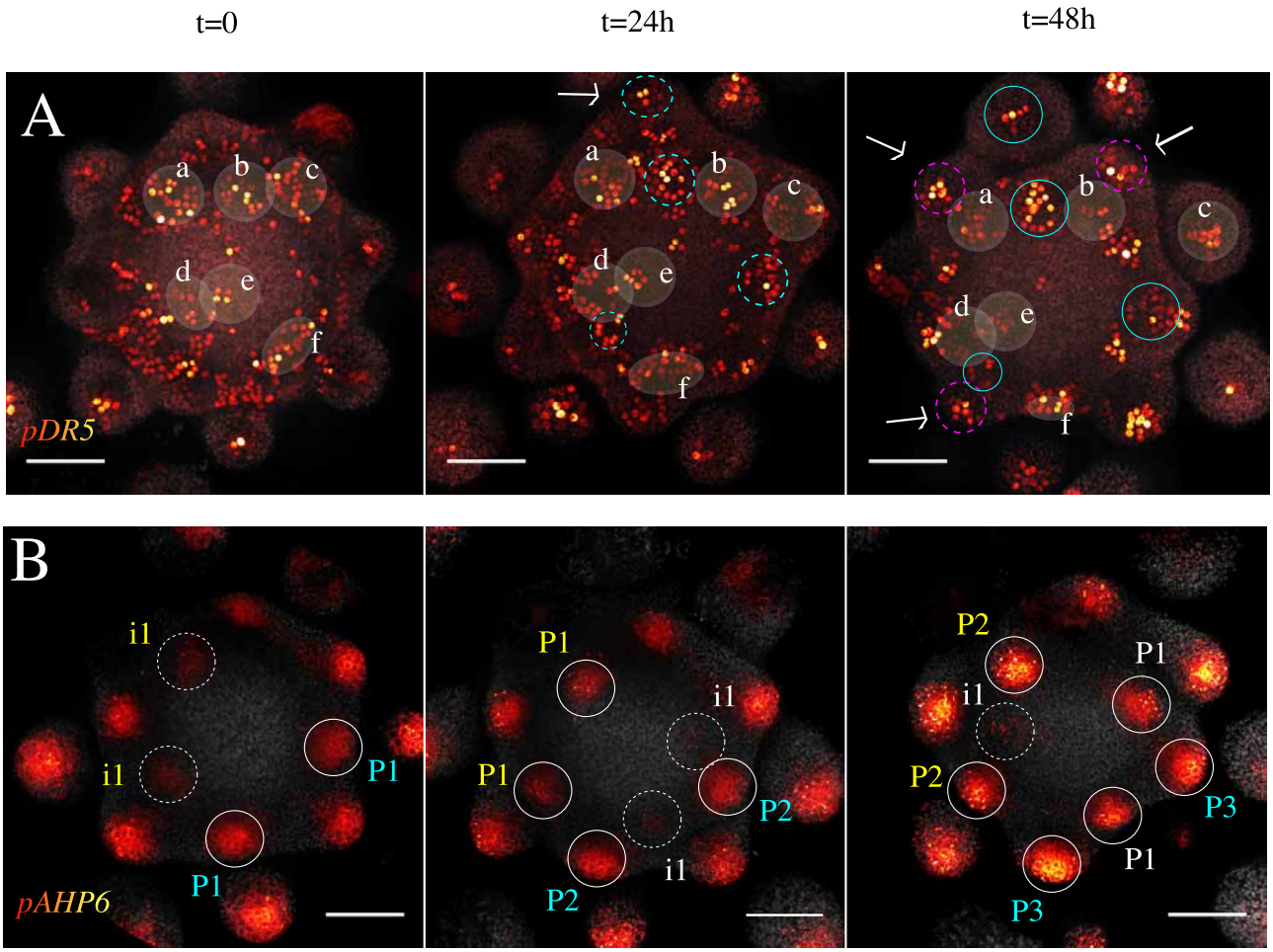

Figure I.7: Time courses of DRB27 mutant meristems expressing *DR5* (A) or *AHP6* (B) transcriptionnal reporters at t=0, 24h, 48h. A) *pDR5*. Light disc shows group of cells (labelled arbitrarily "a" to "f") to follow throughout time; dotted circles show groups of cells expressing *de novo DR5* signal; full circles follow these signals in time with the same colour code; white arrows show *DR5* signal and primordia arising from the periphery. B) *pAHP6*. White circles mark primordia, labelled P1, P2 onwards, according to their age from the youngest to elders. Dotted circles show initia, which are not marked by *pFIL* reporter, a white arrow marks the probable i1 position instead. At t=0, i1 to P2 are coloured in yellow, blue and pink respectively. All marked organs keep their assigned colour as they shift to the next stage in the following time point. Scale bars=50µm.

I.B.4.a – DIZORGANIZED AUXIN SIGNALING CONFUSE THE STARTING SIGNAL FOR ORGANOGENESIS IN DRB27

In the mutant (Figure I.7.A), meristem was crowded with cells showing *DR5* activity all across the peripheral zone, and ectopic expression was found in the centre. In this context, it was not obvious to determine which group of cells would give rise to a primordium, and to follow the route of DR5-signalling-cells in time. Nevertheless, some group of cells (examples are labelled as a to f) could be traced from t=0 according to their relative arrangement. We could then observe a distortion of growth as these groups sometimes remained at the same position in the centre ("e") or at the periphery ("a" and "b"), whereas others were pushed away to the periphery and ultimately formed separate organs ("c"). Several groups of cells showed *de novo DR5* activity after 24 and 48 hours, strikingly some of them marked already mature primordia on the outside of the meristem and outside existing signal (white arrows). Finally in this case, we identified at least seven *de novo DR5* peaks around the DRB27 meristem in 48 hours, for two in the wild type (Figure I.6.A). As this does not reflect the difference between wild type and mutant's number of organs at the scale of the whole shoot (Figure I.2.A-B), it shows that organogenesis can burst in the mutant, producing the clusters we quantified previously. Altogether these observations show disorganized auxin signalling in the shoot apical meristem of DRB27 inducing bursts of organogenesis with no sign of pattern at this stage.

The irregular presence of *DR5* signal throughout the meristem periphery without much interruption indicated that the auxin inhibitory fields were perturbed. In the shoot apical meristem, auxin peaks in developing primordia induce auxin depletion around them by cell-to-cell auxin transport, creating the auxin inhibitory field where no organogenesis can occur (Douady & Couder, 1996; Reinhardt *et al.*, 2003, Heisler *et al.*, 2005; Bainbridge *et al.*, 2008; Vernoux *et al.*, 2011). This patterning agent is a major player in phyllotaxis (see introduction) and is superimposed on another hormone-based inhibitory field, which is that of *ARABIDOPSIS HISTIDINE PHOSPHOTRANSFERASE PROTEIN 6 (AHP6)*, a cytokinin signalling inhibitor. *AHP6* was previously shown to participate in spacial-temporal robustness of the phyllotactic pattern (Besnard *et al.*, 2011), and its promoter activity was thus investigated in DRB27 (Figure I.7.B). Surprisingly, primordia were marked in the mutant

similarly as in the wild type, and did not show further perturbation than the abnormal pattern of organogenesis, which is described below with the *pFIL* transcriptional reporter.

I.B.4.b – OBSERVATION OF CRESCENT ORGANOGENESIS USING LIVE IMAGING

We monitored organogenesis using the *FIL* transcriptional reporter because it marks cells from P1 stage onwards, i.e. when the meristem surface shows a new dome-shaped deformation of the epidermis. Most of the times, the DRB27 meristems did not behave as described for the wild type in Figure I.6. We discriminated organs by range of signal sizes and distance to the centre, and named them P1, P2 (…) accordingly. Secondly, it appeared that organogenesis did not use all the space available around the peripheral zone: some domains were left idle with no organogenesis. The Figure I.8.A illustrates this phenomenon, as organogenesis occurs in the most crowded side of the meristem. In fact, half of the meristem is totally inactive although there is much space for organogenesis with less influence from elder organs in this zone, whereas organogenesis occurs on the other side where the available space is scarce. The fact that the largest gaps between organs were not the position for organogenesis, and on the contrary were idle domains of the peripheral zone, was consistent with the crescent-shaped clusters observed in section I.B.3. However, this behaviour of the meristem might as well have a pattern that is only disturbed by the presence of zones where the classical signalling does not occur. Further investigations are necessary to confirm this hypothesis: which identity do cells have in these zones? Which signal is lacking for organogenesis? It could be also interesting to use modelling to test whether such inactive zones in the meristem are sufficient to explain the angles that were measured.

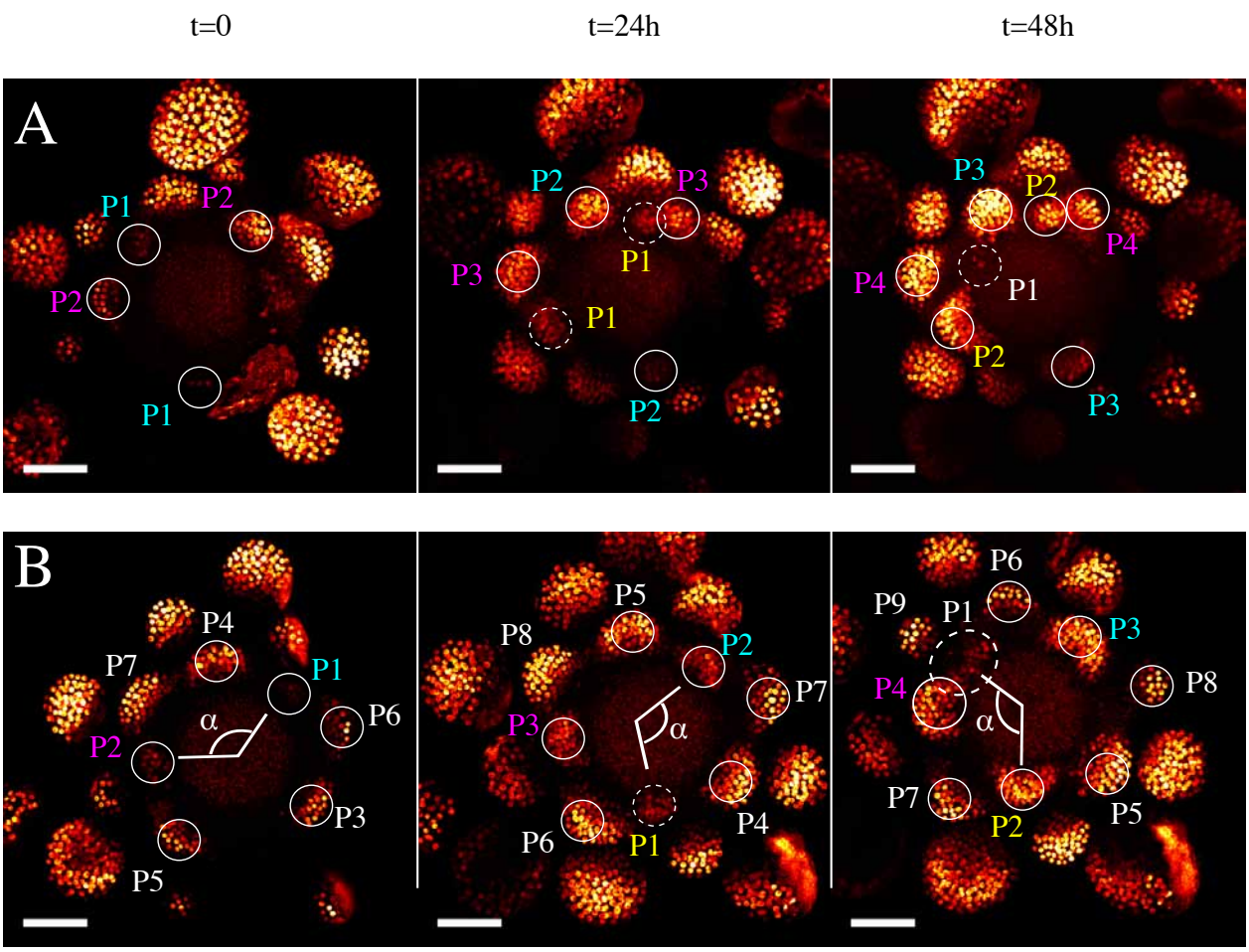

Figure I.8: Time course imaging of organogenesis in DRB27 mutant meristems expressing the *FIL* transcriptionnal reporter, at t=0, 24h, 48h. Organogenesis occurs in the most crowded space in (A) whereas classical α≈137,5° divergence angles separate two successive organogenesis in (B), indicated here between P1 and i1. White circles mark primordia, labelled P1, P2 onwards, according to their age from the youngest to elders. Dotted circles show de novo organogenesis, a white arrow marks the probable i1 position instead. At t=0, i1 to P2 are coloured in yellow, blue and pink respectively. All marked organs keep their assigned colour as they shift to the next stage in the following time point. Scale bars=50µm.

Strikingly, meristems with no such idle zone did follow the canonical pattern in terms of organ positioning. The Figure I.8.B illustrates such a meristem where elder primordia can be traced up to at least P9 at t=24h, with a constant divergence angle close to α. This was consistent with the slight preference for the golden angle observed on the shoot phyllotaxis, and quantified in Figure I.3.C, where only DRB27 angles not arranged in clusters were considered. In this case however, the peripheral zone is much more crowded with the elder organs than the wild type, indicating a different balance ratio between plastochron and post-meristematic growth, i.e. between the timing of organogenesis and the time needed to free space around the peripheral zone.

To conclude, the crescents we described earlier in Figure I.4 are most likely the result of the presence of idle zones in the meristem, which disturb classical phyllotaxis pattern. This phenomenon could be associated with the growth distortions we observed with the *DR5* reporter in Figure I.7.A. However not all organogenesis occurred this way, phyllotaxis pattern was maintained in some meristems at the moment we observed them. The DRB27 mutant phenotype is fully penetrant. Moreover clusters are found all along the shoot, and they include all the sorts of lateral organs encountered in DRB27 mutants (see next section). The fact that all organogenesis do not organize similarly confirms that 1) the phyllotaxis phenotype is not correlated with organogenesis of the arising lateral organs; 2) an occasional phenomenon may interfere with the establishment of phyllotaxis in DRB27.

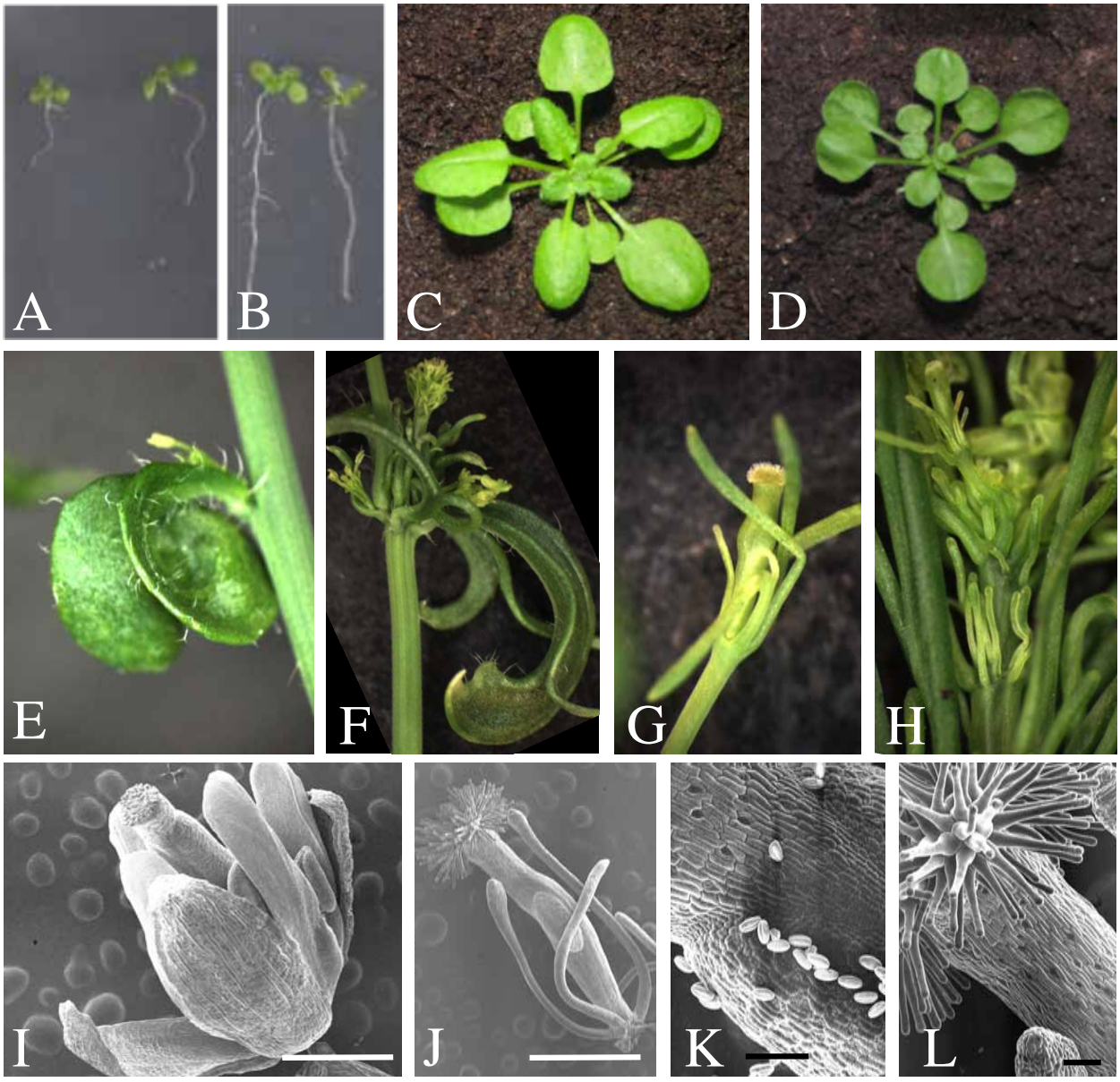
A
B
C
D
E
F
G
H
I
J
K
L

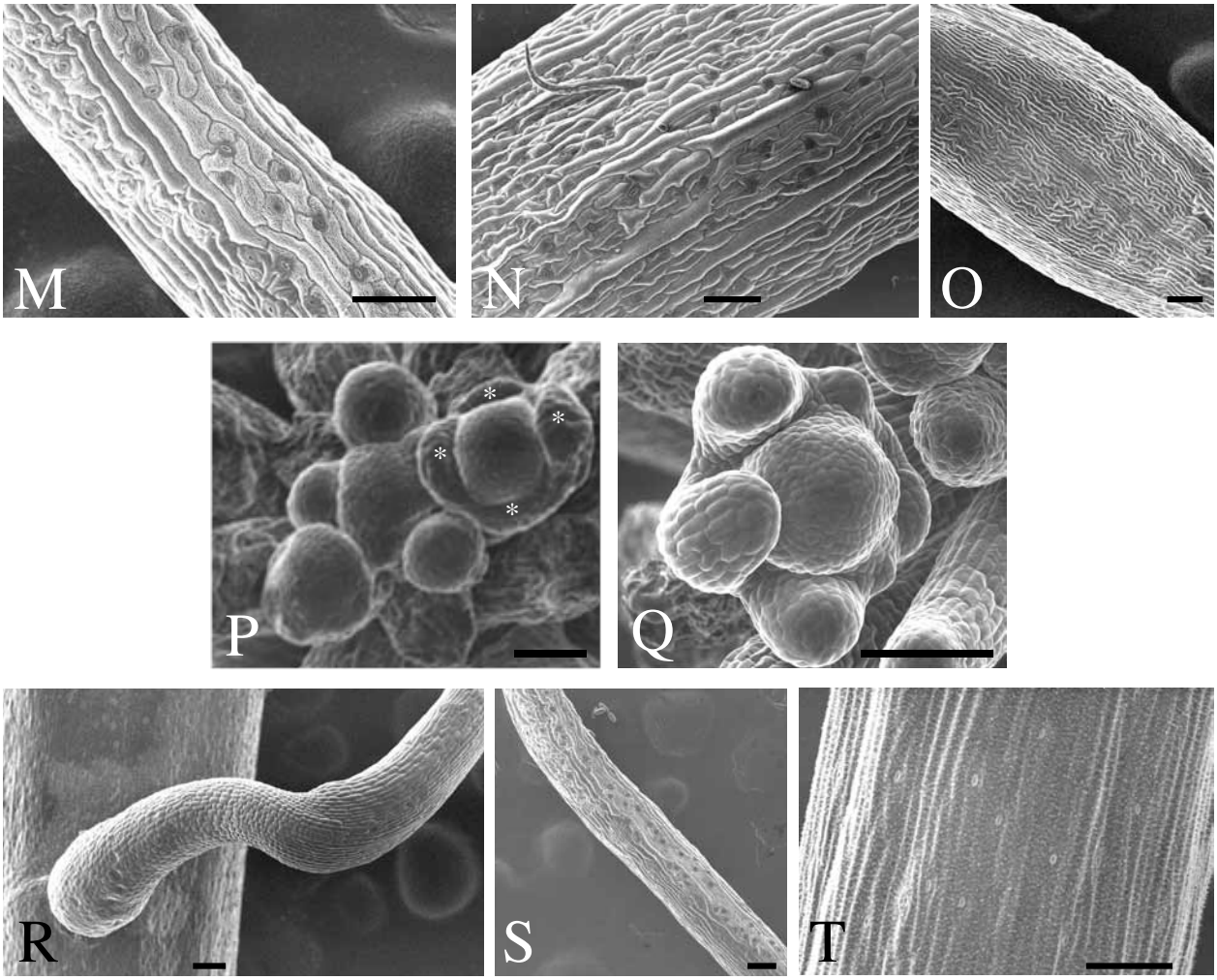

Figure I.9: Pleiotropic phenotype of DRB27 mutants. Wild type (A-C) and DRB27 (B-D) 5-days old seedlings (A-B) and 2-week old rosettes (C-D). E-H) Lateral organs produced along the DRB27 stem: curled leave (E), cluster of all sorts of lateral organs (F), abnormal flowers lacking petals and stamen (G) and radial symetry structures (H, white arrows). I-T) SEM images of wild type (I) and DRB27 (J) mature flowers; wild type (K) and DRB27 (L) carpels; DRB27 sepaloïd (M) compared to wild type adaxial (N) and abaxial (O) sides of sepals, Wild type (P) and DRB27 (Q) early flowers illustrate abnormal growth of sepals (white stars) in DRB27. Basis (R) and middle (S) of filamentous structures in DRB27 do not ressemble to wild type pedicel (T). White scale bars = 500µm. Black scale bar = 50µm.

I.C – DRB27 PRODUCES LATERAL ORGANS WITH PERTURBED ADAXIAL-ABAXIAL POLARITY

I.C.1 – DRB27 PLANTS DISPLAY PLEIOTROPIC PHENOTYPES.

Some elements of the phenotype were already visible at early stages of DRB27 development: seedlings were more vigorous and seemed to produce more lateral roots in the mutant (Figure I.9.A-B), whereas its rosette looked more juvenile and less developed than the wild type's at the same stage (Figure I.9.C-D). Indeed the wild type rosette leaves of *A. thaliana* normally are slightly hyponastic and round before elongating and growing epinastic; whereas the mutant bore persistent hyponastic rosette leaves with abnormal growth that resulted in smaller and rounder blades, similarly to the wild type's first two leaves. Bolting occurred simultaneously with the wild type when grown together in the same conditions, and cauline leaves on the contrary systematically bended downward (strong epinasty, Figure I.9.E), suggesting overgrowth of the adaxial side compared to the abaxial side.

Along the inflorescence shoot, DRB27 produced leaves with abnormal shapes (Figure I.9.E, F), abnormal flowers baring only two whorls (Figure I.9.G) and filamentous structures with radial symmetry (Figure I.9.H). As opposed to wild types, all these organs were mixed together in the clusters described in the previous section (Figure I.9.F), which was another illustration of the disturbed pattern of DRB27. Indeed this was not consistent with the regular distribution of lateral organs in fully-grown wild type shoots that restrain siliques to the upper part, and lateral meristems to the lower part of the shoot. In order to better understand how lateral organs were affected, and to better characterize filament-like structures, scanning electron microscopy study of the lateral organs epidermis was performed.

I.C.1.a – DRB27 FLOWERS LACK THE TWO B-FUNCTION WHORLS

All flowers were composed exclusively of only two whorls: carpels in the centre, and sepaloïd filamentous structures (Figure I.9.I, J) outside, the characteristic cell shapes of petal (papillae) and stamen epidermis were nowhere to be seen. Carpels epidermis looked similar to the wild type, with aligned rectangle-shaped cells regularly interspaced with stomata (Figure I.9.K, L). However they showed underdeveloped valves that were incapable of developing further after pollination by the wild type.

Sepal-like structures were of radial symmetry; their epidermis bore elongated cells interspaced with stomata and long giant cells (Figure I.9.M), and was similar to the epidermis of the abaxial side of sepals observed in the wild type (Figure I.9.I, N), but not to the adaxial epidermis (Figure I.9.O). In addition to the abaxialized sepals, another indication of abaxial/adaxial imbalance in the flowers was the overgrowth of the abaxial sepals, relatively to the meristem. Indeed in the wild type, sepals are the first floral organs to appear, in the following order: a unique abaxial sepal, then the two lateral ones, and ultimately the adaxial sepal (Smyth *et al.*, 1990; Alvarez-Buylla *et al.*, 2010; Chandler *et al.*, 2014). The four sepals then grow altogether and the adaxial sepal grows and catches up with the abaxial sepal size (Figure I.9.P). In DRB27, adaxial sepals kept a smaller size whereas the abaxial one kept growing, at the stage we observed (Figure I.9.Q). This persistent polar imbalance in the whorl formation was accompanied with the ectopic growth of small sepals on the adaxial side.

Intermediary stages of flower development could not be observed, but DRB27 flowers had only two whorls visible: carpels and narrow sepal-like structures (Figure I.9.G, J). Homeotic mutants impaired in the B-function, which specifies petals and stamens, usually display a conversion of inner whorls into sepals and carpels. Hence, the absence of whorls n°2 and n°3 shows that DRB27 flowers produce less organs and suggests a mis-regulation of stem-cells renewal and /or floral meristem size rather than a direct perturbation of the B-function.

I.C.1.b – FILAMENTOUS STRUCTURES GROW ALL ALONG THE STEM

Similar structures were previously described in literature as flowerless pedicel (Chen *et al.*, 1999), undeveloped flowers (Sawa *et al.*, 1999) or bracts (Lugassi *et al.*, 2010). Our SEM observations of their epidermis revealed a more complex identity. At the basis, rectangular cells were tightly packed and aligned with scarce interspaced stomata at the basis (Figure I.9.R). Then a transition, sometimes accompanied with a torsion and formation of an angle that shifted the orientation of the filaments from diagonal to upward (Figure I.9.R), led to a differently structured epidermis that was similar to the abaxialized sepaloïd filaments observed in DRB27 flowers, with elongated cells interspaced with stomata and long giant cells (Figure I.9.S).

Comparison of these filaments with other lateral organs in the wild type and DRB27 highlighted that the basis of the filaments wasn't similar to any other type of organ's, not even a pedicel, which epidermis was very similar to that of a stem of both wild type and mutant (Figure I.9.T). We concluded that the identity of the filaments could not be simply deduced from the epidermis and should be considered as a completely new structure that mix original features with some abaxial-like elements.

I.C.2 – GENE EXPRESSION IN DRB27 INFLORESCENCE MERISTEM INDICATE UNDERDEVELOPED STRUCTURES

To describe further how abaxial-adaxial polarity was affected in the mutant, polarity gene expression was assessed in the meristem and early flowers. We chose for adaxial markers the five HD ZIP III transcription factors, *i.e. PHABULOSA (PHB), PHAVOLUTA (PHV), REVOLUTA (REV) ATHB8* and *ATHB15* (also called *CORONA*). They are expressed in the early developing flowers and are repressed on the abaxial side by the micro RNAs 165 and 166. These micro RNAs are composed of nine members, two *MIR165* with identical mature sequence, and seven *MIR166* also with identical mature sequence, the two groups only diverging from one nucleotide (Jung *et al.*, 2007). Although specificity mechanism of HD ZIP III regulation by these miRNAs is not clear yet, *MIR166A* was shown to repress more

drastically *ATHB15* and *PHV* in aerial parts of Arabidopsis (Kim *et al.*, 2005), or *PHV* and *PHB* in wheat germ extracts (Tang *et al.*, 2003), and overall HD ZIP III regulation was shown to be mediated by spacial-temporal sequestration of these MIR (Zhou *et al.*, 2015). In DRB27 meristems, expression of *MIR166A* and HD ZIP III genes were not much perturbed, with p-values indicating non-significant differences (NS, Figure I.10).

Other abaxial markers were chosen with *KANADI1 (KAN1), FILAMENTOUS FLOWER* (*FIL*, or *YABBY1*, *YAB1*) and *YABBY3 (YAB3)*. Whereas the first could not be considered as significantly downregulated (p-value=0,77), two other abaxial markers tested here were downregulated in DRB27 compared to controls. Indeed, *FIL* and *YAB3* RNAs were in respectively 2,45 and 4,09 times lower quantities in DRB27 than in the control, with significantly low error probabilities of 0,03 and 0,009 respectively. This was consistent with the fact that the phenotype shared similarities with that of *fil* alleles (see next section). Noticeably, the expression pattern of the *FIL* transcriptional reporter we discussed in the section I.B.4.b (Figure I.8) was strong and ectopic in the lateral organs, which indicates the presence of a feedback on *FIL*.

Altogether these results indicated a rather adaxialized identity of the meristem and surrounding lateral organs. This was consistent with the epinastic leaves we observed along the shoot (Figure I.9.E). However, how could we reconcile these molecular data with the apparent abaxialization of epidermis in sepaloïds and at the tip of filaments? (Figure I.9.M) Since growth is known to proceed from the abaxial side in early stages of floral development (Sawa *et al.*, 1999; Eshed *et al.*, 1999, 2001; Kwiatkowska *et al.*, 2006), DRB27 sepaloïds and filaments could be seen as underdeveloped structures, resulting from impaired inter-regulation of polarity factors. As described in section III.B of the introduction, polarity genes from both abaxial and adaxial sides are closely regulated, and downregulation of abaxial markers results in developmental defects. In the filaments, the flower formation may be limited to its stage 1, i.e. the formation of the abaxial sepal. At stage 1 of flower development, the two B-function floral genes APETALA3 and PISTILATA are not yet induced (Weigel & Meyerowitz, 1993; Parcy *et al.*, 1998), and therefore cannot induce the formation of petals and stamen. In this point of view, the apparent adaxialisation would be the result of underdevelopment rather than polarity problem.

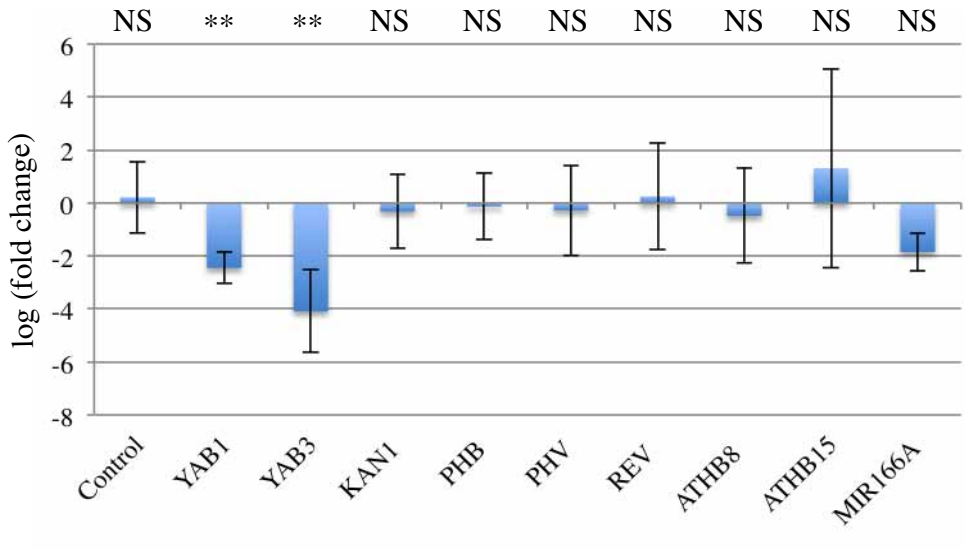

Figure I.10: relative polarity gene expression in DRB27 meristems compared to wild type. *AT1G04850* housekeeping gene is used as control. pvalues, from left to right: 0.9; 0.03; 0.009; 0.77; 0.9; 0.8; 0.8; 0.7; 0.4; 0.25

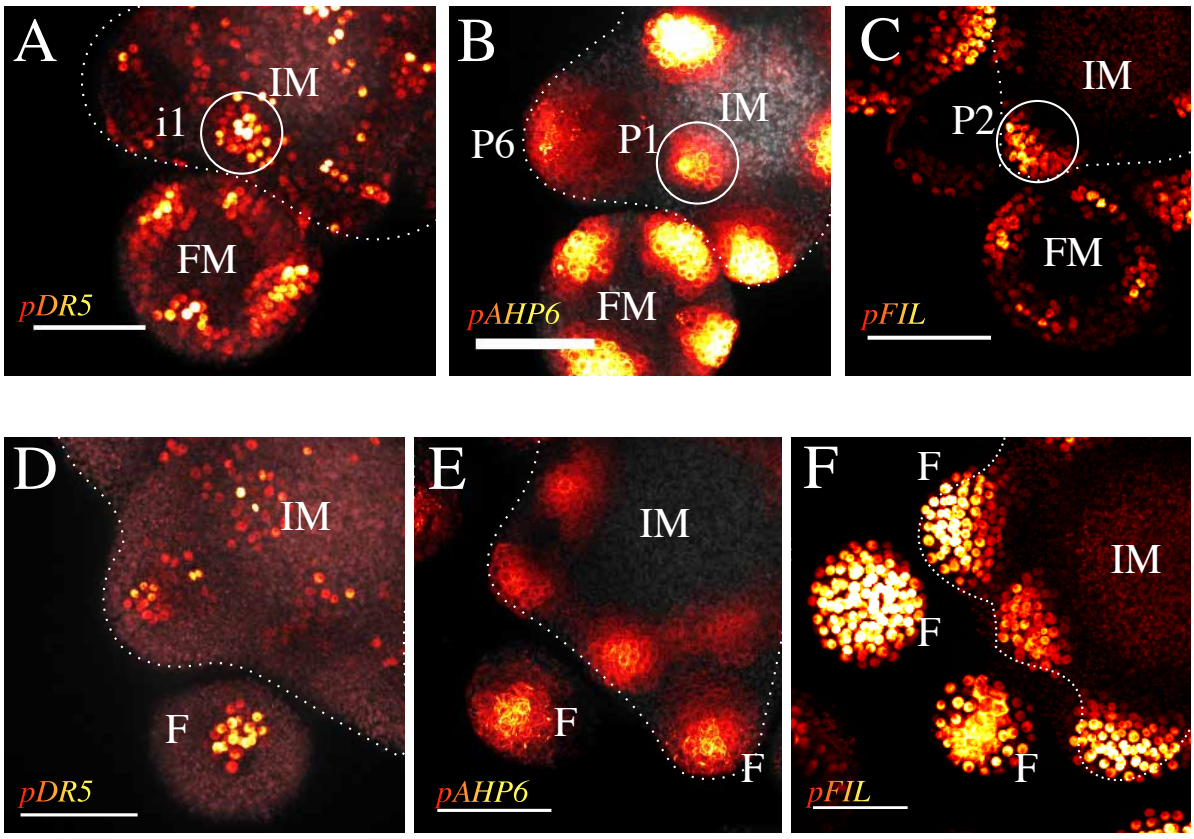

Figure I.11: Growing filaments around the shoot apical meristem show juvenile characteristics. Wild type (A-C) and DRB27 (D-F) imaging of early lateral organs in confocal microscopy, using the *DR5* (A, D), *AHP6* (B, E) and *FIL* (C, F) transcriptional reporters. IM = Inflorescence Meristem, FM= Flower Meristem, F=Filament. Dotted lines show the inflorescence meristem periphery. Scale bars= 50µm.

The observation of the *FIL, AHP6* and *DR5* markers described in Figures I.7 and I.8 also drew our attention on the many filaments that the DRB27 mutants produced around the stem, and described in section I.C.1 of the results. These three markers are expressed in sepal primordia during early flower development, and not in the centre of the flower meristem (Figure I.11.A-C). The expression domains in the flowers were not that of the wild types. The DRB27 lateral organs only displayed *DR5* activity in a small central group of cells, similarly to a primordium (Figure I.11.D). Similarly, the pAHP6 signal in the DRB27 filaments remained that of a growing primordium, with no sign of sepal formation (Figure I.11.E). As AHP6 is an early marker for organogenesis, this pattern may be associated with juvenile structures in DRB27. Interestingly in the lateral organs, whereas the *FIL* domain looked similar to the wild types in early stages of primordium development in DRB27 (crescent-shaped signal on the abaxial side of the primordia), it showed a strong expression throughout all lateral organs instead of being restricted to abaxial side of sepals as in the wild type (Figure I.11.F). This showed that no dorso-ventral pattern was clearly defined in the DRB27 filaments.

Altogether these markers behaviours are consistent with the hypothesis that filaments are underdeveloped structures that fail to differentiate into functional organs, as suggested by our phenotypical analysis (section I.C.1). The fact that flower development was shown to start from the formation of a rudimentary bract on the abaxial side of primordia (Kwiatkowska *et al*., 2006; Chandler & Werr, 2014) further supports the role of abaxial regulators such as FIL and MIR166A in early stages of flower development. Moreover, as demonstrated in the section III.B of the introduction, the establishment of polarity, and molecular crosstalk with polarity regulators is crucial for the shoot apical meristem functioning, which would thus be impaired when producing such under-developed organs.

I.C.3 – SIMILARITIES BETWEEN DRB27 AND FIL MUTANTS

An intriguing feature of this mutant was its strong phenotype similarities with that of mutant's alleles of *FILAMENTOUS FLOWER*. The DRB27 aberrant flowers showing only carpels surrounded by sepal-like structures, and the many-filamentous structures observed along the DRB27 shoot and around its meristems, where very similar to what was previously

described as type A and B flowers in *FILAMENTOUS FLOWER* strong mutant alleles, i.e. aberrant flowers with homeotic changes and filaments respectively. The three most described *fil* mutants are shown in Figure I.12: *fil-1* from Sawa *et al.*, 1999; *fil-5* from Chen *et al.*, 1999; *fil-9* from Lugassi *et al.*, 2010. An additional *fil* allele was recently described in a *brevipedicellus* mutant of the *Ler* genetic background with similar features (Douglas *et al.*, 2017). All mutant lines mentioned in the literature are summed up in Figure I.13 (Sawa *et al.*, 1999; Chen *et al.*, 1999; Lugassi *et al.*, 2010; Douglas *et al.*, 2017). Regrettably, phyllotaxis was not precisely described in these mutants, and no quantification of divergence angles or organogenesis monitoring can be found in the literature. Nevertheless scanning electron microscopy was performed, showing some *fil* meristems with clear spirals (Figure I.12.C, F, I). The one showing the closest phenotype to that of DRB27 mutants was *fil9*; but it showed a high variability in floral phenotypes, and its reporter phyllotaxis defects were not fully penetrant as they appeared only in late developmental stages. Nevertheless, all these lines show aberrant flowers and filamentous structures, similarly to DRB27; this suggests that the phyllotaxis phenotype of the DRB27 mutant could not be simply the result of a change in ad-abaxial polarity in lateral organs, although analysing phyllotaxis in a variety of mutants affected in ad-abaxial polarity would be required to clarify this point.

To conclude, DRB27 showed a strong and pleiotropic phenotype. Some of its aspects, such as the similarities with the *fil* phenotype, the many filamentous and undefined structures surrounding the meristem and the curled morphology of the leaves, constituted hints that DRB27 mutants were afflicted with identity or polarity defects. These defects were genetically linked with the phyllotaxis phenotype that interested us, as they segregated together in DRB27, but were not necessarily linked with phyllotaxis in the literature. The loss of polarity and the phyllotaxis phenotype in DRB27 could be due to a same gene acting in the two processes, but the question remains of whether the loss of polarity perturb the regular spacing of organs into Fibonacci spirals, or are these phenotypes mechanistically unlinked?

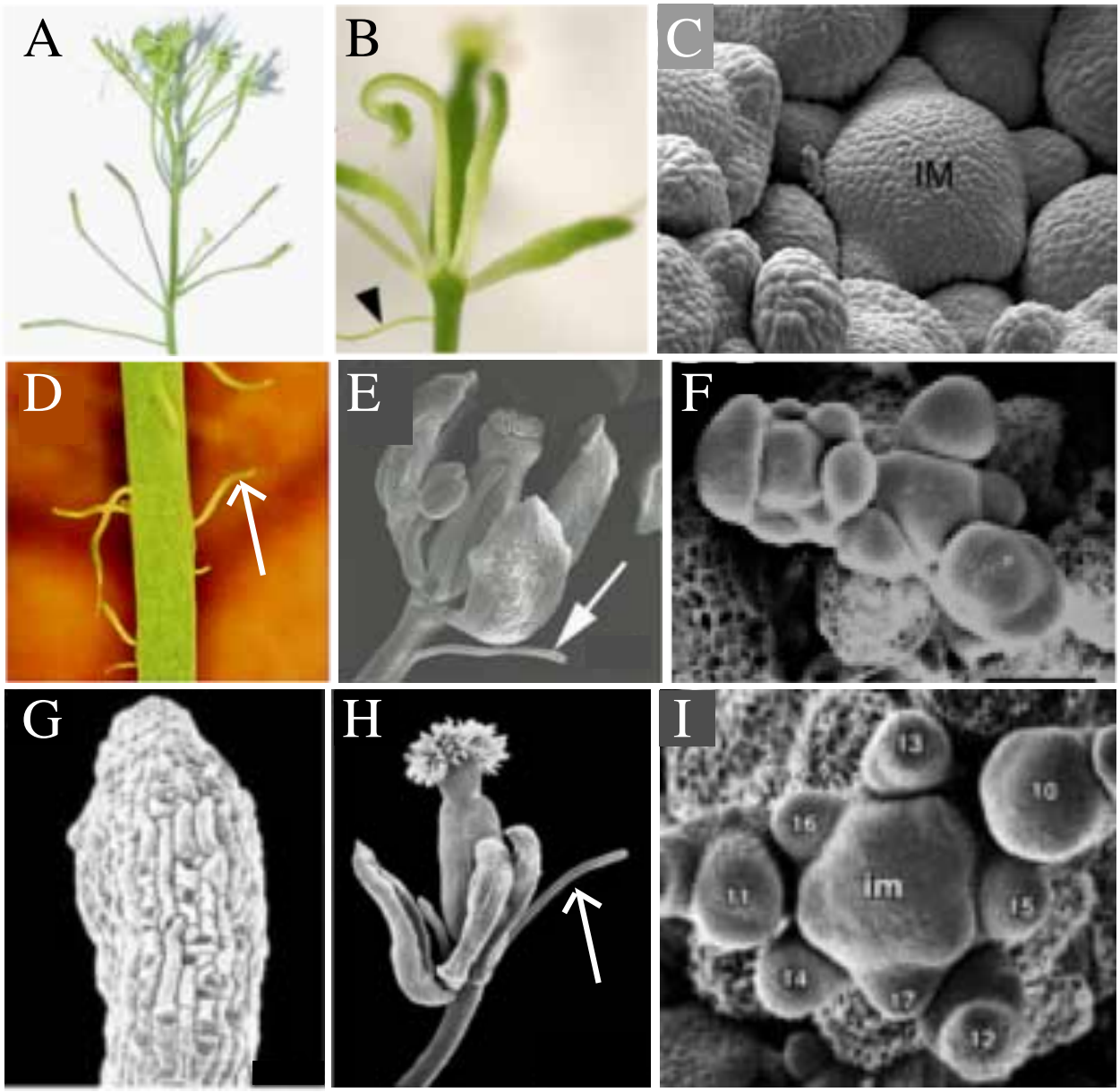

Figure I.12: *fil* strong alleles show filamentous structures and abnormal flowers but not necessary disturbed phyllotaxis. A-C) *fil9*. D-F) *fil1*. G-I) *fil5*. All three alleles show aberrant flowers with homeotic changes, with sepal-like structures and filaments (B, E, H). Although one shows aberrant phyllotaxis from the meristem (A-C), others have spiraled phyllotaxis at the meristem (F, I). Arrows show filamentous structures, with a close-up on their typical tip in G.

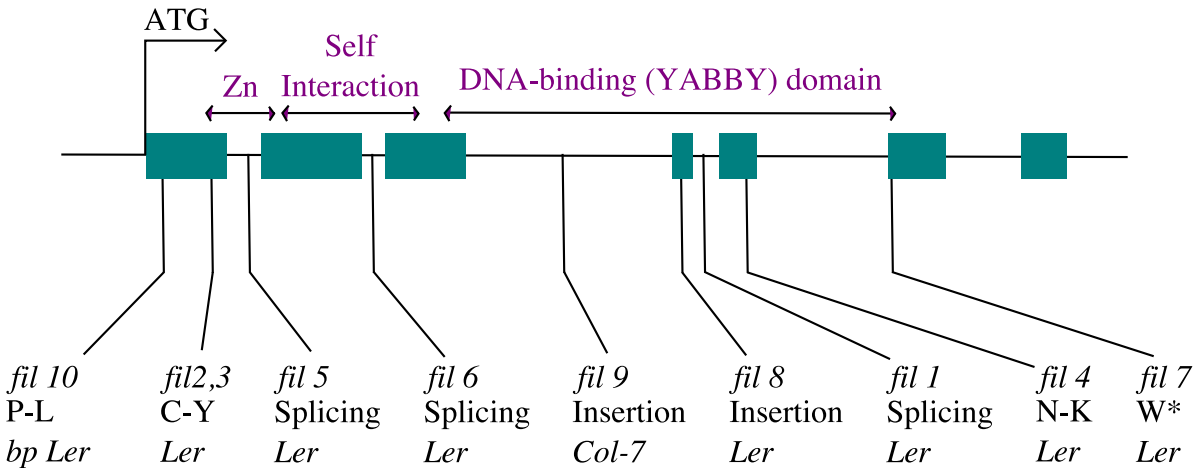

Figure I.13: The *FIL* gene contains 7 exons, and 10 alleles are mentionned in the litterature. Functional domains are indicated above. For each allele (1-10), the mutational event and the genetic background are indicated. Splicing = new splicing acceptor site. Insertion = T-DNA insertion. The alleles mentionned in Figure I.11 fall into the Zinc finger domain (*fil5*) or the DNA binding domain (*fil 1*, *fil9*).

II – IS DRB27 A FIL MIR166A DOUBLE MUTANT?

II.A – DRB27 IS A RECESSIVE SINGLE-LOCUS MUTANT MAPPING AT THE END OF CHROMOSOME 2.

II.A.1 – IDENTIFICATION OF AN INSERTIONAL MUTATION NEAR ATG8E

The DRB27 line is an insertion mutant isolated from an agrobacterium random mutagenesis on a *Ws-4* genetic background, with the binary vector pGKB5 as the T-DNA insert (see methods). Since T-DNA insertion in the gene-coding locus can disrupt the gene's function, the precise locus of T-DNA insertion is the first obvious candidate mutation responsible for the phenotypes isolated from the mutagenesis.

To locate T-DNA insertion, we performed selective PCR on T-DNA flanking regions, a strategy described by O'Malley et al. (2007). This method enables to directly sequence the junction between T-DNA borders and genomic DNA after a selective amplification of this sequence through an adapter ligation-mediated PCR (see methods). This strategy is efficient to map a single insertion event but was not designed for complex situations (T-DNA inserted in a complex manner lacking borders, like tandem or partial inserts).

Adapter ligation-mediated PCR yielded a single band, which sequence matches the right border of the pGKB5 T-DNA and the promoter of *AUTOPHAGY RELATED PROTEIN*

8E (*ATG8E, AT2G45170*), a gene positioned at the end of chromosome 2 (Figure II.1.A). Genotyping analysis showed that only plants homozygous for this insertion showed the DRB27 phenotype (Figure II.1.B), confirming that the DRB27 phenotype was recessive and monolocus (see section I.A and Table I.A). Gene expression analysis showed that *ATG8E* was down regulated in DRB27 (Figure II.1.C) with 2,89 times less mRNA than the wild type (pvalue=0,049).

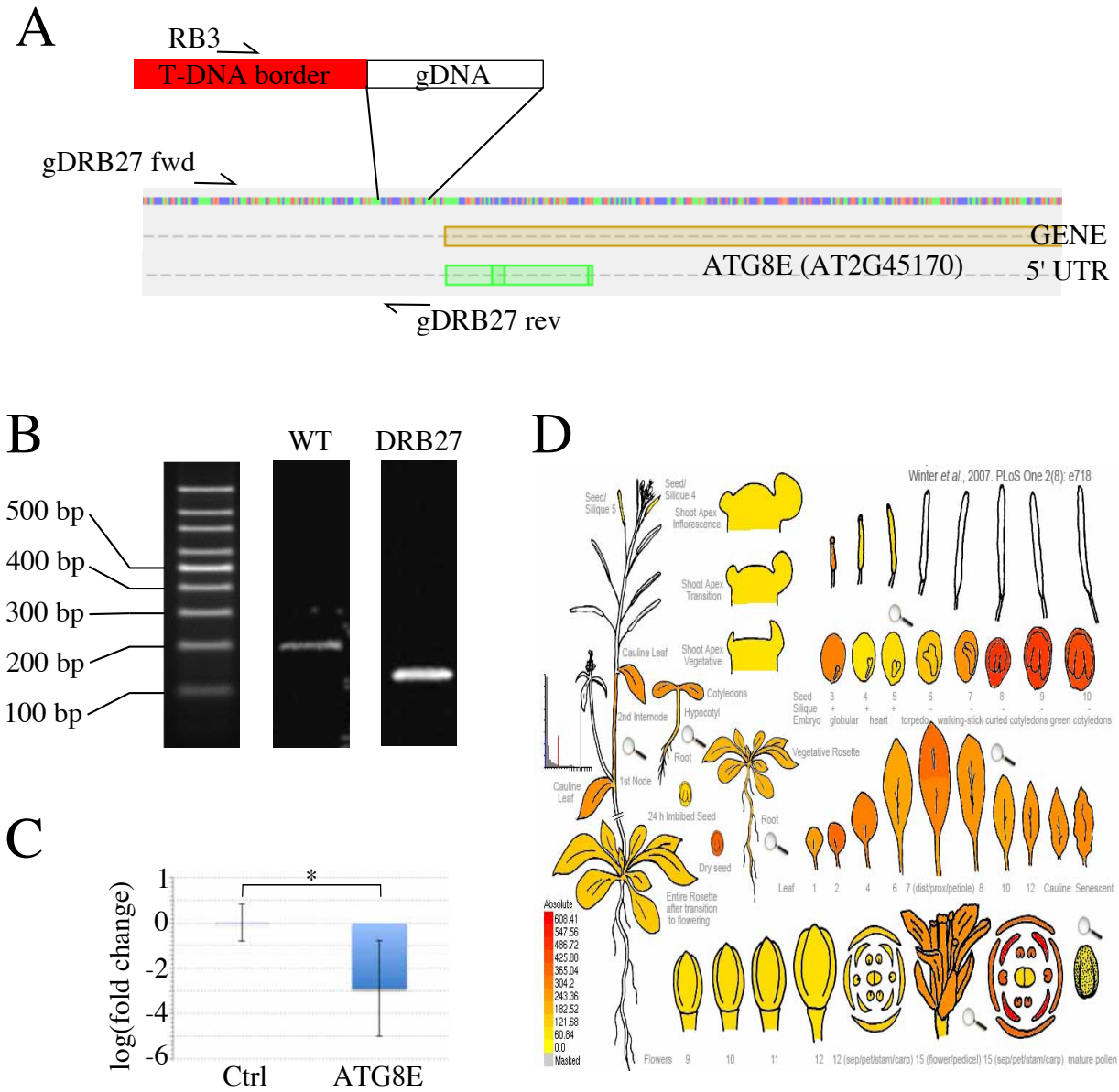

Figure II.1: Identification of ATG8E as a candidate gene responsible for the DRB27 phenotype. A) The ATG8E locus in DRB27 was identified by adapter ligation-mediated PCR (see methods; Figure M.2) and controlled with independant primers gDRB27 forward (fwd) and reverse (rev), and the T-DNA border primer RB3. B) PCR products on 2% agarose gel shows theapproximately 200 bp band for wild type, and 150 bp band for T-DNA insertion. C) Gene expression analysis confirms ATG8E misexpression in DRB27. pvalue=0,048 D) eFB Browser expression data for ATG8E shows weak expression in the shoot apical meristem and early flowers.

II.A.2 – IS DRB27 AN ATG8E LOSS-OF-FUNCTION MUTANT?

ATG proteins are described as acting during macro-autophagy, a cellular recycling function based on membrane trafficking and involved in stress responses as well as cellular housekeeping. A double membrane, called phagophore, expands and engulfs portions of the cytoplasm to deliver it to the vacuole. The core mechanism consists in an ubiquitin-like conjugating system composed of ATG proteins, where ATG8 is the membrane anchor that expands the phagophore and connects it to recyclable targets (reviewed by Wesselborg *et al.*, 2015; Michaeli *et al.*, 2015). In yeast, ATG8 is a single protein whereas in plants, ATG8 proteins compose a multigenic family of 9 members with up to 99% homology (Katelaar *et al.*, 2004) and thus high-expected redundancy. To our knowledge, their function has not been linked to developmental patterning in the literature. Neither functional difference between ATG8 proteins nor phenotype like the one described for DRB27 have been reported, as the classical phenotype for *atg* mutants is normal growth under favourable conditions and hypersensitivity to starvations (Michaeli *et al.*, 2015), and functional overexpressors displayed normal growth (Contento *et al.*, 2005). Moreover, available data on *ATG8E* gene expression in development (weak in shoots and induced by starvation stresses, Slavikova *et al.*, 2005) doesn't support a role of the protein in the shoot apical meristem (Figure II.1.D).

ATG8E is an unexpected candidate gene with low support from literature and available mutants. In addition, the insertion *locus* is surrounded by loci coding for transcription factors acting in shoot apical meristem development, such as the GRAS family-member *HAIRY MERISTEM (ATHAM1;* Schulze *et al.*, 2010) at a 4,2 Kb upstream distance, and the YABBY family-member *FIL (*Sawa *et al.*, 1999) at a 4 Kb downstream distance. Considering the problem of adaxialization and the impaired expression of *FIL* reported in DRB27 (see phenotype description in section I.C), we suspected that another or several mutations closely linked to the T-DNA inserted in *ATG8e*, for example in the *FIL* locus, could cause the DRB27 phenotype, either alone or in combination. Before undertaking further experiments to validate the candidate gene *ATG8e*, we re-sequenced the DRB27 strain to analyse its mutational landscape.

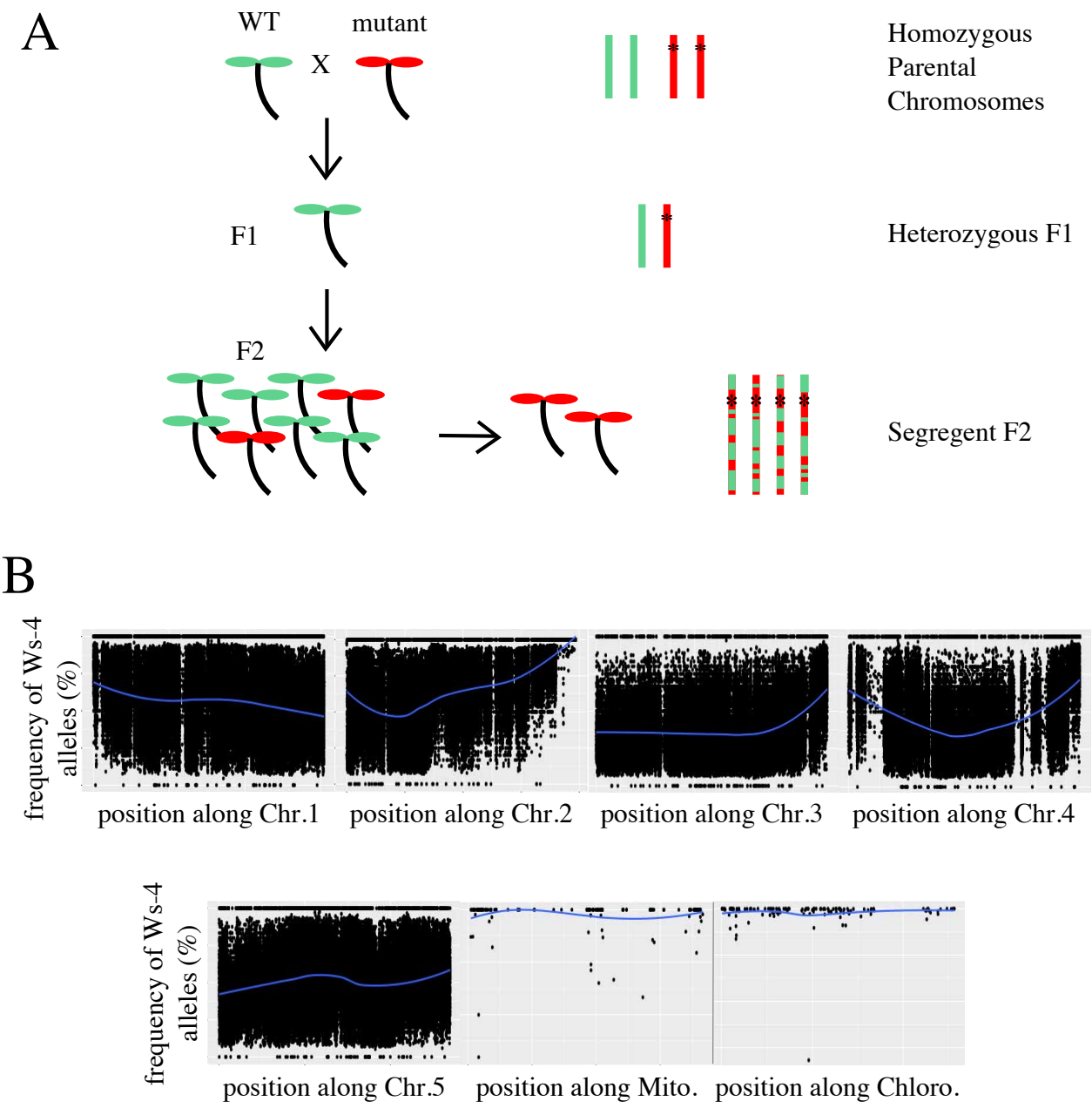

Figure II.2: Bulk segregent analysis of DRB27. A) Principle of the method: an homozygous polymorphic wild type mapping strain and the recessive mutant are crossed, and mutants from segregating F2 population are sequenced in bulk. Crossing-overs performed in F1 germinal cells produce sets of allele combinations in F2 that keep half of each parent's genomic background. The mutation and its genetic region are conserved from the mutant parental line in every F2 individuals that present the mutant phenotype. B) *Ws-4* variant frequencies along the five Arabidopsis chromosomes, mitochondrial DNA and chloroplastic DNA, in mutants from segregating F2 population of outcross with *Col-0*. The end of chromosome 2 shows 100% *Ws-4* alleles. Blue lines are a local regression (LOESS) of the *Ws-4* variant frequency.

II.B – MAPPING-BY-SEQUENCING IDENTIFIES SEVERAL CANDIDATE MUTATIONS IN THE DRB27 STRAIN

II.B.1 – MAPPING-BY-SEQUENCING ALLOWS MAPPING, IDENTIFICATION AND SELECTION OF THE BEST CANDIDATE MUTATIONS.

Whole genome re-sequencing can potentially identify all mutations in the genome, like T-DNA insertions, SNPs, InDels or even complex rearrangements (copy number variations, inversions, etc.); it should then be sufficient to pinpoint all mutations present in the genome of the DRB27 mutant. However, the causal mutation can easily be missed by just a re-sequencing of the mutant strain. First, due to bias in the sequencing strategies and the downstream variant analysis programs, SNPs and small InDels are much easier to identify (Pabinger *et al.*, 2014; Pirooznia *et al.*, 2014). Second, the genetic background of the strain DRB27 is *Ws-4*, a natural accession with high genetic divergence from the reference genome published, *Col-0*, and from other *Ws* accessions (Păcurar *et al.*, 2012). This difference of genetic background can produce many false or true positives during variant analysis. Third, T-DNA mutation lines can be amplified for many generations for selection and maintenance: they can accumulate a certain number of random variations by drift (Ossowski *et al.*, 2014), which will not be responsible of the selected phenotype of the mutant.

To maximise our chances to identify the true causative mutations, we chose a mapping-by-sequencing approach (Schneeberger K. *et al.*, 2014). Briefly, this method consists in bulk-sequencing a F2 population bearing a recessive mutant phenotype. F2 mutants are obtained from a cross with the original mutant strain and a genetically divergent strain, non-mutant and polymorphic at many sites throughout the genome (called a mapping strain). In such a pool of F2 mutants, polymorphic sites that are not linked to the causal mutations are expected to segregate randomly: the alleles that distinguish the two parental strains will be sequenced at equal frequency. However, if polymorphic markers are linked to

the causal mutations, the alleles corresponding to the mapping strain will be counter-selected in the F2 mutant pool and their frequencies will decrease close to the causal mutation, down to zero immediately around it (Figure II.2.A). Whole-genome analysis of the allelic proportion of polymorphic markers between the mutant and the mapping strain thus map the region genetically linked to the causal mutation. As a consequence, only the mutations found in this mapping interval are relevant candidates, filtering out many false positive genomic variants. Conversely, if no mutations stand out in this interval, further efforts can be spent on this region to discover complex mutations missed by classical variant analysis.

In practice, we performed the analysis of our mapping-by-sequencing approach as follows:

- First, we mapped the mutant interval thanks to the variations introduced with a mapping strain (here *Col-0*).

- Second, we analysed all mutations present in this mutant interval in the DRB27 strain.

- Third, we designed a program to specifically track T-DNA insertion sites (since these long insertion events were missed by the variant caller).

II.B.2 – THE DRB27 PHENOTYPE MAPS AT THE END OF THE CHROMOSOME 2

As DRB27 mutants were sterile, we crossed heterozygous DRB27 fertile plants with the reference accession *Col-0*. Seven F2 mutant plants were selected and their DNA sequenced in bulk after equimolar pooling (*Ws-4* accession was also re-sequenced in parallel, see methods). A 500-bp insert library was paired-end sequenced by Illumina sequencing to produce 150-bp reads at an expected coverage of at least 15X. After quality checks and mapping, the actual average coverage reached 10.2X and 13.9X for *Ws-4* and DRB27 respectively.

We first used whole-genome sequencing data of *Ws-4* wild-type strain to define a high-confidence set of 744,639 polymorphic SNPs with *Col-0* (one SNP every 160 bp on average). Then, from bulk sequencing of F2 DRB27 mutants, we computed the proportion of

Ws-4 and *Col-0* alleles for each markers of this dense set along the five nuclear chromosomes and along the mitochondrial and chloroplastic genomes (Figure II.2.B). Despite an important variability in allele proportions between markers, a local regression of the plot (loess) clearly identifies a mapping interval at the end of the chromosome 2, where the allele frequency of the mutant background *Ws-4* peaks toward 100%. Elsewhere in the nuclear genome, the local regression sometimes deviates from 50% (expected for unlinked regions) but it never indicates region of pure *Ws-4* background. The high variability of the allele frequencies is likely a result of the small number of F2 plants pooled in our mapping population. More F2 individuals increase the number of independent crossing over at meiosis and average out allele frequencies at each position, so that proportions of both parental alleles are close to 50% away from the selected mutations. Moreover, increasing F2 numbers is also expected to narrow down the mapping interval. However, the coverage needs to increase accordingly to at least twice the number of F2s, so that sequencing reads can statistically represent all information from each diploid genome. Further assays will be needed to find the best compromise between coverage (hence sequencing cost) and quality of the mapping.

Despite these limitations, our data define a ~1,7 Mb mapping interval at the end of the chromosome 2. This interval contains *ATG8e* coding sequence, partially confirming the results obtained by adapter-ligation-mediated PCR (see above, II.A.1, Figure II.1).

II.B.3 – DRB27 MAPPING INTERVAL CONTAINS MUTATIONS UNRELATED TO T-DNA INSERTIONS

To identify all possible mutations in the mapping interval, we first selected homozygous variants from the mutant F2 sequencing data, a requirement for a recessive causative mutation. Chromosome 2 only bore 247 homozygous variants and only 61 fell in the DRB27 mapping interval. We then assessed the putative functional impact of each mutation with a variant annotator (SnpEff, see Methods), which classifies them into four categories of deleteriousness according to their predicted impact: "high" (the mutation disrupts the amino acid sequence of a protein-coding gene), "moderate" (non-disruptive change in a protein-coding sequence, like amino-acid substitution or in frame InDel) "low" (e.g. synonymous variants) (see methods for a detailed description about the classification of variant effects into functional impact) and "modifier" (all other variant effects).

So as not to miss any mutations, we considered all mutations present in chromosome 2, even outside the mapping interval and retained the "high" and "moderate" impact mutations (table II.A). The chromosome 2 of bulk F2 DRB27 mutants had only 2 high impact mutations and only one within the DRB27 mapping interval and 7 moderate impact mutations (2 in the mapping interval). No T-DNA insertion site was detected in this set of filtered variants, which can be explained by the weak performance of variant caller (here GATK, see methods) to detect large insertions.

All mutations found in the mapping interval are supported by genetic evidence and must then be considered as serious candidates. The most striking variation is the high impact mutation: it consists in a 29-nucleotide deletion disrupting *ATG8E* coding sequence. Direct inspection of aligned reads confirmed that this deletion was not an artefactual variant call due to the T-DNA insertion identified in *ATG8E* promoter region (Figure II.3.A). This deletion very likely results in a loss-of-function, confirming that *ATG8E* function is compromised in DRB27 mutants. Yet, this mutational event comes redundantly in addition to the T-DNA insertion in the promoter described in section II.A.1.

Moreover, two missense-variants were found inside *AT2G40520* and *AT2G46440* coding sequences (table II.A, moderate impact). The first is an unknown protein of the Nucleotidyltransferase family and no reported correlation with phyllotaxis, whereas the second is the CYCLIC NUCLEOTIDE-GATED CHANNEL 11 (CNGC11), a positive regulator of fungal resistance. None of these two genes had reported function or phyllotaxis phenotype. To assess the relevance of these polymorphisms in the DRB27 mutant, we compared them to existing polymorphism within *A. thaliana* accessions or to other species according to the Uniprot database (http://www.uniprot.org/). The affected amino-acid residues are not conserved and equivalent substitutions found in homologous proteins suggest that they have no deleterious impact (Figure II.3.B). We thus consider that these mutations are very unlikely to cause the DRB27 phenotype.

To conclude, this first variant analysis selected *ATG8E* as the best candidate gene within the mapping interval. However, the standard variant calling procedure we applied obviously missed T-DNA insertions. We thus designed a specific analysis pipeline to track T-DNA insertion in the genome.

	Locus	distance to T-DNA 1		mutational event
High impact	**AT2G45170 4th exon**	**1 150 bp**	**0,004 cM**	**disruptive inframe deletion GAAGAGAATCAAACTAAGTGCAGAGAAA**
	AT2G08986	14 999 418	52 cM	disruptive inframe deletion GACACCAAGCCAAAGACTCATATAGACTTTGGCTACAC CATGAAAGCTTTCAGAT
Moderate impact	AT2G02490	17 956 462 bp	62 cM	missense variant T->C
	AT2G08986	15 002 404 bp	52 cM	missense variant G->T
	AT2G20550	9 777 262 bp	34 cM	missense variant T->C
	AT2G21420	9 452 640 bp	33 cM	disruptive inframe deletion GATGAC
	AT2G22795	8 925 379 bp	31 cM	disruptive inframe deletion CACTCTCTTCGGTAC
	AT2G40520	**1 698 968 bp**	**6 cM**	**missense variant A -> C, Lys388Thr**
	AT2G46440	**438 615 bp**	**1,5 cM**	**missense variant G -> A, Arg188Lys**

Table II.A: homozygous variants of "high" and "moderate" predicted impact. Physical and genetic distances are indicated relatively to the first T-DNA insertion identified, in the promoter of ATG8E. Bold text pinpoint the three variants falling into the mapping interval of DRB27.

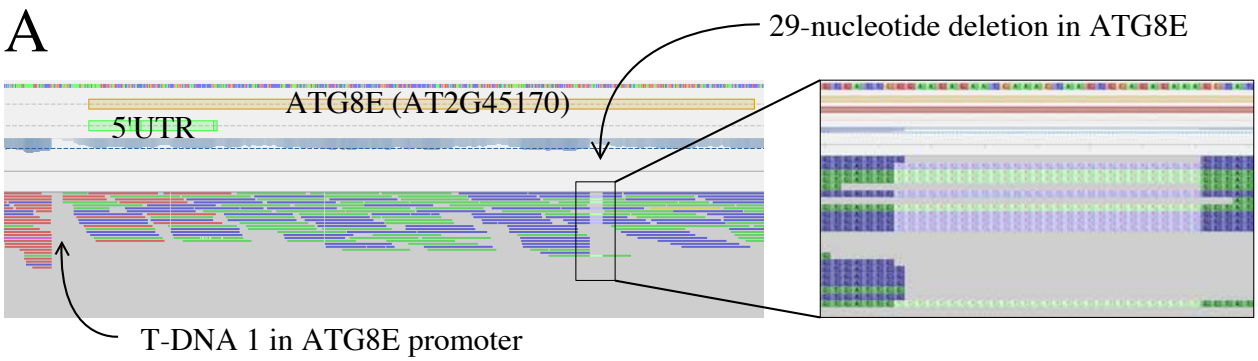

B

AT2G40520: LYS388THR

LYS388

```
B20170802A7434721E10EE658.. 351  LEKFFNVSLERNGKGQRQDVEEPVVAFGTGAADYSQLKGDFDRYRNNLIYGKWFHGES--  408
D7LF51      D7LF51_ARALL     351  LEDFFGNSLDRNGKGQRQDVEEPVIPFGTGKADYSNLRGDFYGYFLCFIYGKWFHRES--  408
R0FUZ5      R0FUZ5_9BRAS     351  LEKFFANSLDRNGKGQRQDAEEPIYAFGTGRAELSDLRGDFEGNFRSLVYGKWFHGETT-  409
A0A1J3JTD5  A0A1J3JTD5_NOCCA 345  LEKFFSNSLDRNGKGQRQDVEEPVFAFGTGRSNLSQLRGDFEGYFKSLVSAKLFHGEIQ-  403
A0A1J3ES02  A0A1J3ES02_NOCCA 360  LEKFFRNSLERNGKGQRQDVNDPVTAFGTGRSELSELGGNFEGYFERLVYGQMYHGYSLP  419
V4NEE5      V4NEE5_EUTSA     361  LEKFFGNSLERNGKGQRLDVNDPVTAFGTGRSELSELSGDFEGYFGRLVYGQMYHGYSLP  420
M5XS50      M5XS50_PRUPE     334  LEKFFVTTIDRNGRGERPDVNAPVCAFGIGRSEESDLWGEYDSYYSSMLYGQAFHRSTH-  392
                                  **.**  :::***:*:* *.: *:  ** * :: *:* *::      :: .: :*
```

AT2G46440: ARG188LYS

ARG188

```
B20170802A7434721E10EE658.. 181  PLYKEVTRAFGTVAESKRVGAALNFFLYMLHSYVCGAFWYLSSIERKSTCWRAACARTSD  240
Q9SKD6      CNG11_ARATH      181  PLYKEVTRAFGTVAESKRVGAALNFFLYMLHSYVCGAFWYLSSIERKSTCWRAACARTSD  240
A0A178VR19  A0A178VR19_ARATH 176  PLYKEVTKAFGTVAESKRVGAALNFFLYMLHSYVFGAFWYLSSIERKSTCWRAACARTSD  235
B3FXQ4      B3FXQ4_ARATH     173  PLYKEVTKAFGTVAESKRVGAALNLFLYMLHSYVFGAFWYLSSIERKSTCWRAACARTSN  232
Q8GWD2      CNG12_ARATH      181  PLYKEVTRAFGTVAESKWAGAALNLFLYMLHSYVFGAFWYLSSIERKSKCWRAACARTSD  240
B3FXQ3      B3FXQ3_ARATH     181  PLYKEVTRAFGTVAESKWAGAALNLFLYMLHSYVFGAFWYLSSIERKSKCWRQACARTSD  240
F4II92      F4II92_ARATH     158  PLYKEVTRAFGTVAESKWAGAALNLFLYMLHSYVFGAFWYLSSIERKSKCWRAACARTSD  217
                                  *******:********* .*****:********* *************.*** ******:
```

Figure II.3: Analysis of homozygous variants falling into the mapping interval of DRB27. A) Local alignment of WGS reads indicate a 29-nucleotides deletion in ATG8E, 0,004 cM downstream of the first identified T-DNA (T-DNA 1). B) Missense variants found inside the mapping interval do not concern conserved amino-acids among homologous proteins. The wild type residues are indicated in green. A "*" indicates positions which have a single, fully conserved residue; a ":" indicates conservation between groups of strongly similar properties (scoring > 0.5 in the Gonnet PAM 250 matrix); a "." indicates conservation between groups of weakly similar properties (scoring =< 0.5 in the Gonnet PAM 250 matrix) (source: UniProt).

II.B.4 – T-DNA MAPPING REVEALS 3 INDEPENDENT INSERTIONS IN THE MAPPING INTERVAL.

We followed a multi-step bio-informatics procedure to track all possible insertions of a known T-DNA sequence in the genome.

First, computing the coverage of the T-DNA sequence in DRB27 bulk-F2 sequencing data strongly suggests the presence of multiple T-DNA insertions in the genome (Figure II.4.A). While the average coverage of *A. thaliana* genome was 13.9X +/- 11.4, the average coverage of the T-DNA was approximately four times higher: 54.0X +/- 20.6 (median coverage are 13X and 58X and for *A. thaliana* and T-DNA genome, respectively). Moreover, local variations in the coverage of the T-DNA sequence (up to 90X) suggest complex T-DNA insertions, involving either incomplete insertions or local duplications.

Second, we specifically looked for the signature of T-DNA insertion: paired-end reads mapping to the T-DNA sequence on one end and to *A. thaliana* genome on the other end. We started by aligning DRB27 bulk-F2 sequencing reads on the T-DNA and extracted all singletons (defined as a read paired in sequencing, mapping to the sequence but whose mate is unmapped). T-DNA singletons mapped on both strands at the end of the sequence, but also in the middle, which confirmed possible partial insertions (Figure II.4.A). We then mapped all paired-end reads containing T-DNA singletons onto *A. thaliana* genome, revealing six putative loci of insertions: a single insertion in chromosome 4, and five insertions in chromosome 2 (Figure II.4.B and table II.B).

Third, to further assess these candidate insertions (labelled as T-DNA 1 to 6, table II.B), we directly inspected read alignments on *A. thaliana* genome around each locus and checked how corresponding singletons map on the T-DNA sequence (Figure II.4.B, panel a). Three putative insertion loci (T-DNA 1, 2, 4) correlated with a gap in the aligned sequences of DRB27 bulk-F2 reads with the plant genome (Figure II.4.B, panel d), suggesting that T-DNA insertion deleted a few nucleotides, as described previously (Gheysen *et al.*, 1991; Waterworth *et al.*, 2011). In addition, no pairs map over this gap and singleton orientations on both sides are coherent with a long insertion at this locus (median insert size of the

sequencing library is around 500 bp). Finally, the corresponding mate reads on the T-DNA showed compatible orientations, which allowed to deduce the direction of the T-DNA insertion and to reconstruct the whole insertion. For instance T-DNA 1 and 2 were almost full-length insertion in the reverse orientation while T-DNA 4 is likely a tandem of two inverted T-DNAs, because both forward and reverse singletons map to the left-border. Finally, we excluded the three other putative insertions (T-DNA 3, 5 and 6) because of the absence of gap in the global alignment of DRB27 bulk-F2 reads and inconsistent orientations of singletons between genomes. Singletons corresponding to these insertions mapped in the middle of the T-DNA and could indicate partial insertions, but since they also map where coverage is more variable, they could just be mapping errors. Moreover, two of them fall outside the mapping interval (T-DNA 5 & 6; Table II.B).

To sum-up this specific bio-informatics search for T-DNA insertions, we retained three insertion loci (Table II.B): one in the promoter of *ATG8E* (*AT2G45170, T-DNA 1*), confirming the result of adapter ligation-mediated PCR (see above II.A.1), one in the coding sequence (5th intron) of *FILAMENTOUS FLOWER* (*AT2G45190, T-DNA 2*) and one (made of two T-DNAs) in the promoter of *MIR166A* (*AT2G46685, T-DNA 4*). These three T-DNA insertions fall into the DRB27 mapping interval and we estimated that they lie inside a genetic distance of 1,9cM, based on a recent study of the genome-wide recombination landscape in *A. thaliana* (Salome *et al*., 2012).

To conclude on this part, whole-genome sequencing identified several mutations in the same genetic interval, that affect three genes: *ATG8E* (one deletion + T-DNA insertion in the promoter), *FILAMENTOUS FLOWER* (T-DNA insertion in the coding sequence) and *MIR166A* (potentially a tandem mirrored insertion in the promoter). All three were supported by genetic evidence, and their insertion *loci* were confirmed by PCR. Whether or not these genomic mutations are the origin of the phyllotactic phenotype of DRB27 mutants was tackled by functional experiments.

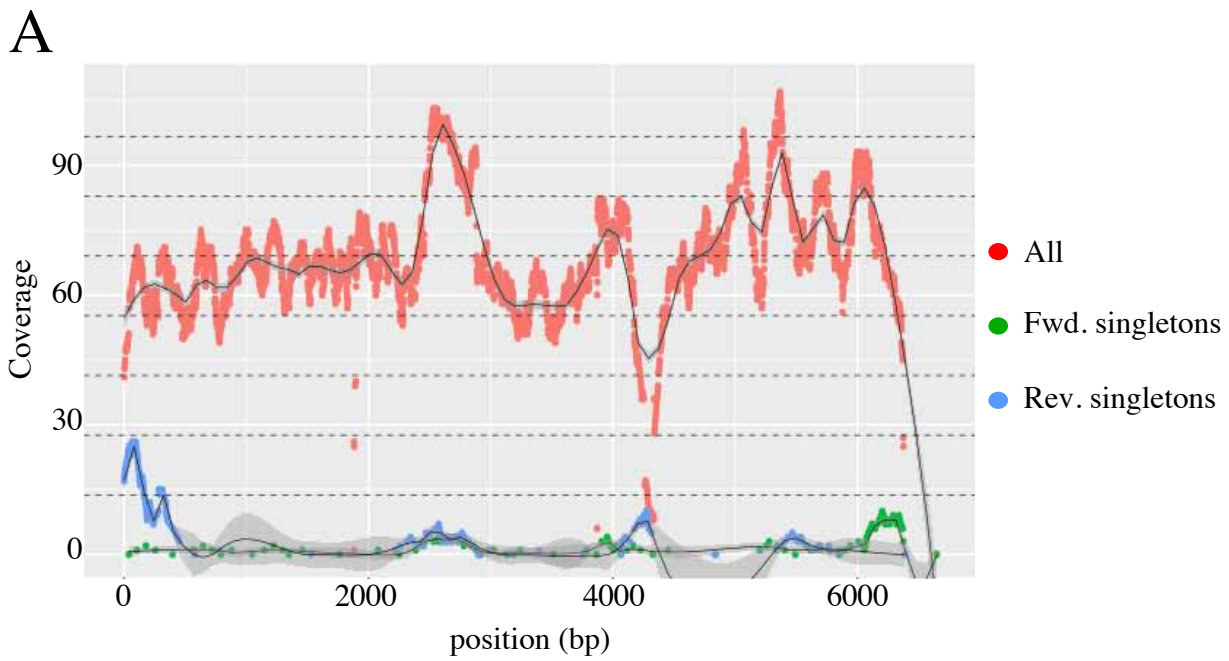

Figure II.4: T-DNA insertions in DRB27. A) Coverage of the T-DNA sequence with the reads of DRB27 (red dots). Single forward and single reverse reads are represented in green and blue dots respectively. Horizontal dotted lines indicate increasing coverage by multiples of the DRB27 mean coverage (14X). B) T-DNA insertions 1 to 6 in the genome of DRB27. For each insertion: a) selection of singletons from (A) which mates map on a single locus of *Ws-4* genome (b); read alignments of these singletons on the DRB27 genome, and whole data are shown in panel b and c respectively. Annotated genes are shown in yellow with 5'UTR in green showing the orientation (a); all forward reads are represented in green (panel c & d) whereas reverse reads are in blue; on panels c & d only, red reads are singletons.

B

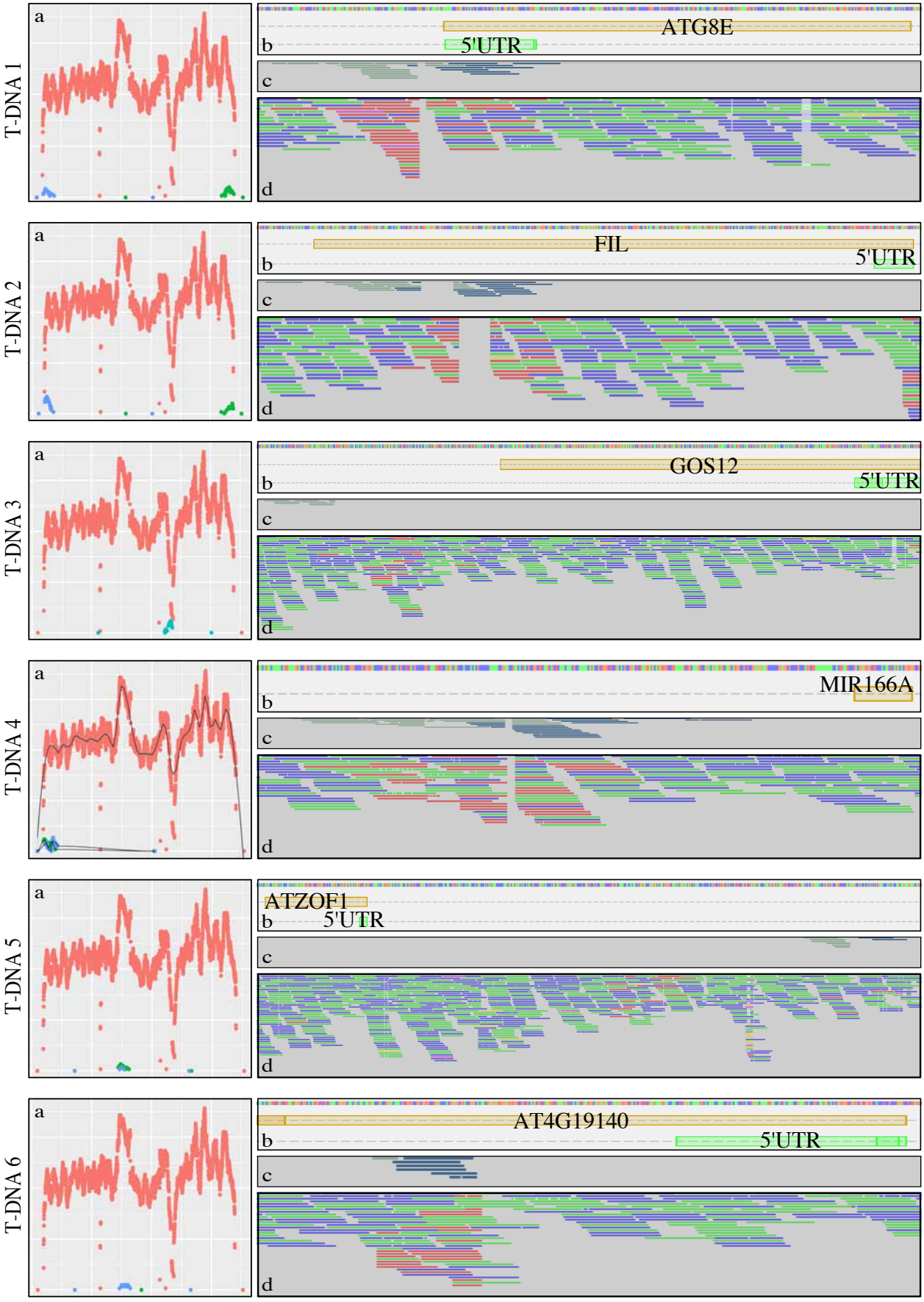
T-DNA 1
a
b
ATG8E
5'UTR
c
d
T-DNA 2
a
b
FIL
5'UTR
c
d
T-DNA 3
a
b
GOS12
5'UTR
c
d
T-DNA 4
a
b
MIR166A
c
d
T-DNA 5
a
ATZOF1
b
5'UTR
c
d
T-DNA 6
a
b
AT4G19140
5'UTR
c
d

	Locus	distance to T-DNA 1	Orientation	T-DNA integrity	Associated mutational event
T-DNA 1	**promATG8E (AT2G45170)** **338 bp before START**	/	Reverse	Complete	deletion of 23 bp: ACAAGCTAAGCTGACGTGTCTAA
T-DNA 2	**FIL (AT2G45190)**	**3 304 bp** **0,01 cM**	Reverse	Complete	deletion TGTGGGGGAAGTGGGCCCACTGCATTACACATAAACAACATACGTACAAGACACATATCAACTTGTGTTATAACCCGACAAAATTCTTTACTCCTAATTTCAGCTATACCTACATATATGACTGTTTAATATAT
T-DNA 3	promGOS12 (AT2G45200)	12 177 bp 0,04 cM	Reverse	Truncated right border	/
T-DNA 4	**promMIR166A (AT2G46685)** **881 bp before mature MIR**	**554 Kb** **1,9 cM**	Tandem insertion Left borders facing out	Left borders complete No data on right borders	deletion AATATGTACTGTTTGTTGC
T-DNA 5	promATZOF1 (AT2G19810) 2kb before START	10 083 Kb 34,59 cM	Forward	Partial insertion	/
T-DNA 6	AT4G19140	/	Forward	Partial insertion right half	/

Table II.B: T-DNA insertions in DRB27. Bold text pinpoint the three homozygous T-DNAs falling into the mapping interval

II.C – FUNCTIONAL VALIDATION OF THE CANDIDATES

Thorough genomic analysis of DRB27 identified three candidate genes that could be responsible for the complex phenotypes described in section I. Two of them were downregulated in DRB27 meristems, as shown by qRT-PCR (figures I.10 and II.1.C). MIR166A also seemed to be downregulated but this observation was not statistically confirmed when the independent experiments were pooled (p-value = 0,25). However the high redundancy between the *MIR165/166* might impact on those results, and the similarly opposite behaviour of *ATHB15*, which was shown to be specifically regulated by *MIR166A* (Kim *et al*., 2005), indicate that producing additional replicate might be necessary to better understand these results. The adaxialisation observed is thus very likely caused by two direct mutations acting in the same direction in the genetic balance of polarity establishment: a loss of function of the abaxial identity gene *FIL* and a loss of function of the adaxial inhibitor *MIR166A*.

However, our project focuses on the perturbed phyllotaxis of DRB27 mutant. In order to determine the role played by each candidate in this specific phenotype, we started two independent approaches. First, rescuing the phyllotactic phenotype by insertion of the full wild-type sequence of each candidate gene in the mutant, separately or in combination. Conversely, re-creating mutant lines using CRISPR-Cas9 genome edition, targeting candidate genes either separately or in combination.

II.C.1 – ATG8E CANNOT RESCUE THE SEVERE PHYLLOTACTIC PHENOTYPE OBSERVED IN DRB27

To assess the impact of *ATG8E* loss-of-function in our phenotype, we observed the phenotypes of an *atg8e* mutant (Figure II.5.A; Table M.A). No phyllotaxis phenotype was visible nor described in the literature (Michaeli *et al*., 2015) in normal growth conditions, and the plants were not distinguishable from the wild types. CRISPR lines were generated to observe independent lines and are still in process of screening.

We also generated two constructs of mVENUS-ATG8E fusion protein for complementation with different promoters: one line was driven by the endogenous promoter, and the other by the RPS5A promoter, which expression is strong in the shoot apical meristem (Weijers *et al*., 2001). The first showed almost undetectable fluorescence that could as well be artefactual (Figure II.5.B), which could be due to low endogenous level of expression, (Slavikova *et al*., 2005; Contento *et al*., 2005). On the other hand, we could observe typical *ATG8* fluorescence signal in the line driven by the strong *RPS5A* promoter (Figure II.5.C-D from Slavikova *et al*., 2005 and Contento *et al*., 2005), with a cytoplasmic fluorescence and bright aggregates that could correspond to autophagosomes. F2 progeny displayed the same signals with no sign of phenotype rescue (Figure II.5.E-F). In case the *pRPS5A* construct was not functional, we also crossed DRB27 with an overexpressor line of a functional GFP-ATG8E fusion protein whitch expression was driven by the strong cauliflower *35S* promoter (Contento *et al*., 2005). F2 seedlings expressing the GFP in shoot tissues (Figure II.5.G) showed no change of phenotype at later stages.

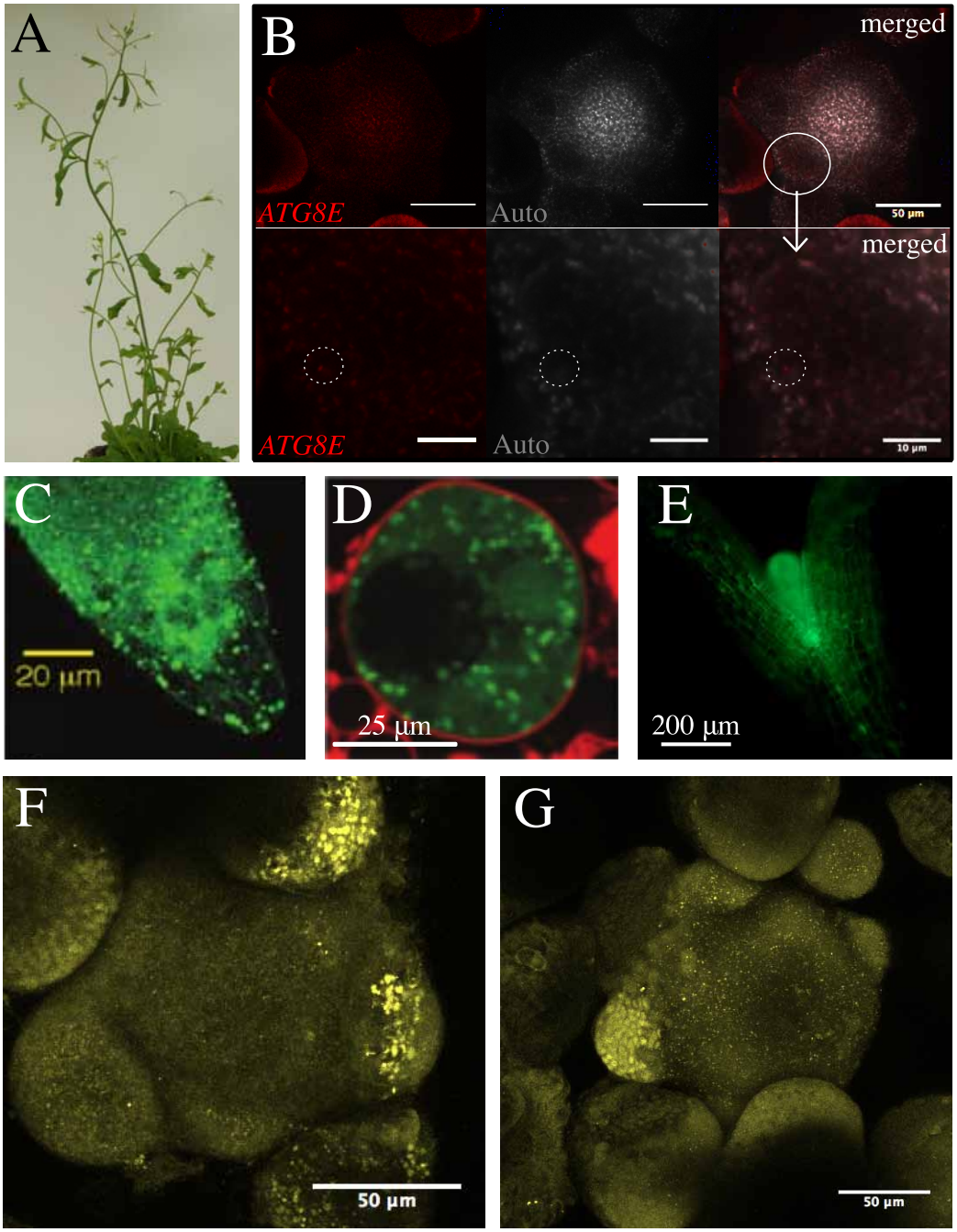

Figure II.5: *ATG8E* is not responsible for the DRB27 phenotype. A) Fully grown *atg8e* mutant does not show DRB27-like phenotype. B) Confocal imaging of T2 lines transformed with *pATG8E::mVENUS-ATG8E* shows almost undetectable fluorescence at the shoot apical meristem, and close up on a primordium where autofluorescence is limited. C-D) Classical *p35S::GFP-ATG8E* fluorescence signal in the root (C, from Slavikova *et al.*, 2005) and protoplast (D, from Contento *et al.*, 2005) shows mild fluorescence in the cytoplasm and bright aggregates when autophagophores are formed. E) F2 DRB27 seedling from cross with *p35S::GFP-ATG8E* line shows expression in the shoot apical meristem. F-G) Confocal imaging of T1 lines transformed with *pRPS5A::mVENUS-ATG8E* shows classical ATG8E pattern in wild type (F) as well as mutant (G) shoot apical meristems.

II.C.2 – STUDY OF THE ROLE OF *FILAMENTOUS FLOWER* AND *MIR166A* IN THE DRB27 PHENOTYPE

We generated independent lines carrying constructs to generate disruptive in frame deletions in the two candidate genes using the CRISPR-Cas9 technology. We also transformed DRB27 lines with the full wild type sequence, from the end of the previous annotated gene in 5' to the end of the 3' UTR, either of *FILAMENTOUS FLOWER* or *MIR166A*. All these lines are in process of screening. Baring in mind the published documentation on *fil* phenotypes in the literature that does not necessarily relate to meristem patterning (see section I.C.3), we also observed independent mutants' meristems, such as *fil8* and WiscDsLox367E6_049, two alleles of *fil*, baring transposons inside the 4th and the last introns of *FILAMENTOUS FLOWER* respectively (Figure II.6.A-D). We could not have access to any *mir166* mutant, but as *MIR166A* was shown to participate in vascular development of the inflorescence stem through downregulation of *ATHB15* (Ochando et al., 2006), we observed *icu4*, which is an *ATHB15* mutant resistant to *MIR165/166* with occasional co-initiations along the stem (Figure II.6.E-H).

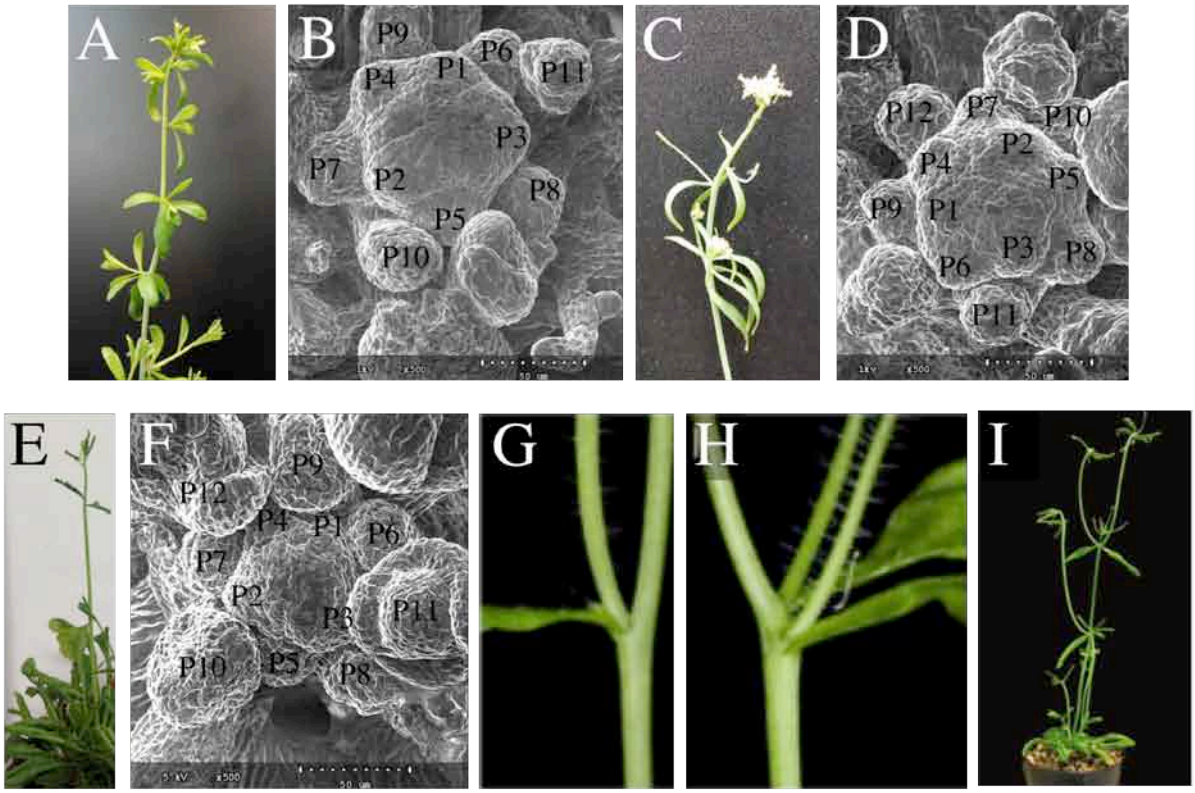

Figure II.6: Single *fil* and *icu4* alleles do not show the DRB27 phyllotaxis phenotype. A-B) *fil8* mutant does not show DRB27-like phenotype (A) and has a spiralled meristem (B). C-D) WiscDsLox367E6_049 mutant allele of *FIL* shows similarities with DRB27 with clustering of lateral organs (C) but has a recognizable spiral pattern at the meristem. E-H) *icu4* mutant shows spiral phyllotaxis at the shoot (E) and meristem (F) despite documented clustering of secondary shoots (G: wild type, H: *icu-4* from Ochando *et al.,* 2006). I) *fil3 icu4* double mutant shows similarities with DRB27 phyllotaxis (from Ochando *et al.,* 2008). B, D, F) Primordia are marked P1, P2, ... according to their relative size

None of these mutants recapitulated the phyllotaxis of DRB27, as they all displayed spiralled organ initiation in meristems. Even for the strong *fil* allele (WiscDsLox367E6_049), which showed similarities with DRB27 concerning its lateral organs' phenotype. In this case, clustering of lateral organs along the stem most likely result from post-meristematic growth, as indicated by the accumulation of young primordia around the meristem (Figure II.6.D). However, an unrelated study has observed a similar phyllotaxis phenotype on the *icu4 fil3* double mutant (Ochando et al., 2006, 2008; Figure II.6.I), consisting of clustering of two secondary shoots along the stem. Unfortunately we could not obtain this line to look at organogenesis at the meristem. However, *MIR166A* was shown to share high identity with the eight others MIR165/166s' mature sequences (Jung *et al.*, 2007; Zhu *et al.*, 2011, Zhou *et al.*, 2015; Merelo *et al.*, 2016), so that loss-of-function of *MIR166A* alone was not likely to be the cause of so strong a phenotype.

To conclude, three candidates were selected after genetic and genomic study of the DRB27 mutant, but *ATG8E* seemed unlikely to cause such phenotype as that of DRB27. The implication of the two others, *FIL* and *MIR166A*, still need to be functionally validated. However *fil* independent mutants did not recapitulate the DRB27 phenotype, and no phenotype for *mir166a* loss-of-function was documented so far. Indeed there is a high redundancy between the nine *MIR165/166*, and a single mutant is not likely to produce so strong a phenotype. However, the addition of down-regulations of *FIL* and *MIR166A*, is likely to cause the phenotype of the DRB27.

III – STRUCTURAL MODIFICATIONS OF THE INFLORESCENCE ACCOMPANY PHYLLOTAXIS DEFECTS IN DRB27

The phenotype of the DRB27 line combines two important characteristics: atypical phyllotaxis (with longitudinal clusters and radial crescents) and imbalanced polarity of organs. Although we have not yet confirmed the genetic origin of this original phenotype, our analysis suggests that it likely results from two independent T-DNA insertions impairing two positive regulators of abaxial identity: *FILAMENTOUS FLOWER* and *miR166A*.

Polarity genes are activated after a certain delay during organogenesis (see introduction section III.B and *pFIL* signal at P1 in Figure I.5). Therefore loss of function does not prevent organ initiation. However, spatial-temporal sequence of organ initiation was modified in DRB27, which suggests that the regulation of abaxial-adaxial polarity of organs feedbacks on the mechanisms that normally control organ initiation and phyllotactic patterning. Those mechanisms are notably the auxin-mediated induction of organogenesis in the peripheral zone and the subsequent inhibitory fields created by auxin depletion (Reinhardt *et al.*, 2003), AHP6 inhibitory fields (Besnard *et al.*, 2014), mechanical modulation of cell wall stiffness allowing growth (Peaucelle *et al.*, 2008; Peaucelle *et al.*, 2011a, b; Braybrook *et al.*, 2013, and geometry of the SAM (Douady & Couder, 1996). In a series of experiments, we tried to study several of these mechanisms in *DRB27* inflorescence meristems, to decipher the dynamics governing the formation of abnormal phyllotactic patterns in this mutant line.

III.A – CHANGES IN GEOMETRY AFFECT THE RATIO BETWEEN CENTRAL AND PERIPHERAL ZONE IN DRB27

III.A.1 – DRB27 MUTANT MERISTEMS ARE WIDER AND HIGHER THAN WILD TYPES

The first striking observation about the DRB27 meristem is that it seemed to be larger than the wild type's (Figure III.1.A, B). In order to quantify this observation, we used the autofluorescence signal on confocal microscopy to measure meristem diameter. We established a reproducible metrics to compare Wild type and DRB27 meristems (see Methods). As shown in Figure III.1.C, the wild type displayed an average meristem diameter of 113.44 µm, whereas DRB27's meristem diameter reached an average of 153.76 µm, which represents a significant increase of 35.6% (pvalue=$2.2.10^{-16}$). Similarly, wild-type meristems were of 36.79 µm high in average, for 66.75 µm in DRB27 (Figure III.1.D), which represents an increase of 81% of meristem height in DRB27 (p-value=$2.2.10^{-16}$). Such enlargement of meristem proportions was observed previously in the *fil9* allele (Lugassi *et al.*, 2010), as well as in multiple polarity mutants (see introduction section III.B.2).

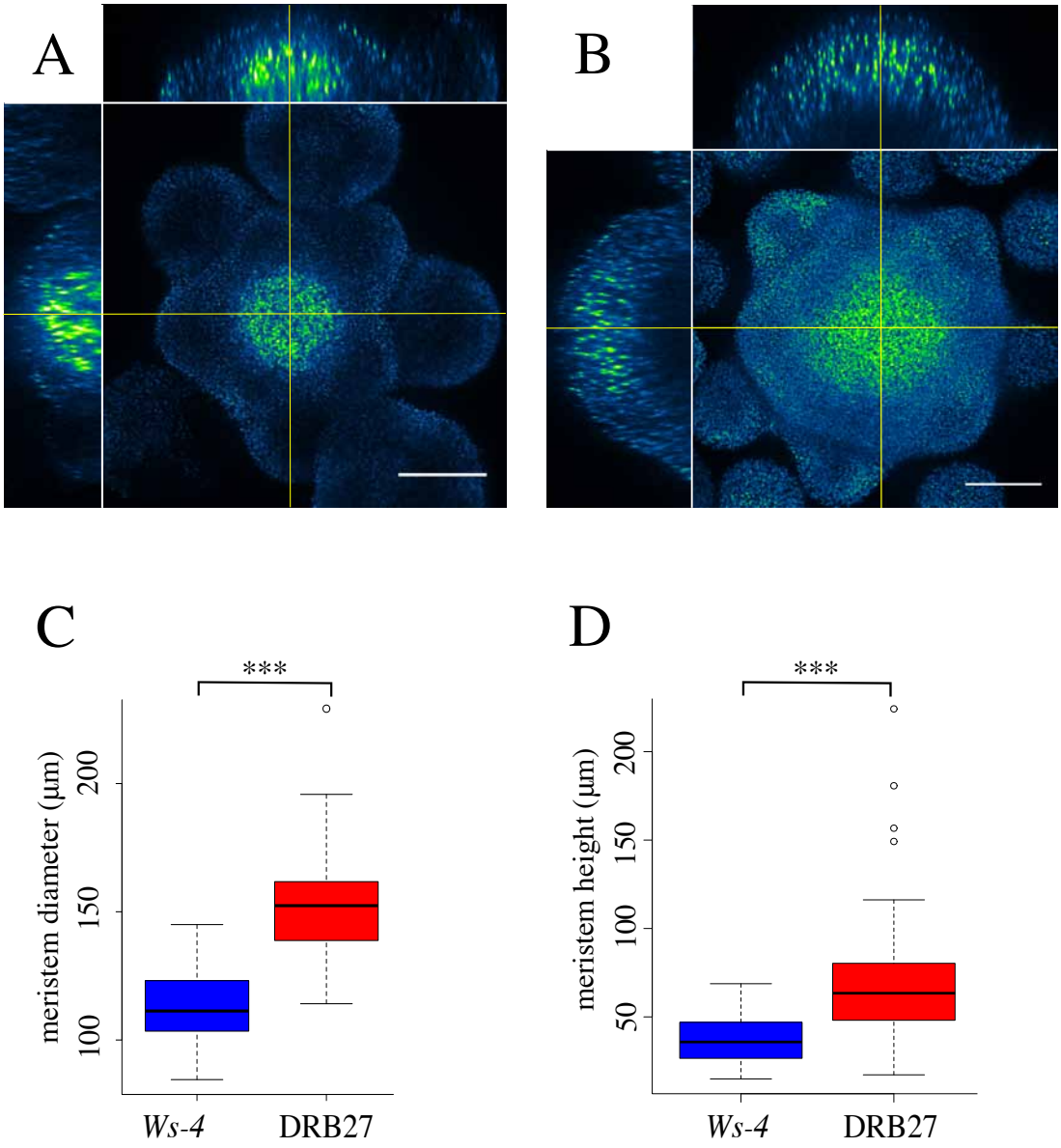

Figure III.1: The shoot apical meristem of DRB37 is larger and taller than that of *Ws-4*. A-B) Z-projections and orthogonal views of autofluorescence signals show different proportions of the wild type (A) and DRB27 (B) meristems; scale bars=50µm. Quantifications of meristem diameter (C) and height (D) in *Ws-4* and DRB27. Both p-values $=2.2.10^{-16}$. n=178 wild types & 136 mutants

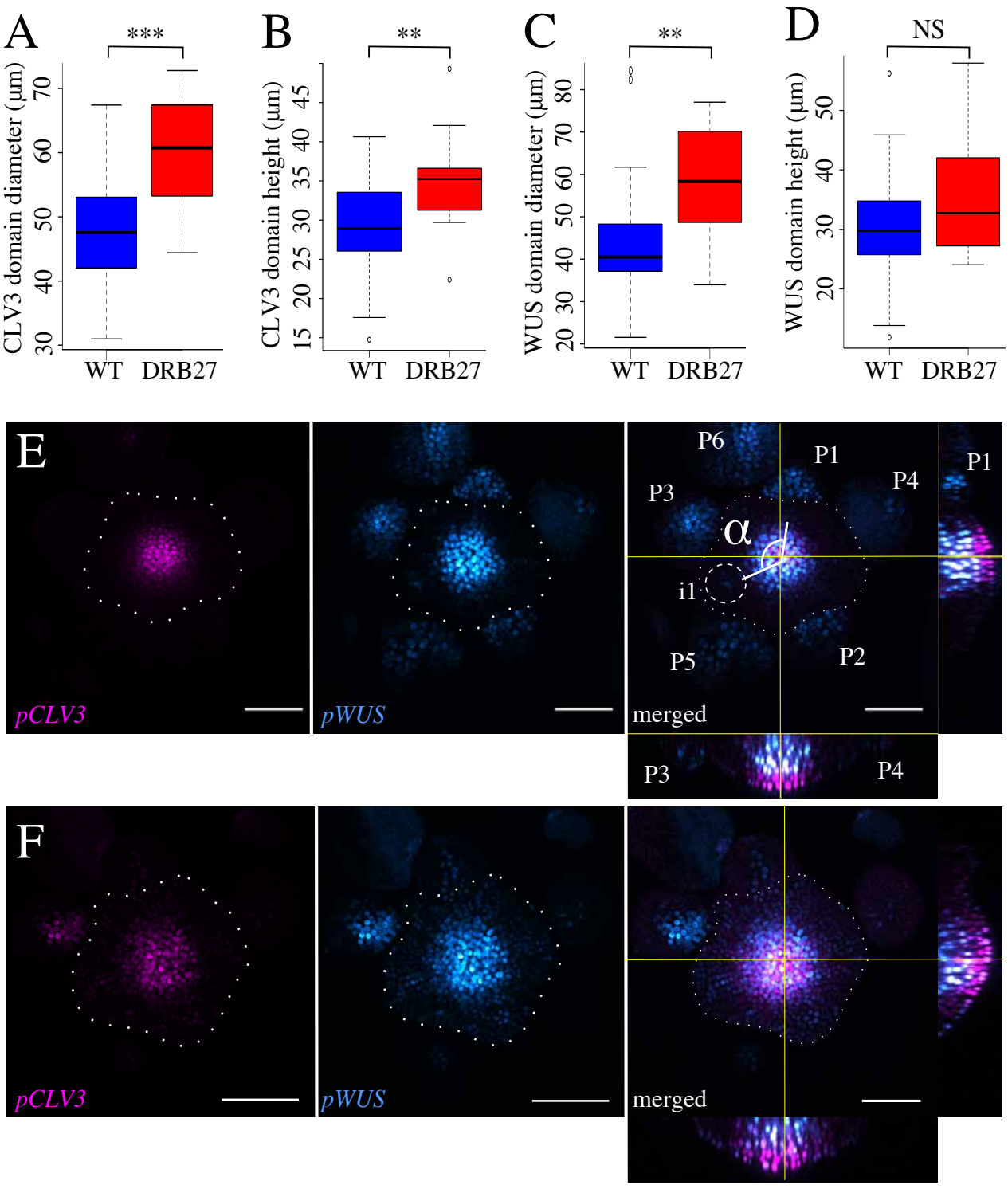

Figure III.2: *WUS-CLV3* expression domains in DRB27 compared to the wild type. A-D) quantifications of *CLV3* (A, B) and *WUS* (C, D) diameter expansion (A, C) and height increase (B, D) in DRB27 compared to the wild type. E-F) Z-projections of *WUS* (cyan) and *CLV3* (magenta) channels alone (left panels) and merged (right panels) in the wild type (E) and a DRB27 with high expansion of the *WUS-CLV3* domains (F). Orthogonal views associated to merged images correspond to the signal at the slices indicated by yellow lines. Dotted lines indicate the periphery of the meristem. n= 74 wild types & 15 mutants. Scale bars=50µm

III.A.2 - PHYLLOTAXIS PERTURBATION IN DRB27 IS CORRELATED WITH ABNORMAL WUS-CLV3 EXPRESSION DOMAINS

Meristem size modifications have already largely been correlated with phyllotaxis defects in the literature (see introduction section III.A). However, models predict that absolute meristem size does not matter as much as the proportions between the different domains in the meristems, namely the diameter of the central zone and the diameters of organ-centred inhibitory fields (Douady et Couder, 1996).

Further investigation was thus necessary to assess whether this increase of size was followed by an upscale of the other zones' sizes or not. We observed a significant increase of the *CLV3* domain by 26% in diameter (Figure III.2.A, pvalue=1,8.10^{-5}) and by 20% in height (Figure III.2.B, pvalue=3.10^{-3}) as well as a significant increase of the WUS expression central domain in diameter by 35% (Figure III.2.C, pvalue=1,9.10^{-3}) but not in height (Figure III.2.D, pvalue=0,2).

A striking example of the *WUS-CLV3* increase of the expression domains is given in Figure III.2.E-F. In the wild type shown here (Figure III.2.E) and consistently with the literature, *CLV3* is expressed exclusively in the central zone, and the WUS domain is restricted to the organizing centre of the meristem, except for the growing primordia. As shown in the orthogonal views, the two domains are well defined as well in depth. In the mutant (Figure III.2.F) the *pCLV3* domain expanded radially and low *pWUS* signals corresponding to what is seen in the wild type primordia were visible all over the peripheral zone. Moreover both domains' limits were blurred, as shown by the orthogonal views, where both *WUS* and *CLV3* signals were heterogeneous (Figure III.2.F).

To conclude, only the *WUS* domain expanded radially and proportionally to the wild type meristem size, whereas CLV3 up scaled to a lesser extent.

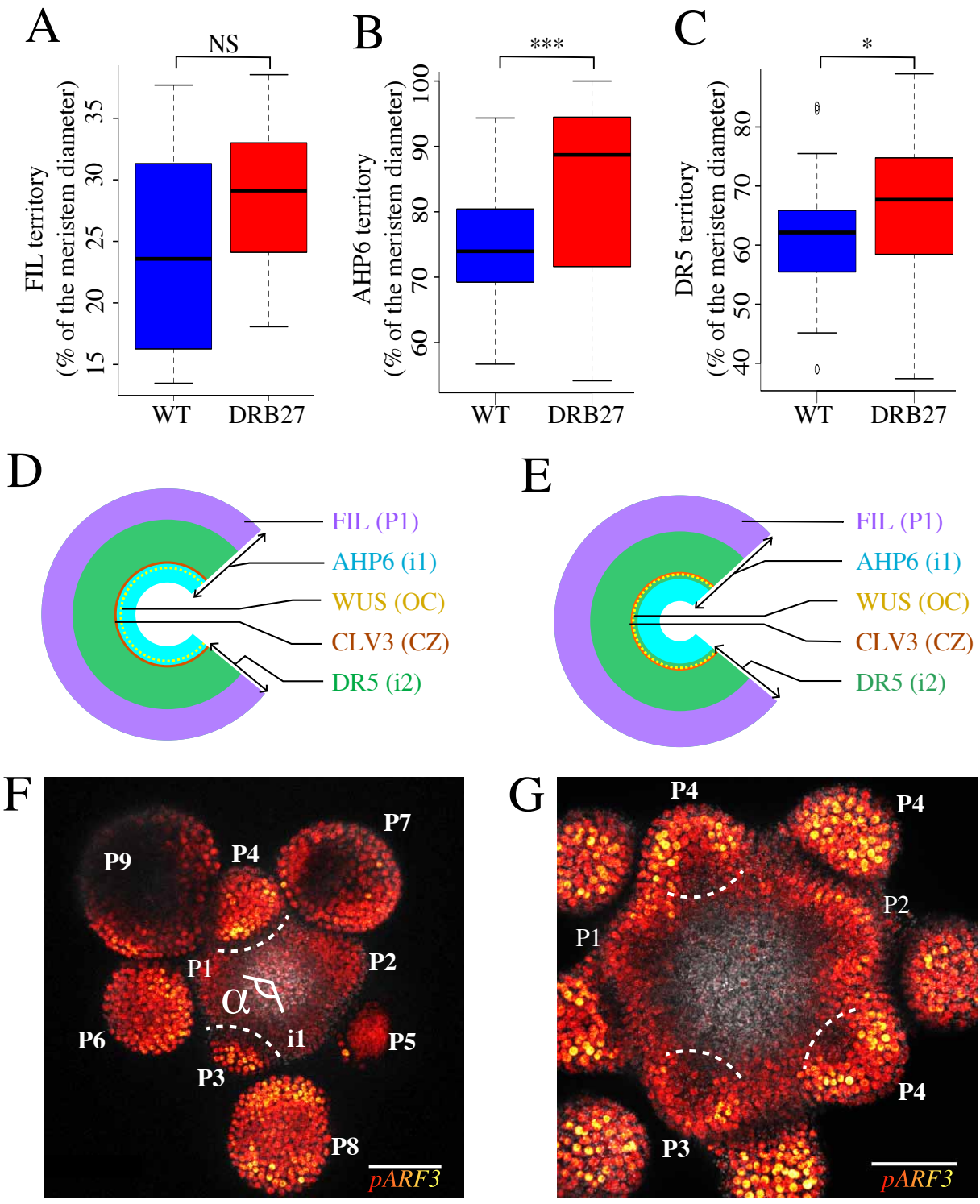

Figure III.3: Markers of functional domains across the meristem. A-C) *FIL* (A, n= 16 WT & 16 mutants), *AHP6* (B, n= 68 WT & 42 mutant) and *DR5* (C, n= 32 WT & 34 mutants) occupancy of the meristem territory was calculated from the shortest distance between opposite signals across the centre, and reported in percentage of the meristem diameter. These data are summed up and added to *WUS-CLV3* diameter data in D (wild type) and E (DRB27 mutant). F-G) Confocal microscopy of wild type (F) and DRB27 mutant (G) plants bearing the *ARF3* transcriptional reporter. Dotted lines pinpoint boundary domains of the growing primordia. Scale bars=50µm.

III.A.3 – PATTERNING OF OTHER MERISTEMATIC FUNCTIONAL ZONES IS IMPAIRED IN DRB27

Conversely to *WUS-CLV3* expression domains in the central zone, we measured the diameters of the zones devoid of *FIL, DR5* and *AHP6* expression, i.e. the smallest distance between signals through the centre, to estimate the occupancy of these domains, relatively to the diameter. The average ratio between meristem diameter, and other markers' territories were compared between wild types and mutants (Figure III.3) to assess whether the increase in total meristem size was followed by modification of the ratio between the sizes of meristem functional zones.

The *pAHP6* and *pFIL* signals are proxies for the zone where organogenesis occurs; baring in mind that *pFIL* only marks the abaxial part of organs starting from P1. In DRB27 inflorescence meristems, *FIL* expression domain up scaled to the same proportion as in the wild type (Figure III.3.A), as it occupied 24.7% of the meristem diameter in WT and 28.69% in DRB27, an increase that was not significant according to Wilcoxon sum rank test (p-value = 0.1). This maintenance of proportions was not at all followed by the AHP6 promoter, which average domain increased drastically from 74.62% to 83.92% of the meristem diameter, a 12% increase that was highly significant (Figure III.3.B; p-value=2.10^{-4}). Auxin signalling domain also proportionally expanded towards the centre to a lesser extent, with a significant increase of 8.7% of the meristem diameter occupancy, from 61.03% in the wild type to 66.34% in DRB27 (p-value = 0.03), as shown in Figure III.3.C. Altogether the DRB27 mutants showed mostly expansions of *AHP6* and *DR5* territories across the meristem (summed up in Figure II.3.D-E), indicating a large overlap of a PZ regulator on the CZ/OC, whereas *FIL* territory remained proportionally equal to that of the wild type. This result indicated that although organogenesis seemed to reach i1 stage closer to the centre in DRB27 than in the wild type (AHP6 signal shown in Figure I.7.B clearly marked a phyllotactic pattern), it was retained from reaching P1 stage until it grew further away from the centre.

The organizational modification of the mutant's meristem was also visible with the *AUXIN RESPONSE FACTOR 3 (ARF3)* fluorescent marker. In the wild type (Figure III.3.F), the *pARF3* signal remains low throughout the meristem, and increases drastically in the

growing primordia as soon as P1 stage. The boundaries are then clearly marked by the contrasted absence of *ARF3* from P3 stage onward (Zhao *et al., 2013*). In the mutant, the *pARF3* signal was stronger and uninterrupted around the meristem periphery, and across young primordia furrows (named here P1 to P3 after their corresponding size in the wild type), which were only visible as organs separated from the meristem (Figure III.3.G). Here, the boundaries seemed not to be specified as early as in the wild type.

These results were consistent with the literature, as loss-of-function of *FIL* was shown to increase *WUS* domain through *LAS* misregulation (Goldshmidt *et al.*, 2008; and see section III.B.4 of the introduction). Altogether this indicated that organogenesis signal position was not so clear in DRB27. On the centripetal axe, it started closer to the centre in a context where the organizing centre (inhibiting cell differentiation, Negin *et al.*, 2017) was larger. Radially, the lack of boundary specification also indicated that the limit between differentiating and proliferating cells, and undifferentiated meristematic cells (Hussey *et al.*, 1970; Reddy *et al.*, 2004; Breuil-Broyer *et al.*, 2004; Ha *et al.*, 2003, 2007) was not so clear in the DRB27 mutant, thus potentially blurring the positioning signal around the meristem. It was also visible with the *DR5* and even sometimes with the *AHP6* signals (Figure I.11.E), which could be quite continuous in the peripheral zone. This suggests that there is a perturbation of boundaries that could interfere with a precise definition of the organogenesis sites, contributing in perturbing the spatial-temporal pattern of DRB27.

III.B – MECHANICAL PROPERTIES OF THE DRB27 MERISTEM

As mechanical properties of the shoot apical meristem have been shown to impact on phyllotaxis (Peaucelle *et al.*, 2008, 2011a; Milani *et al.*, 2011; Kierzkowski *et al.*, 2012; Braybrook *et al.*, 2013), we explored the mechanical properties of DRB27 shoot apical meristem. We measured by Atomic Force Microscopy (AFM) the mechanical properties of cell walls at the surface of the meristem. Preliminary results shown in Figure III.4 provided insight in the mechanical properties of DRB27. In the meristem, cell wall relaxation is needed

before tissue deformation is visible, to allow cell division (Peaucelle *et al.*, 2008; Peaucelle *et al.*, 2011a, b; Braybrook *et al.*, 2013). As a consequence, local elasticity of the meristem corresponds to its permissiveness to tissue deformation. For instance in the central zone, a higher force (quantified as elasticity value, in Mpa) is necessary for tissue deformation whereas the peripheral zone is softer with lower elasticity values (Hamant *et al.*, 2008).

In wild-types *Ws-4* plants, the expected elasticity pattern were confirmed at the surface of cell walls: 48.4 Mpa in the central zone versus 32.2 Mpa in the peripheral zone (Figure III.4.A). This means that a higher force is necessary to deform the surface of the central zone. Similar value was measured on the mutant's central zone, although more variable. However the periphery showed extreme stiffness, with a mean elasticity value of 218 Mpa (Figure III.4.B). Moreover, the regularity and progressive changes of surface stiffness that we observed in the wild type were not seen in DRB27, where cells could show abrupt changes of elasticity compared to their immediate neighbours (illustrated with white stars). However, this exploratory measurement should be interpreted cautiously, because of the high variability we faced. Indeed the high range of stiffness that we encountered didn't allow us to always use the same cantilever between measurements. Moreover the morphology of the DRB27 meristem didn't allow us to make series of measurements on single meristems as we did on wild types, especially around the peripheral zone.

However, these observations indicate a potentially very low permissiveness to organogenesis in the peripheral zone, although organogenesis is not impaired in DRB27 mutants (section I.B.1, Figure I.2.B). This might be correlated with the fact that in DRB27 mutants, whereas the AHP6 domain (i1) expands toward the centre, the FIL domain (P1, when a visible deformation of the epidermis marks the primordium) remains at the periphery (Figure III.3.D, E). In other words, development from initiated organs (i1) to primordia (P1) is delayed until they grow away from the centre, and this could be correlated with the presence of this high surface stiffness at the periphery. Further investigation will be necessary to confirm these observations.

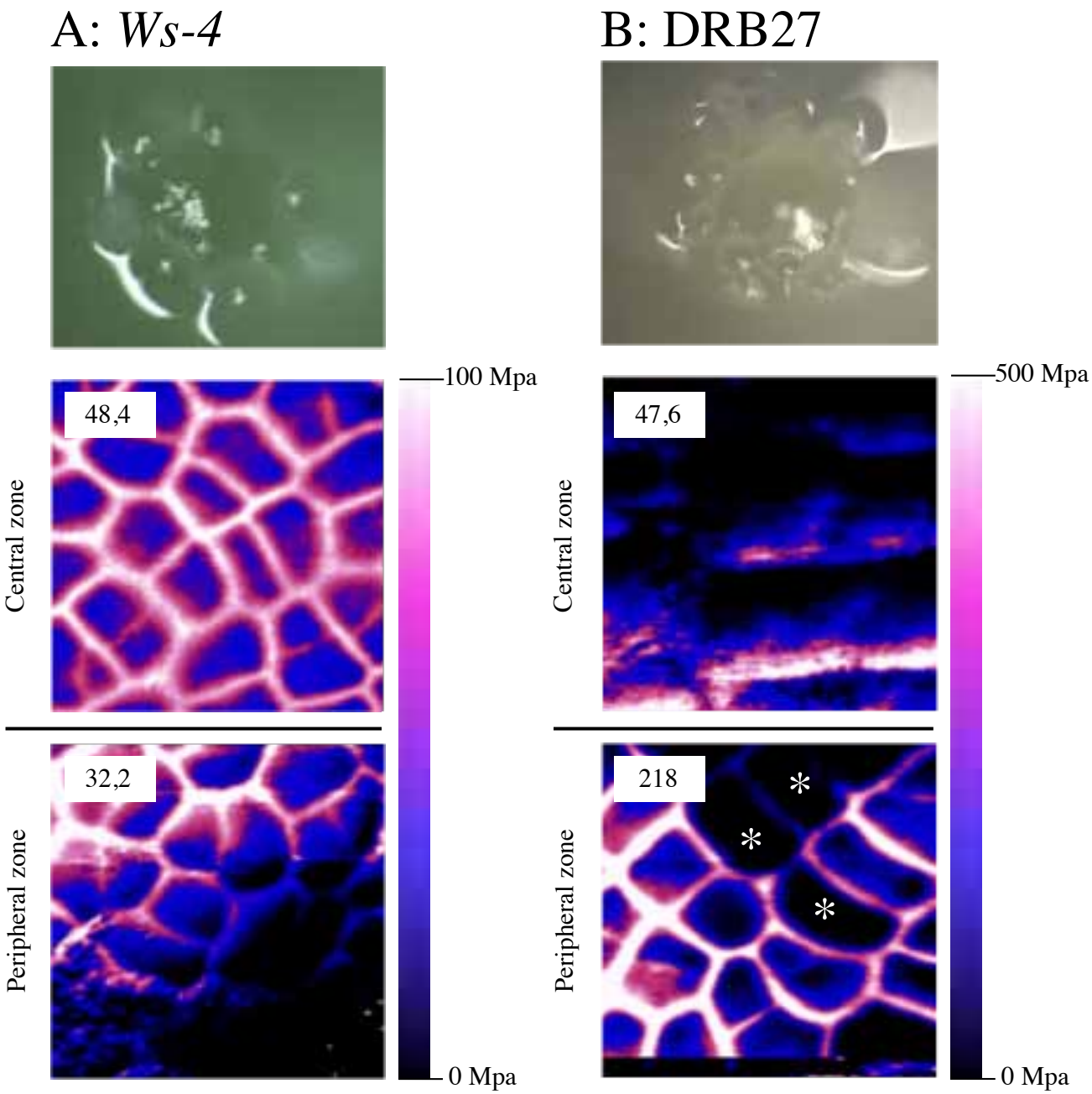

Figure III.4: Measure of the surface stiffness of wild type (A) and DRB27 (B) shoot apical meristems by Atomic Force Microscopy. For each genotype, elasticity was measured with Atomic Force Microscopy on the central zone and the peripheral zone. Mean elasticity values are indicated on the top left of each picture. For each genotype, a different scale is indicated. White stars show abrupt fall of elasticity in neighbouring cells.

REFERENCE LIST

Alvarez-Buylla Elena, R et al. 2010. "Flower Development." *The Arabidopsis Book* 8(1): 1–57. http://dx.doi.org/10.1199/tab.0127.

Bainbridge, Katherine et al. 2008. "Auxin Influx Carriers Stabilize Phyllotactic Patterning." *Genes and Development* 22(6): 810–23.

Besnard, Fabrice, Frédérique Rozier, and Teva Vernoux. 2014. "The AHP6 Cytokinin Signaling Inhibitor Mediates an Auxin-Cytokinin Crosstalk That Regulates the Timing of Organ Initiation at the Shoot Apical Meristem." *Plant Signaling & Behavior*: 4–7.

Besnard, Fabrice, ENS Lyon, France. 2011. "Study of the Role of the AHP6 Gene in the Control of Phyllotaxis in Arabidopsis Thaliana Robustness and Coupling between Space and Time during Pattern Formation." *Thesis*: 344.

Besnard, Y Refahi, V Morin, B Marteaux, G Brunoud, P Chambrier, F Rozier1, V Mirabet, J Legrand, S Laine, E Thevenon, Et Farcot, C Cellier, P Das, A Bishopp, R Dumas, F Parcy, Y Helariutta, A Boudaoud, Y Guedon & C Godin, J Traas, and T Vernoux. 2014. "Cytokinin Signalling Inhibitory Fields Provide Robustness to Phyllotaxis ´." *Nature*: 2–9.

Braybrook, Siobhan a., and Alexis Peaucelle. 2013. "Mechano-Chemical Aspects of Organ Formation in Arabidopsis Thaliana: The Relationship between Auxin and Pectin." *PLoS ONE* 8(3).

Breuil-Broyer, Stephanie et al. 2004. "High-Resolution Boundary Analysis during Arabidopsis Thaliana Flower Development." *Plant Journal* 38(1): 182–92.

Burian, a. et al. 2015. "The CUP-SHAPED COTYLEDON2 and 3 Genes Have a Post-Meristematic Effect on Arabidopsis Thaliana Phyllotaxis." *Annals of Botany*: 807–20. http://aob.oxfordjournals.org/cgi/doi/10.1093/aob/mcv013.

Chandler, J. W., and W. Werr. 2014. "Arabidopsis Floral Phytomer Development: Auxin Response Relative to Biphasic Modes of Organ Initiation." *Journal of Experimental Botany* 65(12): 3097–3110.

Chen, Q et al. 1999. "The Arabidopsis FILAMENTOUS FLOWER Gene Is Required for Flower Formation." *Development (Cambridge, England)* 126(12): 2715–26.

Contento, Anthony L., Yan Xiong, and Diane C. Bassham. 2005. "Visualization of Autophagy in Arabidopsis Using the Fluorescent Dye Monodansylcadaverine and a GFP-AtATG8e Fusion Protein." *Plant Journal* 42: 598–608.

Douady, S. 1996. "Phyllotaxis as a Dynamical Self Organizing Process Part II: The Spontaneous Formation of a Periodicity and the Coexistence of Spiral and Whorled Patterns." *Journal of Theoretical Biology* 178(3): 275–94. http://linkinghub.elsevier.com/retrieve/pii/S0022519396900259.

Douglas, Scott J et al. 2017. "A Novel Filamentous Flower Mutant Suppresses Brevipedicellus Developmental Defects and Modulates Glucosinolate and Auxin Levels." *PLoS ONE* 1: 1–30.

Eshed, Yuval, Stuart F. Baum, and John L. Bowman. 1999. "Distinct Mechanisms Promote Polarity Establishment in Carpels of Arabidopsis." *Cell* 99(2): 199–209.

Gheysen, Godelieve, Raimundo Villarroel, and Marc Van Montagu. 1991. "Illegitimate Recombination in Plants: A Model for T-DNA Integration." *Genes and Development* 5(2): 287–97.

Goldshmidt, Alexander, John Paul Alvarez, John L Bowman, and Yuval Eshed. 2008. "Signals Derived from YABBY Gene Activities in Organ Primordia Regulate Growth and Partitioning of Arabidopsis Shoot Apical Meristems." *The Plant cell* 20(5): 1217–30. http://www.pubmedcentral.nih.gov/articlerender.fcgi?artid=2438466&tool=pmcentrez&rendertype=abstract (December 19, 2013).

Guédon, Yann et al. 2013. "Pattern Identification and Characterization Reveal Permutations of Organs as a Key Genetically Controlled Property of Post-Meristematic Phyllotaxis." *Journal of Theoretical Biology* 338: 94–110. http://dx.doi.org/10.1016/j.jtbi.2013.07.026.

Ha, Chan Man et al. 2003. "The BLADE-ON-PETIOLE 1 Gene Controls Leaf Pattern Formation through the Modulation of Meristematic Activity in Arabidopsis." *Development (Cambridge, England)* 130(1): 161–72.

Ha, Chan Man, Ji Hyung Jun, Hong Gil Nam, and Jennifer C Fletcher. 2007. "BLADE-ON-PETIOLE 1 and 2 Control Arabidopsis Lateral Organ Fate through Regulation of LOB

Domain and Adaxial-Abaxial Polarity Genes." *The Plant cell* 19(6): 1809–25. http://www.pubmedcentral.nih.gov/articlerender.fcgi?artid=1955725&tool=pmcentrez&rendertype=abstract.

Hamant, O. et al. 2008. "Developmental Patterning by Mechanical Signals in Arabidopsis." *Science* 322(5908): 1650–55. http://www.sciencemag.org/cgi/doi/10.1126/science.1165594.

Heisler, Marcus G. et al. 2005. "Patterns of Auxin Transport and Gene Expression during Primordium Development Revealed by Live Imaging of the Arabidopsis Inflorescence Meristem." *Current Biology* 15: 1899–1911.

Hofmeister Allgemeine HW, der Gewächse M. Handbuch Der Physiologischen Botanik I-2. Leipzig: W. Engelmann; 1868

Hussey, G. 1970. "Vitro Growth of Vegetative Tomato Shoot Apices." *Journal of Experimental Botany* 22(72).

Jung, Jae-hoon Park, Chung-mo. 2007. "MIR166 / 165 Genes Exhibit Dynamic Expression Patterns in Regulating Shoot Apical Meristem and Floral Development in Arabidopsis." *Planta*: 1327–38.

Ketelaar, Tijs et al. 2004. "Arabidopsis Homologues of the Autophagy Protein Atg8 Are a Novel Family of Microtubule Binding Proteins." *FEBS Letters* 567: 302–6.

Kierzkowski, Daniel et al. 2012. "Elastic Domains Regulate Growth and Organogenesis in the Plant Shoot Apical Meristem." *Science* 335(6072): 1096–99. http://www.ncbi.nlm.nih.gov/pubmed/22383847.

Kim, Joonki et al. 2005. "microRNA-Directed Cleavage of ATHB15 mRNA Regulates Vascular Development in Arabidopsis Inflorescence Stems." *Plant Journal* 42(1): 84–94.

Kwiatkowska, Dorota. 2006. "Flower Primordium Formation at the Arabidopsis Shoot Apex: Quantitative Analysis of Surface Geometry and Growth." *Journal of Experimental Botany* 57(3): 571–80.

Landrein, Benoit et al. 2015. "Meristem Size Contributes to the Robustness of Phyllotaxis in Arabidopsis." *Journal of Experimental Botany* 66(5): 1317–24.

Landrein, Benoît et al. 2013. "Impaired Cellulose Synthase Guidance Leads to Stem Torsion and Twists Phyllotactic Patterns in Arabidopsis." *Current Biology* 23(10): 895–900.

Lugassi, Nitsan, Naomi Nakayama, Rachel Bochnik, and Moriyah Zik. 2010. "A Novel Allele of FILAMENTOUS FLOWER Reveals New Insights on the Link between Inflorescence and Floral Meristem Organization and Flower Morphogenesis." *BMC plant biology* 10: 131. http://www.pubmedcentral.nih.gov/articlerender.fcgi?artid=3017777&tool=pmcentrez&rendertype=abstract.

Merelo, Paz et al. 2016. "Regulation of MIR165 / 166 by Class II and Class III Homeodomain Leucine Zipper Proteins Establishes Leaf Polarity." *Proceedings of the National Academy of Sciences* 166: 3–8.

Michaeli, Simon et al. 2015. "Autophagy in Plants - What's New on the Menu?" *Trends in Plant Science* 21(2): 134–44. http://dx.doi.org/10.1016/j.tplants.2015.10.008.

Milani, Pascale et al. 2011. "In Vivo Analysis of Local Wall Stiffness at the Shoot Apical Meristem in Arabidopsis Using Atomic Force Microscopy." *Plant Journal* 67: 1116–23.

Negin, Boaz, Or Shemer, Yonatan Sorek, and Leor Eshed Williams. 2017. "Shoot Stem Cell Specification in Roots by the WUSCHEL Transcription Factor." *Plos One* 12(4): e0176093. http://dx.plos.org/10.1371/journal.pone.0176093.

O'Malley, Ronan C et al. 2007. "An Adapter Ligation-Mediated PCR Method for High-Throughput Mapping of T-DNA Inserts in the Arabidopsis Genome." *Nature protocols* 2: 2910–17.

Ochando, Isabel et al. 2006. "Mutations in the microRNA Complementarity Site of the INCURVATA4 Gene Perturb Meristem Function and Adaxialize Lateral Organs in Arabidopsis." *Plant physiology* 141(2): 607–19. http://www.pubmedcentral.nih.gov/articlerender.fcgi?artid=1475466&tool=pmcentrez&rendertype=abstract.

———. 2008. "Alteration of the Shoot Radial Pattern in Arabidopsis Thaliana by a Gain-of-Function Allele of the Class III HD-Zip Gene INCURVATA4." *International Journal of Developmental Biology* 52(7): 953–61.

Ossowski, Stephan et al. 2014. "The Rate and Molecular Spectrum of Spontaneous Mutations in Arabidopsis Thaliana." *Science* 327(5961): 1–9.

Pabinger, Stephan et al. 2014. "A Survey of Tools for Variant Analysis of next-Generation Genome Sequencing Data." *Briefings in Bioinformatics* 15(2): 256–78.

Păcurar, Daniel Ioan et al. 2012. "A Collection of INDEL Markers for Map-Based Cloning in Seven Arabidopsis Accessions." *Journal of Experimental Botany* 63(7): 2491–2501.

Parcy, Francis et al. 1998. "A Genetic Framework for Floral Patterning." *Nature* 395(6702): 561–66.

Peaucelle, Alexis et al. 2008. "Arabidopsis Phyllotaxis Is Controlled by the Methyl-Esterification Status of Cell-Wall Pectins." *Current Biology* 18: 1943–48.

Peaucelle, Alexis, Siobhan a. Braybrook, et al. 2011. "Pectin-Induced Changes in Cell Wall Mechanics Underlie Organ Initiation in Arabidopsis." *Current Biology* 21: 1720–26.

Peaucelle, Alexis, Romain Louvet, et al. 2011. "The Transcription Factor BELLRINGER Modulates Phyllotaxis by Regulating the Expression of a Pectin Methylesterase in Arabidopsis." *Development* 4741: 4733–41.

Peaucelle, Alexis, and Patrick Laufs. 2007. "Phyllotaxy: Beyond the Meristem and Auxin Comes the miRNA." *Plant signaling & behavior* 2(May 2015): 293–95.

Pinon, Violaine et al. 2013. "Local Auxin Biosynthesis Regulation by PLETHORA Transcription Factors Controls Phyllotaxis in Arabidopsis." *Proceedings of the National Academy of Sciences of the United States of America* 110(24): 1107–12. http://www.pubmedcentral.nih.gov/articlerender.fcgi?artid=3549086&tool=pmcentrez&rendertype=abstract.

Pirooznia, Mehdi et al. 2014. "Validation and Assessment of Variant Calling Pipelines for next-Generation Sequencing." *Human Genomics* 8(1): 14. http://humgenomics.biomedcentral.com/articles/10.1186/1479-7364-8-14.

Prasad, Kalika et al. 2011. "Arabidopsis PLETHORA Transcription Factors Control Phyllotaxis." *Current Biology* 21: 1123–28.

Ragni, Laura, Enric Belles-Boix, Markus Günl, and Véronique Pautot. 2008. "Interaction of KNAT6 and KNAT2 with BREVIPEDICELLUS and PENNYWISE in Arabidopsis Inflorescences." *The Plant cell* 20(4): 888–900. http://www.ncbi.nlm.nih.gov/pubmed/18390591.

Reddy, G Venugopala, Marcus G Heisler, David W Ehrhardt, and Elliot M Meyerowitz. 2004. "Real-Time Lineage Analysis Reveals Oriented Cell Divisions Associated with Morphogenesis at the Shoot Apex of Arabidopsis Thaliana." *Development (Cambridge, England)* 131(17): 4225–37. http://www.ncbi.nlm.nih.gov/pubmed/15280208 (December 12, 2013).

Reinhardt, Didier et al. 2003. "Regulation of Phyllotaxis by Polar Auxin Transport." *Nature* 426: 255–60.

Salomé, P a et al. 2012. "The Recombination Landscape in Arabidopsis Thaliana F2 Populations." *Heredity* 108(4): 447–55. http://dx.doi.org/10.1038/hdy.2011.95.

Sawa, S, T Ito, Y Shimura, and K Okada. 1999. "FILAMENTOUS FLOWER Controls the Formation and Development of Arabidopsis Inflorescences and Floral Meristems." *The Plant cell* 11(1): 69–86. http://www.pubmedcentral.nih.gov/articlerender.fcgi?artid=144087&tool=pmcentrez&rendertype=abstract.

Sawa, Shinichiro et al. 1999. "Filamentous Flower, a Meristem and Organ Identity Gene of Arabidopsis, Encodes a Protein with a Zinc Finger and HMG-Related Domains." *Genes and Development* 13(9): 1079–88.

Schneeberger, Korbinian. 2014. "Using next-Generation Sequencing to Isolate Mutant Genes from Forward Genetic Screens." *Nature Reviews Genetics* 15(10): 662–76. http://www.nature.com/doifinder/10.1038/nrg3745.

Slavikova, S. 2005. "The Autophagy-Associated Atg8 Gene Family Operates Both under Favourable Growth Conditions and under Starvation Stresses in Arabidopsis Plants." *Journal of Experimental Botany* 56(421): 2839–49. http://jxb.oxfordjournals.org/lookup/doi/10.1093/jxb/eri276.

Smyth, D R, J L Bowman, and E M Meyerowitz. 1990. "Early Flower Development in Arabidopsis." *Plant Cell* 2(8): 755–67. http://www.ncbi.nlm.nih.gov/pubmed/2152125.

Vernoux, T. et al. 2011. "The Auxin Signalling Network Translates Dynamic Input into Robust Patterning at the Shoot Apex." *Molecular Systems Biology* 7(1): 508–508. http://msb.embopress.org/cgi/doi/10.1038/msb.2011.39.

Waterworth, Wanda M., Georgina E. Drury, Clifford M. Bray, and Christopher E. West. 2011. "Repairing Breaks in the Plant Genome: The Importance of Keeping It Together." *New Phytologist* 192(4): 805–22.

Weigel, Detlef, and Em Meyerowitz. 1993. "Activation of Floral Homeotic Genes in Arabidopsis." *Science* 261(1973): 1–4. http://www.sciencemag.org/content/261/5129/1723.short.

Weijers, D et al. 2001. “An Arabidopsis Minute-like Phenotype Caused by a Semi-Dominant Mutation in a RIBOSOMAL PROTEIN S5 Gene.” *Development (Cambridge, England)* 128(21): 4289–99. http://www.ncbi.nlm.nih.gov/pubmed/11684664.

Wesselborg, Sebastian, and Björn Stork. 2015. “Autophagy Signal Transduction by ATG Proteins: From Hierarchies to Networks.” *Cellular and Molecular Life Sciences*. http://link.springer.com/10.1007/s00018-015-2034-8.

Zhou, Yuyi et al. 2015. “Spatiotemporal Sequestration of miR165/166 by Arabidopsis Argonaute10 Promotes Shoot Apical Meristem Maintenance.” *Cell Reports* 10(11): 1819–27. http://linkinghub.elsevier.com/retrieve/pii/S2211124715002053.

Zhu, Hongliang et al. 2011. “Arabidopsis argonaute10 Specifically Sequesters miR166/165 to Regulate Shoot Apical Meristem Development.” *Cell* 145(2): 242–56. http://dx.doi.org/10.1016/j.cell.2011.03.024.

DISCUSSION

INITIAL QUESTIONS OF MY PH.D PROJECT: OPENING THE TOOLBOX OF PHYLLOTACTIC DIVERSITY

In this work, we intended to extend our knowledge about phyllotaxis towards other patterns than the most studied spiral. In particular, we focused on whorls, the dominant arrangement in angiosperm flowers which also occurs in vegetative or inflorescence shoots in some species. A first question was to study how plants make whorls, and whether current knowledge still applies in this case. A second question was to understand how plants switch between different phyllotaxis. Indeed, phyllotaxis is very robust and displays low variance, at least for the radial distribution of organs (Besnard *et al.*, 2014, Landrein *et al.*, 2015). However, robustness does not preclude plasticity: most plants produce at least two distinct phyllotaxis, one for the vegetative or inflorescence shoot and one for the flowers. In this case, the different phyllotaxis are produced by two distinct meristems, the shoot apical meristem and the floral meristem (Bartlett *et al.*, 2014). But in some species, the same meristem undergoes transitions between phyllotaxis (Kwiatkowska 1995). Theoretical models can predict which parameters should change and how they evolve to perform such phyllotactic switches. Yet, the nature of the causal changes occurring in the genetic network controlling organogenesis and meristem patterning and how this translates at the molecular and cellular levels are totally unknown.

With a Fibonacci spiral in the shoot and whorls in flowers, *A. thaliana* allows studying different phyllotaxis. However, whorl formation in flowers is barely observable because sepals rapidly hide the entire floral meristem. Moreover, indeterminate shoots ease the study of phyllotaxis, because of iterative organ formation: a single snapshot of a SAM displays several organs at different stages of development, capturing the dynamics of the system. Changing the phyllotaxis of *A. thaliana* shoots then appears as an interesting experimental trick to study different phyllotaxis while keeping the convenient advantages of this system. To our knowledge, and despite very likely intense trials (F. Besnard, personal communication),

there is no report of *A. thaliana* mutants with a proper change in phyllotaxis, i.e. a switch from the wild-type Fibonacci spiral to another regular arrangement observed in nature. Interestingly, such "homeotic" mutants of phyllotaxis (Kuhlemeier *et al.*, 2007) have been found in maize (*abphyl1* and *abphyl2*) (Giulini *et al.*, 2004; Yang *et al.*, 2015) and rice (*decussate*) (Itoh *et al.*, 2012) where the wild-type vegetative distichous phyllotaxis is modified into a decussate arrangement. Whether this difference in the mutational spectrum of *A. thaliana* versus maize and rice is due to differences in the underlying genetic network or from different properties of the initial phyllotaxis (Fibonacci spiral versus distichous) is an open question.

Despite the absence of regular changes in phyllotactic mutants of *A. thaliana*, some mutants display peculiar arrangements. We chose the *Arabidopsis* T-DNA mutant DRB27 for the particular pattern of inflorescence phyllotaxis, which was reminiscent of vegetative whorls observed in unrelated species.

ORGANOGENESIS IN CRESCENTS: A VIOLATION OF CLASSICAL PHYLLOTACTIC RULES

Instead of a whorled pattern, we observed the formation of many crescents along the stem (Figures I.3.E & I.4.G), as well as around the meristem in confocal imaging (Figure I.8.A), but we also observed spiral patterns approaching the Fibonacci spiral.

In the first case, we observed growth distortions at the meristem (Figure I.7.A) and no clear pattern was visible, although it might be shifted by variable meristem growth. Therefore the crescents happened to originate in early stages of organogenesis, and not to be the result of post-meristematic growth variation. This abnormal phyllotactic pattern also occurs in a context of high production of organs, meaning that the pattern is not correlated to a defect in the organogenesis-starting program. This discovery was completely new, and opposite to Hofmeister's rule and all phyllotactic models. Indeed in DRB27, organogenesis did not necessarily occur in the largest gap available in the meristem peripheral zone. In the second case, old primordia were still close to the centre, indicating a possible post-meristematic effect as well.

Meristem homeostasis includes typical growth pattern, as stem cell divide slowly and peripheral zone cells can proliferate rapidly. These distortions could be due to ectopic growth, but considering our observations of *DR5* (Figure I.7.A), it is most likely that they are in fact due to the presence of idle zones. Moreover, the variability of the patterns observed at the meristem indicates that the growth distortions inducing formation of crescents might be an episodic phenomenon.

THE POWER OF FORWARD GENETICS: DRB27 IS LIKELY AN IMPROBABLE DOUBLE *fil mir166a* MUTANT

Forward genetics offers an unbiased approach to study the development of phenotypes. It leads to the discovery of either totally unknown genes, or sheds a new light on the function of already known genes. Thanks to a thorough genomic analysis, we found that the DRB27 line bears a complex mutant locus with multiple insertions and other mutational events. The most serious candidates are mutations in *FILAMENTOUS FLOWER (FIL)* and *MIR166A,* although definitive validation is still needed. These genes are not new, as they were already described as two positive regulators of abaxial identity. However, this unique combination was never described before, which can easily be understood regarding the very short genetic distance between the two main loci (1.89 cM, Table II.B), which seriously complicates crosses between mutant alleles of those two genes. Moreover, this study shows the importance of the initial question guiding any mutagenic screen, especially in case of pleiotropic phenotypes. DRB27 could also have been isolated as a polarity mutant, but we selected this line for its pseudo-whorled phyllotaxis. Altogether, this illustrates the power of forward genetic approaches.

Some mutant alleles of *fil* have already been associated with progressive phyllotaxis defects and meristem enlargement (see Result section I.C.3 and Figure I.12), a phenotype that led Lugassi *et al*. (2010) to suggest that *fil* mutants were potential tools to study meristem organization. Moreover, co-initiations were occasionally seen on the *MIR166A*-resistant *icu4* mutant (Kim *et al*., 2005; Ochando *et al*., 2006), and if there is no mention in the literature of a single *mir166a* loss-of-function mutant (most likely because of high redundancy), the *men1* overexpressor of *MIR166A* displays enlarged and fasciated meristem with over proliferation of flowers (Kim *et al*., 2005). However, spiral still seemed to be the main phyllotactic pattern

observed in all these lines, even in *fil* enlarged meristems, where canonical angles could still be seen (Figure I.12.C, F, I; Lugassi *et al*. 2010). These observations were similar to what we observed in DRB27 in the absence of crescent-shaped stretches of organogenesis (Figure I.8.B), but this specific part of the phenotype was not seen in any of the *fil* mutants described in the literature. It is likely that these two abaxial regulators only have a limited role on phyllotaxis when separated, whereas the combination of them disables the plant to develop correctly and induce the formation of crescent-shaped bursts of organogenesis.

Nevertheless, functional validation should be completed. Production of independent lines recapitulating the phenotype is essential to confirm the present results. Due to the very short distance between *FIL* and *MIR166A*, it will be necessary to perform simple mutants separately to the double mutant, which will be obtained by successive mutagenesis with the two constructs. The inconvenient of generating independently simple and double mutants might be that mutational events will be different. A close attention on this will be necessary to confirm or not that the difference between two lines is due to the addition of another mutation, and not of the creation of another allele. Moreover, all described *fil* or *mir166a*-related mutants are in different genetic backgrounds, as well as our transcriptional reporters (*Col-0*). It might be interesting to introduce these mutations into *Ws-4* as well as *Col-0* wild types to verify that the DRB27 phenotype is not impacted by genetic background.

MIR166A and *FIL* are expressed in lateral organs, but their mutants induce defects in SAM and phyllotaxis phenotypes. Perturbation of these genes thus necessarily induces non cell-autonomous effects (likely indirect). We conducted several experiments to understand how organogenesis, auxin signalling and SAM homeostasis was perturbed in this mutant, especially during the episodes of organ crescent formation. We propose two possible mechanisms, not necessarily mutually exclusive, to explain the phyllotactic perturbations: they would be a consequence 1) either of local feedbacks from the under-development of organs, which perturb organ initiation in the PZ; 2) either of a global feedback effect on the geometry of the meristem.

HOW POLARITY DEFECTS FEEDBACK ON PHYLLOTAXIS: THE HYPOTHESIS OF LOCAL PERTURBATION OF INHIBITORY FIELDS

The balance between the polarity players is crucial in many aspect of plant development. During organogenesis, it is essential for the progression throughout developmental sages. Indeed, lateral organ outgrowth was shown to proceed first through abaxialization according to gene expression (Sawa *et al.*, 1999; Eshed *et al.*, 1999, 2001, Chandler *et al.*, 2012), and cell lineage analysis (Kwiatkowska *et al.*, 2006). Newly formed primordia are then abaxial by default in early stages, and abaxial players are thus the earliest regulators of lateral organ differentiation. The double mutation of abaxial regulators in DRB27 most likely results in under-development of structures, as shown by the juvenile-like rosette leaves, and the presence of filaments. This would explain why the loss of abaxial regulators does not produce an adaxialisation of the organs: the apparent abaxialization of the filaments in DRB27, as shown by *FIL* expression lacking the wild type pattern, would rather be due to an arrest in the developmental program instead of being just a signal of abaxialization. The hypothesis of filaments being under-developed flowers is also consistent with the low *WUS* expression in those filaments (Figure III.2.F), showing a low level of stem cell specification together with persistent DR5 activation in the floral meristem (Figure I.11.D). Indeed *WUS* expression starts at late floral stage 2 (Lenhard *et al.*, 2001; Lohmann *et al.*, 2001), and is not as strongly activated in the mutant as in the wild type. Finally, another important phenotype of flowers is the establishment and differentiation of the four whorls, two of which are lacking in DRB27 mutants. Development of the missing stamens and petals development should be led by the B-function flower genes (*PISTILATA* & *APETALA3*), which transcription starts at stage 1 of flowers development (Weigel & Meyerowitz, 1993; Parcy *et al.*, 1998). In the case of the filaments being defined as under-developed flowers,

these transcription factors or their targets might not be activated, a theory that could be verified by observation of their fluorescent reporters, for example.

To summarize, we propose that the developmental program of organs in DRB27 cannot proceed to the next step, and remains abaxial thanks to other abaxial players still expressed. This hypothesis was already put forward by Sawa *et al*. (1999) and Chen *et al*. (1999) in the description of *fil* alleles, after scanning electron microscopy analysis of the epidermis.

How the perturbation of organ development at very early stages, i.e. as soon as stage P1 when FIL expression starts, could impact phyllotaxis? First, at this stage, organs are not separated from the meristem by any physical boundary: the tissue of the PZ is continuous. Inhibitory fields predicted by models (Douady & Couder, 1996) or proxies visualized in vivo (Brunoud *et al*., 2012) are acting in this zone. Locally, each abaxialized-immature DRB27 organs could then interfere in its vicinity with either mechanical properties of the cell walls or auxin transport and signalling in the PZ. Several data could support this hypothesis.

Concerning a feedback on cell wall properties, it was shown previously that mechanical properties of the meristem surface may allow or not the outgrowth of primordia, thanks to the combined actions of PMEs and PME INHIBITORs (PMEI; Peaucelle *et al*., 2008) together with auxin peaks. It was also shown that microtubules adapt their orientation to the tensile forces at the meristem surface, and guide the PIN1 efflux carrier orientation, therefore acting directly on the phyllotactic pattern (Hamant *et al*., 2008). A variable surface stiffness across the meristem would thus be a great source of pattern perturbation (see introduction section III.C; also reviewed by Sampathkumar *et al*., 2014). We have explored the mechanical properties of DRB27 mutant's meristems, and measured huge increase of surface stiffness in the peripheral region (Figure III.4). It is not clear how extended these zones are, but they might be correlated with the presence of idle zones we show in Figure I.7.A. An interesting way to understand the correlation between organogenesis in DRB27 and surface stiffness, would be to make time courses observations of DRB27 lines with fluorescent markers for cell wall stiffness regulators, such as the cell wall modulator *PECTIN METHYLESTERASE 5 (PME5)*, which was shown to participate in primordia outgrowth

(Peaucelle *et al.*, 2008). This marker could be combined with *DR5* or *FIL* to follow simultaneously organogenesis activity.

Concerning auxin signalling, it was shown to occur more on the abaxial side of developing organs (Brandt *et al.*, 2012; Huang *et al.*, 2014; Xie *et al.*, 2015). In DRB27 filaments, it is maintained with no specific pattern (Figures I.11.D). Second, low auxin also is a feature of boundaries between developing organs and meristematic cells (Zhao *et al.*, 2013; Figure III.3.F). DRB27 meristem showed poor definition of lateral organ boundaries as shown by the *pARF3* transcriptional reporter (Figure III.3.G), an observation that could be complemented with the study of other boundary transcriptional reporters such as *CUC*, *BOP*, or even *LAS*, which has been shown to relay a *FIL*-mediated feedback on the meristem (Goldschmidt *et al.*, 2008). Boundaries are important territories for phyllotaxis: PIN1 transporters in this region show a rapid reversal in their polarity, suggesting that boundaries split auxin fluxes between the growing P1 and the rest of the PZ (Heisler *et al.*, 2005). Affecting boundary definition could thus modify the range of inhibitory fields regulating phyllotaxis. A precise analysis of PIN1 polarity in the PZ of DRB27 mutants would be necessary to address this question.

Finally, all the inhibitory fields models that build our knowledge on phyllotaxis are based on the hypothesis that all lateral organs are equivalent (Wardlaw *et al.*, 1949; Richards *et al.*, 1951; Douady & Couder, 1996; Adler *et al.*, 1998; Shipman *et al.*, 2005). Each organ's field is only different according to their age, as they recede away from the central zone (see introduction section II.A), and the whole system is a dynamo, which homeostasis is maintained through the balance between renewal and receding of equivalent lateral organs. However, lateral organs quantified in DRB27 were of several classes: we observed a mixture of filaments, type-A flowers (as defined by Sawa *et al.*, 1999), secondary meristems and cauline leaves, all potentially coming out of a single cluster. At the meristem, we must find markers that define these different classes of organs in early stages, such as LEAFY (Schultz *et al.*, 1991) or AINTEGUMENTA (Elliott *et al.*, 1996; Klucher *et al.*, 1996), so that we could trace them back to the peripheral zone while growth distortions occur, and see if expression of one or a combination of these markers in the peripheral zone are correlated with

growth distortions. On a more theoretical point of view, one might want to see the effect of implementing different classes of fields into the current models.

HOW POLARITY DEFECTS FEEDBACK ON STEM CELLS: THE GEOMETRIC HYPOTHESIS

Together with the poor boundary definition in DRB27, we observed modifications of the global geometry of the SAM. A dramatic increase of meristem diameter (35.6%; Figure III.1.C) and height (81%; Figure III.1.D) were followed by modifications of the proportions of functional domains. For instance, the *CLV3* and *WUS* domains define the central zone and the organizing centre, respectively and in DRB27 mutants, only WUS expanded radially to the wild type proportions, whereas both WUS height and CLV3 domain were proportionally smaller in the mutant than in the wild type. They control the stem cells domain, which represents a central inhibitory field that is crucial for meristem geometry and phyllotaxis. Consequently the central zone volume was proportionally smaller in DRB27 than in the wild type.

On the other hand *AHP6* signalling, normally occuring at the periphery, expanded towards the centre (Figure III.3.B, C, E). No direct link was established between *AHP6* and *WUS* in the literature. However cytokinin signalling promotes *WUS* expression in a positive feedback loop (Shani *et al.*, 2006; Gordon *et al.*, 2009; Chickarmane *et al.*, 2012). But expansion of an inhibitor of CK signalling, such as *AHP6* (Besnard *et al.*, 2014), towards the centre should be correlated with decrease of *WUS* zone. Our results show that in the wild type, the *pAHP6* domain overlaps with that of *WUS*/*CLV3* in diameter (Figure III.3.B & D). This suggests that *AHP6* might be involved in a pathway that is independent or partially independent of the cytokinin-*WUS* signalling pathway controlling the central zone.

In DRB27, the average *AHP6* and *DR5* domains expanded toward the centre, inducing a slight overlap between the auxin signalling domain and that of *WUS* and *CLV3*, (Figure III.3.D-E). However later organogenesis territory (*FIL* domain) is unchanged compared to the wild type, showing that auxin signalling is not sufficient to launch organogenesis in the

central zone. It suggests that the cells from the central zone remain undifferentiated upon the auxin-mediated organogenesis signal, meaning that their stem-cell identity prevents them from doing so. Co-expression of these markers in the DRB27 mutants would provide finer insight on this phenomenon. Moreover, the correlation between DR5 disorganization and the presence of idle zones versus growing zones might indicate that DRB27 have auxin flux defects. Indeed, *pin1* rosette meristems were shown to present similar crescent as that of DRB27 (Guenot *et al.*, 2012), and PIN1 convergence patterns were shown to be correlated with the expression of *ARF5* in the peripheral zone (or *MONOPTEROS*, *MP*) (Bhatia *et al.*, 2016). Confocal observation of the DII auxin sensor and immuno-localization of the PIN1 proteins in DRB27 would lead us to better understand auxin distribution in the meristem.

These confocal microscopy observations altogether with the clustered patterns observed at the shoot scale (Figures I.2, I.3 & I.4), indicated that in this case a clustered phyllotaxis was associated with geometry issues at the meristem scale. Another crucial geometry factor is the plant growth. To maintain the canonical pattern induced by lateral organs inhibitions, there must be a dynamical balance between organ production and the post-meristematic growth that will push them away and free space for the young ones (Douady & Couder, 1996). In DRB27, we have shown that overall more organs are produced for a similar plant height (Figure I.2.A & B). Moreover, we observed some co-initiations, but not to the extent of the clusters sizes (Figure I.2.F), indicating that most likely these clusters are formed partially as successive organs with variable post-meristematic growth. However, the clustering events we observed at the meristem (Figure I.8.A) were most likely associated with growth distortions in the peripheral zone (Figure I.7.A). Great insight on this phenomenon might come from future time-course observations of a cell-wall marker such as the LOW TEMPERATURE INDUCED 6B PROTEIN (LTI6B; Thompson *et al.*, 2008), associated with the previous markers (*DR5, AHP6, FIL*) in confocal microscopy. One could then trace cell division while identifying organogenesis steps, and see how far these two phenomenon are linked.

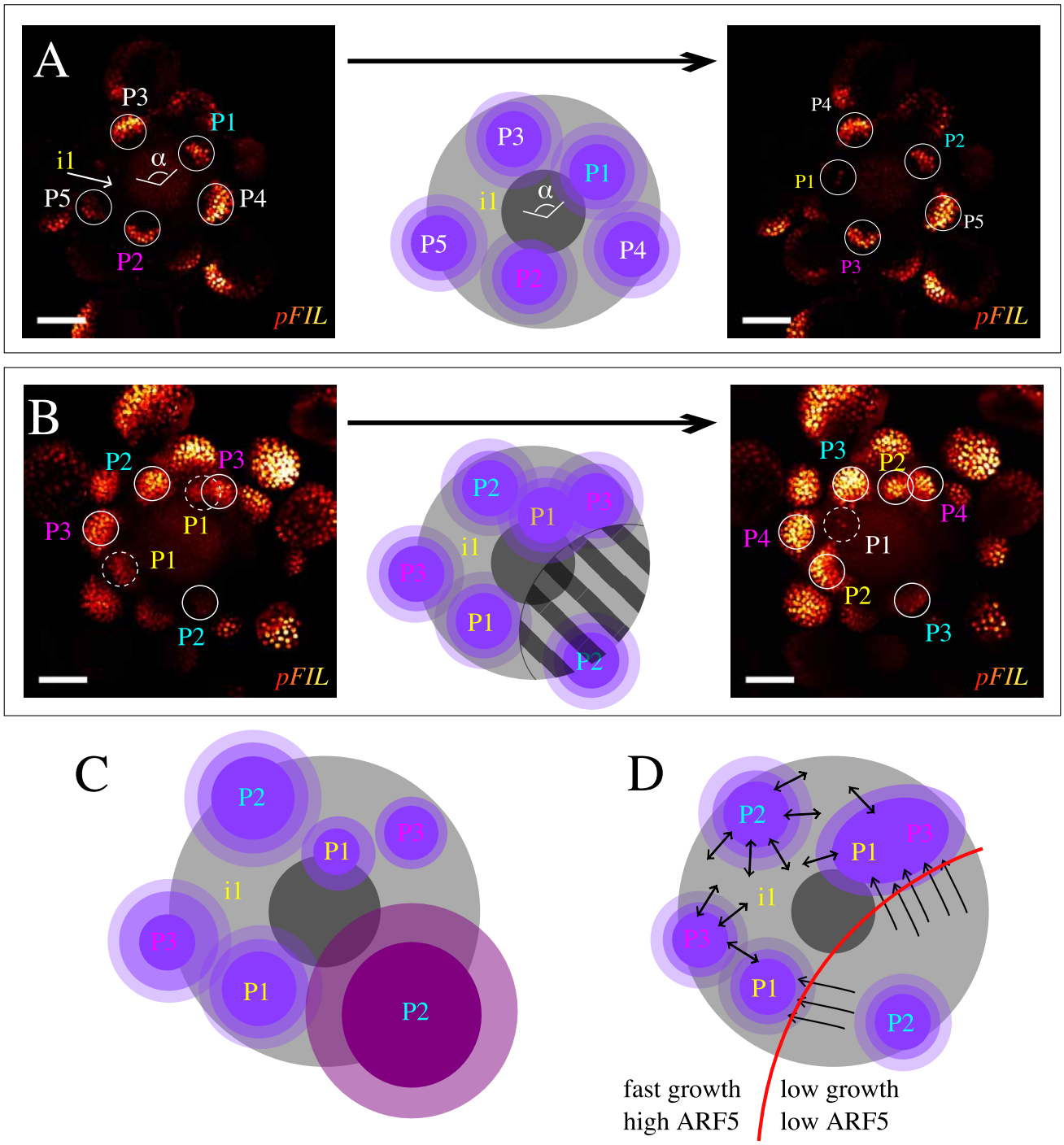

Figure IV: Hypothetical mechanisms inducing the formation of crescents in DRB27 meristems. The Figures 0.3, I., I.6.C and I.8.A are adapted to explain our hypotheses, Scale bars = 50 µm. A) In the wild type existing primordia (numbered from the youngest, P1, to the oldest, P5) generate inhibitory fields that block organ initiation in their vicinity. Growth moves the existing organs away from the tip of the meristem, thus lowering the inhibition and allowing for the next initiation to occur (i1). This process repeats itself as the plant grows, and ultimately successive organs are arranged in a meristem-centred spiral. B) In DRB27 this phenomenon only occurs in a portion of the peripheral zone whereas the striped zone remains idle. Fields might be of variable sizes or natures (C); or geometry of auxin fields might be modified by impaired fluxes (black arrows), for example due to misexpression or AFF5 (D).

CONCLUSION

We have identified a mutant which phenotype questions the rules of phyllotaxis. It sequencially produces bursts of organogenesis in crescent-shaped zones of the meristem, whereas other parts of the meristem remain idle. Moreover, Our work strongly suggests that mutations in the two abaxial regulators *FIL* and *MIR166A* are causing these defects, most likely in combination. We hypothesized that impaired communication of lateral organs to the meristem create growth variability, and unusual patterns of organ initiation in crescent shape. Auxin and the cytokinin inhibitor AHP6 have already been discovered as inhibitory fields. The defects in developing organs of DRB27 mutants could perturb these fields, in particular auxin depletion areas, or any other field emitted by organs towards the meristem, and which strength or nature would depend on their developmental stage or identity. There is in DRB27 a link between lateral organ polarity, meristem geometry, and cell wall mechanics. All these pillars of plant development are most likely very intricate in the complex gene regulation networks underlying meristem homeostasis and the emergence of phyllotactic patterns.

REFERENCE LIST

Adler, I. 1998. "The Role of Mathematics in Phyllotaxis." *Worl Scientific Publishing*: 171–74.

Bhatia, Neha et al. 2016. "Auxin Acts through MONOPTEROS to Regulate Plant Cell Polarity and Pattern Phyllotaxis." *Current Biology* 26(23): 3202–8.

Bartlett, Madelaine E, and Beth Thompson. 2014. "Meristem Identity and Phyllotaxis in Inflorescence Development." *Frontiers in plant science* 5(October): 1–11.

Besnard, Fabrice, Frédérique Rozier, and Teva Vernoux. 2014. "The AHP6 Cytokinin Signaling Inhibitor Mediates an Auxin-Cytokinin Crosstalk That Regulates the Timing of Organ Initiation at the Shoot Apical Meristem." *Plant Signaling & Behavior*: 4–7.

Brandt, Ronny et al. 2012. "Genome-Wide Binding-Site Analysis of REVOLUTA Reveals a Link between Leaf Patterning and Light-Mediated Growth Responses." *Plant Journal* 72(1): 31–42.

Brunoud, Géraldine et al. 2012. "A Novel Sensor to Map Auxin Response and Distribution at High Spatio-Temporal Resolution." *Nature* 482(7383): 103–6. http://www.nature.com/doifinder/10.1038/nature10791.

Chandler, J. W. 2012. "Floral Meristem Initiation and Emergence in Plants." *Cellular and Molecular Life Sciences* 69(22): 3807–18.

Chickarmane, Vijay S et al. 2012. "Cytokinin Signaling as a Positional Cue for Patterning the Apical-Basal Axis of the Growing Arabidopsis Shoot Meristem." *Proceedings of the National Academy of Sciences of the United States of America* 109(10): 4002–7. http://www.pnas.org/content/109/10/4002.full.

Douady, S. 1996. "Phyllotaxis as a Dynamical Self Organizing Process Part II: The Spontaneous Formation of a Periodicity and the Coexistence of Spiral and Whorled Patterns." *Journal of Theoretical Biology* 178(3): 275–94. http://linkinghub.elsevier.com/retrieve/pii/S0022519396900259.

Elliott, R C et al. 1996. "AINTEGUMENTA, an APETALA2-like Gene of Arabidopsis with Pleiotropic Roles in Ovule Development and Floral Organ Growth." *Plant Cell* 8(2): 155–68.

http://www.ncbi.nlm.nih.gov/pubmed/8742707\nhttp://www.plantcell.org/content/8/2/155.full.pdf.

Eshed, Yuval, Stuart F. Baum, and John L. Bowman. 1999. "Distinct Mechanisms Promote Polarity Establishment in Carpels of Arabidopsis." *Cell* 99(2): 199–209.

———. 2001. "Establishment of Polarity in Angiosperm Lateral Organs." *Trends in Genetics* 18(3): 134–41.

Giulini, Anna, Jing Wang, and David Jackson. 2004. "Control of Phyllotaxy by the Cytokinin-Inducible Response Regulator Homologue ABPHYL1." *Nature* 430: 1031–34.

Goldshmidt, Alexander, John Paul Alvarez, John L Bowman, and Yuval Eshed. 2008. "Signals Derived from YABBY Gene Activities in Organ Primordia Regulate Growth and Partitioning of Arabidopsis Shoot Apical Meristems." *The Plant cell* 20(5): 1217–30. http://www.pubmedcentral.nih.gov/articlerender.fcgi?artid=2438466&tool=pmcentrez&rendertype=abstract (December 19, 2013).

Gordon, Sean P, Vijay S Chickarmane, Carolyn Ohno, and Elliot M Meyerowitz. 2009. "Multiple Feedback Loops through Cytokinin Signaling Control Stem Cell Number within the Arabidopsis Shoot Meristem." *Proceedings of the National Academy of Sciences of the United States of America* 106(16): 16529–34.

Guenot, B et al. 2012. "PIN1-Independent Leaf Initiation in Arabidopsis." *Plant Physiology* 159(4): 1501–10. http://www.ncbi.nlm.nih.gov/entrez/query.fcgi?cmd=Retrieve&db=PubMed&dopt=Citation&list_uids=22723086.

Hamant, O. et al. 2008. "Developmental Patterning by Mechanical Signals in Arabidopsis." *Science* 322(5908): 1650–55. http://www.sciencemag.org/cgi/doi/10.1126/science.1165594.

Heisler, Marcus G. et al. 2005. "Patterns of Auxin Transport and Gene Expression during Primordium Development Revealed by Live Imaging of the Arabidopsis Inflorescence Meristem." *Current Biology* 15: 1899–1911.

Huang, Tengbo et al. 2014. "Arabidopsis KANADI1 Acts as a Transcriptional Repressor by Interacting with a Specific Cis-Element and Regulates Auxin Biosynthesis, Transport,

and Signaling in Opposition to HD-ZIPIII Factors." *The Plant cell* 26(1): 246–62. http://www.ncbi.nlm.nih.gov/pubmed/24464295.

Itoh, Jun Ichi et al. 2012. "Rice DECUSSATE Controls Phyllotaxy by Affecting the Cytokinin Signaling Pathway." *Plant Journal* 72: 869–81.

Kim, Joonki et al. 2005. "microRNA-Directed Cleavage of ATHB15 mRNA Regulates Vascular Development in Arabidopsis Inflorescence Stems." *Plant Journal* 42(1): 84–94.

Klucher, K M, H Chow, L Reiser, and R L Fischer. 1996. "The AINTEGUMENTA Gene of Arabidopsis Required for Ovule and Female Gametophyte Development Is Related to the Floral Homeotic Gene APETALA2." *Plant Cell* 8(2): 137–53. http://www.ncbi.nlm.nih.gov/pubmed/8742706\nhttp://www.plantcell.org/content/8/2/137.full.pdf.

Kuhlemeier, Cris. 2007. "Phyllotaxis." *Trends in Plant Science* 12(4): 143–50.

Kwiatkowska, Dorota. 1995. "Changes of Phyllotaxis in Anagallis Arvensis L." *Acta Societatis Botanicorum Poloniae* 64(4): 319–25.

———. 2006. "Flower Primordium Formation at the Arabidopsis Shoot Apex: Quantitative Analysis of Surface Geometry and Growth." *Journal of Experimental Botany* 57(3): 571–80.

Landrein, Benoit et al. 2015. "Meristem Size Contributes to the Robustness of Phyllotaxis in Arabidopsis." *Journal of Experimental Botany* 66(5): 1317–24.

Lenhard, Michael, Andrea Bohnert, Gerd J??rgens, and Thomas Laux. 2001. "Termination of Stem Cell Maintenance in Arabidopsis Floral Meristems by Interactions between Wuschel and Agamous." *Cell* 105(6): 805–14.

Lohmann, Jan U. et al. 2001. "A Molecular Link between Stem Cell Regulation and Floral Patterning in Arabidopsis." *Cell* 105(6): 793–803.

Lugassi, Nitsan, Naomi Nakayama, Rachel Bochnik, and Moriyah Zik. 2010. "A Novel Allele of FILAMENTOUS FLOWER Reveals New Insights on the Link between Inflorescence and Floral Meristem Organization and Flower Morphogenesis." *BMC plant biology* 10: 131. http://www.pubmedcentral.nih.gov/articlerender.fcgi?artid=3017777&tool=pmcentrez&rendertype=abstract.

Ochando, Isabel et al. 2006. “Mutations in the microRNA Complementarity Site of the INCURVATA4 Gene Perturb Meristem Function and Adaxialize Lateral Organs in Arabidopsis.” *Plant physiology* 141(2): 607–19. http://www.pubmedcentral.nih.gov/articlerender.fcgi?artid=1475466&tool=pmcentrez&rendertype=abstract.

Parcy, Francis et al. 1998. “A Genetic Framework for Floral Patterning.” *Nature* 395(6702): 561–66.

Peaucelle, Alexis et al. 2008. “Arabidopsis Phyllotaxis Is Controlled by the Methyl-Esterification Status of Cell-Wall Pectins.” *Current Biology* 18: 1943–48.

Richards, F. J. 1951. “Phyllotaxis: Its Quantitative Expression and Relation to Growth in the Apex.” *Philosophical Transactions of the Royal Society of London. Series B, Biological Sciences* 235(629): 509–64. http://dx.doi.org/10.1098/rstb.1951.0007\nhttp://rstb.royalsocietypublishing.org/content/235/629/509.abstract\nhttp://rstb.royalsocietypublishing.org/content/235/629/509.full.pdf.

Sampathkumar, Arun, An Yan, Pawel Krupinski, and Elliot M. Meyerowitz. 2014. “Physical Forces Regulate Plant Development and Morphogenesis.” *Current Biology* 24(10): R475–83. http://dx.doi.org/10.1016/j.cub.2014.03.014.

Sawa, Shinichiro et al. 1999. “Filamentous Flower, a Meristem and Organ Identity Gene of Arabidopsis, Encodes a Protein with a Zinc Finger and HMG-Related Domains.” *Genes and Development* 13(9): 1079–88.

Schultz, Elizabeth a, and George W Haughn ’. 1991. “LEAFY, a Homeotic Gene That Regulates Lnflorescence Development in Arabidopsis.” *The Plant Cell* 3(August): 771–81.

Shani, Eilon, Osnat Yanai, and Naomi Ori. 2006. “The Role of Hormones in Shoot Apical Meristem Function.” *Current Opinion in Plant Biology* 9(5): 484–89.

Shipman, P. D., and a. C. Newell. 2005. “Polygonal Planforms and Phyllotaxis on Plants.” *Journal of Theoretical Biology* 236: 154–97.

Thompson, M V, and S M Wolniak. 2008. “A Plasma Membrane-Anchored Fluorescent Protein Fusion Illuminates Sieve Element Plasma Membranes in Arabidopsis and Tobacco.” *Plant Physiology* 146(4): 1599–1610. <Go to ISI>://000256417900012.

Wardlaw, C. W. 1947. “Experimental Production of a Protostele from a Dictyostele in Dryopteris Aristata.” *Nature* 160(4053): 29–31.

Weigel, Detlef, and Em Meyerowitz. 1993. “Activation of Floral Homeotic Genes in Arabidopsis.” *Science* 261(1973): 1–4. http://www.sciencemag.org/content/261/5129/1723.short.

Xie, Yakun et al. 2015. “Meta-Analysis of Arabidopsis KANADI1 Direct Target Genes Identifies a Basic Growth-Promoting Module Acting Upstream of Hormonal Signaling Pathways.” *Plant Physiology* 169(2): 1240–53. http://www.plantphysiol.org/lookup/doi/10.1104/pp.15.00764.

Yang, F et al. 2015. “A Maize Glutaredoxin Gene , Abphyl2 , Regulates Shoot Meristem Size and Phyllotaxy.” *The Plant cell*: 1–12. http://www.ncbi.nlm.nih.gov/pubmed/25616873.

Zhao, Hongtao et al. 2013. “The ATP-Binding Cassette Transporter ABCB19 Regulates Postembryonic Organ Separation in Arabidopsis.” *PLoS ONE* 8(4).

MATERIALS AND METHODS

I – PLANT MATERIALS AND CULTURE CONDITIONS

All *Arabidopsis* lines used are described in Table M.A; Versailles lines is described by Bouchez *et al*. (1993) and corresponding T-DNA is detailed in Figure M.1.

Seeds were sterilized in a 20% bleach 0,1% Triton for 10 min, and washed 3 times prior to sowing. They were plated on MS medium (Duchefa Biochemie, Murashige & Skoog, 1962) supplemented with the adequate antibiotics when required, and grown under short days cycles (8h light/16h darkness) for 10 days at 20°C, before being transferred to soil without antibiotics. Plants were then grown for 5 weeks under the same short day cycle at 20°C, before transfer to a long day cycles (16h light/8h darkness). Lines containing *BIALAPHOS RESISTANCE (BAR)*, *HYGROMYCIN B PHOSPHOTRANSFERASE (HPH)* and *NEOMYCIN PHOSPHOTRANSFERASE II (NPTII)* genes were conferred resistance to phosphinothricin, hygromycin or kanamycin respectively. All genotyping primers are listed in Table M.B.

Other species described in the last result section were collected from the Botanical Garden of Lyon, by cutting 1cm of the apices and planting them into agarose media for immediate dissection and observation (see imaging section). Plants were sampled in spring from wild species, and chosen for their abundant production of young lateral organs in order to observe active meristems.

Line name	ecotype	Associated construct	Resistance genes	Origin
AHP6 reporter	*col-0*	pAHP6::ER-GFP	NPTII	Mahonen *et al.*, 2006
ARF3 reporter	*col-0*	pARF3::NLS-3xGFP	NPTII	Heisler *et al.*, 2005
ATG8E CRISPR line	*Ws-4*	pDE-Cas9 + guide (see Table M.B)	NPTII	unpublished
atg8e mutant line	*col-0*	SALK_126394	NPTII	NASC N668998
ATG8E reporter	*col-0*	p35S::ATG8e-GFP	NPTII	Contento *et al.*, 2005
ATG8E translational reporter	*Ws-4*	pRPS5a::NAE-mVENUS-ATG8e-3'UTR	HPH	unpublished
CLV3 transcriptionnal reporter	*col-0*	pCLV3::mCHERRY-NLS	BAR	Pfeiffer *et al.*, 2016
DR5 reporter	*col-0*	pDR5::3xVENUS-N7	BAR + HPH	Vernoux *et al.*, 2011 Brunoud *et al.*, 2012
DRB27	*Ws-4*	pGKB5 insertion	BAR + NPTII	IJPB Versailles
DZP10	*Ws-4*	pGKB5 insertion	BAR + NPTII	IJPB Versailles
EAV 83	*Ws-4*	pGKB5 insertion	BAR + NPTII	IJPB Versailles
EAT 101	*Ws-4*	pGKB5 insertion	BAR + NPTII	IJPB Versailles
EAT 197	*Ws-4*	pGKB5 insertion	BAR + NPTII	IJPB Versailles
FIL complementation	*Ws-4*	pFIL::FIL	HPH	unpublished
FIL CRISPR line	*Ws-4*	pHEE404 + double guide (see Table M.B)	HPH	unpublished
FIL transcriptionnal reporter	*col-0*	pFIL::dsRED-N7	BAR	Heisler *et al.*, 2005
fil8 mutant line	*Ler*	Ds transposon (Parinov et al., 1999)	NPTII	Goldschmidt *et al.*, 2008
fil	*Ler*	WiscDsLox 367E6_049	BAR	NASC N853104
icu4	*Enk-2*	point mutation	none	Ochando *et al.*, 2006
MIR166A complementation	*Ws-4*	pMIR166A::MIR166A	HPH	unpublished
MIR166A CRISPR line	*Ws-4*	pHEE404 + double guide (see Table M.B)	HPH	unpublished
Ws-4 wild type	*Ws-4*	none	none	NASC N5390
WUS transcriptionnal reporter	*col-0*	pWUS::3xVENUS-NLS	NPTII	Pfeiffer et al., 2016

Table M.A: All lines used in this work are listed with their corresponding ecotype, associated construct or mutational event if applicable, plant resistance genes and origin. Unpublished lines were made internally in the team.

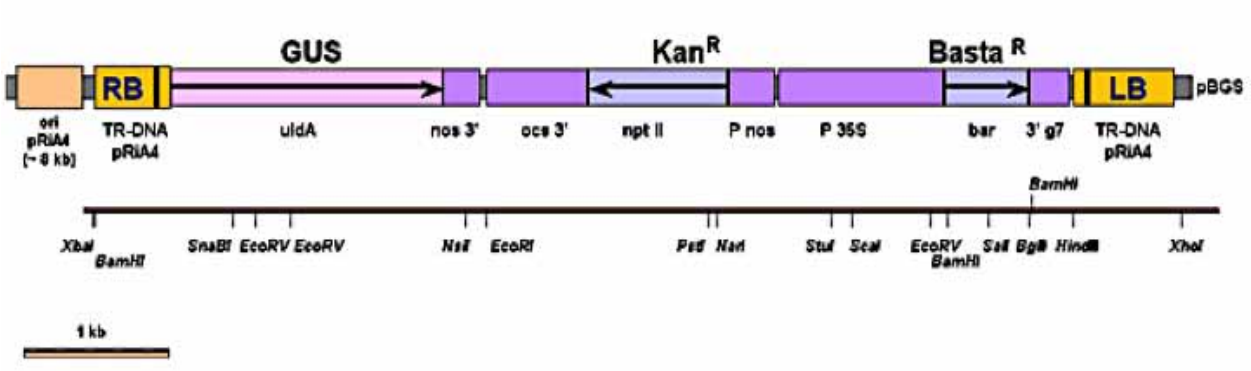

Figure M.1: pGKB5 T-DNA contains a GUS, NPTII and BAR genes, between two insertion borders. Full sequence is available online at http://www-ijpb.versailles.inra.fr/en/bc/equipes/cyto/ressources/pGKB5.html

Oligonucleotides	Forward sequence	Reverse sequence
Adaptors for T-DNA localisation	ACTCACTATAGGGCTCGAGCGGC	GGATCCTAATACGACTCACTATAGGGCTCGAGCGGC
ATG8E CRISPR guides	ATTG*GTCAGAAGCAAAGATGAATAA*	*TTATTCATCTTTGCTTCTGA*AAAC
ATG8E qPCR (Efficiency = 1,99)	TCGAATTCCTGTGATTGTGG	TTAGGTCTGATGGCACAAGGT
ATHB8 qPCR (Efficiency = 2)	CTCAAGAGATTTCACAACCTAACG	TCACTGCTTCGTTGAATCCTT
ATHB15 qPCR Efficiency = 2)	CCGTCAACATACTCCAAATCC	GTCACCACCGATTCACAGC
AT1G04850 qPCR (Efficiency =f 2)	agtggagaggctgcagaaga	ctcgggtagcacgagcttta
BAR genotyping	GCGGTCTGCACCATCGTCAACCACT ACATC	ACGTCATGCCAGTTCCCGTGCTTGAA
DRB27 genotyping on *ATG8E* T-DNA	AGTGAGGGAAAGGCAAATCA	ATGATCTACGGATACAAAGTC
FIL CRISPR guides 1	ATTGGCTCCTGCAGCTGCTAACGT	AAACACGTTAGCAGCTGCAGGAGC
FIL CRISPR guides 2	GCTCCTGCAGCTGCTAACGT	ACGTTAGCAGCTGCAGGAGC
FIL qPCR (Efficiency = 1,99)	ACTCTTACTTCAATCCCCAGGA	TCATATTCATGTTAGACGGTGCAT
HPH genotyping	GGGTCGATGCGACGCAATCGT	GAGCGAGCTTAGCGAACTGT
KAN1 qPCR (Efficiency = 2)	CTAACAAGCCTGCTGCTTCA	CGTTTCCATTTATGCCCATT
MIR166A CRISPR guides 1	GTTGTCTGGCTCGAGGACTC	GAGTCCTCGAGCCAGACAAC
MIR166A CRISPR guides 2	GGTTTTAGCGTCTTCGGACC	GGTCCGAAGACGCTAAAACC
MIR166A qPCR (Efficiency = 2)	GGACTGTTGTCTGGCTCG	GCTAAAACCCTAATCAAATCTGAAATC
NPTII genotyping	TGGAGAGGCTATTCGGCTATGAC	AACTCGTCAAGAAGGCGATAG
PHB qPCR (Efficiency = 1,95)	TTGGTTTCAGAACCGCAGA	CTGTTTGAAGACGAGCAGCTT
PHV qPCR (Efficiency = 2)	TTGGTTCCAGAATCGCAGA	CACTGTCTGAAGACGAGCTGA
RB3	CCAGACTGAATGCCCACAGGCCGTC	
REV qPCR (Efficiency = 2)	CGAGCTTGTTTATATGCAGACG	ATCTCAGGGTCCAGAAATCG
pGKB5 left border	TAATGCACACGGAAATGGCG	
pGKB5 right border	CCAGACTGAATGCCCACAGGCCGTC	
YAB3 qPCR (Efficiency = 2)	GCAACGGAAGATCAGTGGAT	GATGGTACTCTTTGTCGCTTCTC

Table M.B: Oligonucleotides used in this work with their sequences (qPCR and genotyping primers, adaptors)

II – PHYLLOTAXIS

II.A – MEASUREMENTS

Phyllotaxis measurements were performed (as described in Besnard *et al.*, 2014) on well-developed main shoots 4 weeks after transfer to long day conditions, and divided in 2 independent replicates. Azimuths of all lateral organs were measured on the primary shoot, at their separation from the stem and from the base upward (Note that the last measurements towards the tip of the plant can be biased, as internodes shorten and angles become less discernable).

II.B – ANALYSIS

Raw angles were processes into relative angles between consecutive measures on spread sheet tables, after deducing the main orientation of the spiral (clockwise vs. anticlockwise). The orientations of the spirals - measurements from clusters excluded – were determined by assessing the proportion of angles lower than 180°. A majority of angles inferior to 180° indicated a clockwise turning spiral, as opposed to anticlockwise spiral. Afterward, the following function was used to transform absolute angles into relative angles, depending on the direction of the spiral (clockwise or anticlockwise), with n = azimuth measure of an organ and n-1 = previous measurement of the organ (below).

$$Clockwise: angle = IF(SUM\big(n; -(n-1)\big) \geq 0;$$
$$360 - SUM\big(n; -(n-1)\big); 360 - SUM(360; n; -(n-1))$$

$$Anticlockwise: angle = IF(SUM\big(n; -(n-1)\big) \geq 0;$$
$$SUM\big(n; -(n-1)\big); 360 - SUM(360; n; -(n-1))$$

For partial utilization of the data (angles inside clusters only, or angles without clusters), measures were discarded when “n” or “n-1” was out of the considered group of angles. Two independent replicates were analysed and pooled.

III – GENE EXPRESSION ANALYSIS

III.A – RNA PURIFICATION

Inflorescence meristems from freshly bolting soil-grown plants were dissected to remove all flowers older than P2 stage, and immediately frozen in liquid nitrogen and grinded. Total RNA was extracted using the Arcturus PicoPure™ RNA Isolation Kit (Applied Biosystem, protocol supplied). DNase treatment was performed with the TURBO DNA-free™ Kit (ambiont™ , ThermoFisher Scientific), and absence of DNA was assessed by PCR on GLYCERALDEHYDE 3-PHOSPHATE DEHYDROGENASE (GAPDH) housekeeping gene. Transcripts were quantified using UV measurements with the cDrop™ software on a DropSense96 device (Trinean).

III.B – QUANTITATIVE POLYMERASE CHAIN REACTION

Gene expression analysis was performed on at least 2 independent experiments and three technical replicates. RT was performed on total RNA using the RevertAid RT Reverse Transcription Kit (ThermoFisher Scientific™) with random primers. Quantitative PCR was performed on a step one plus cycler (Applied Biosystems) using the Fast SYBR® Green Master Kit (Applied Biosystem). Threshold crossing point and primer efficiencies were used to calculate the relative expression ratios (Pfaffl *et al.*, 2001). The control target is the *UBIQUITIN ASSOCIATED DOMAIN CONTAINING PROTEIN* (AT1G04850) housekeeping gene. All primers used and their efficiencies are listed in Table M.B.

Raw data was analysed and computed into charts and statistical analysis using the MCMCqPCR package on R software (source code available online at: https://rdrr.io/cran/MCMC.qpcr/src/R/mcmc.qpcr.R)

IV – DNA ANALYSIS

IV.A – DNA PURIFICATION

Samples were taken from apical and secondary meristematic tissues on fully-grown inflorescences, frozen in liquid nitrogen and grinded. Samples were resuspended with 500µL of extraction buffer (CTAB 0,2g/L, NaCl 1,4M, EDTA 0,02M pH8, Tris 0,1M pH8) and left 25 min at 60°C. Supernatant was collected and added to 500µL Chlorophorm/Isoamyl alcool 24/1, and centrifugated 10 min at 12000rpm. Second supernatant was collected and added to 500µL of Isopropanol, mixed up and down, and centrifugated alike. Supernatant was discarded and the pellet was washed with EtOH 70%, and centrifugated. EtOH supernatant was discarded, the remaining DNA was dried for 5 min at 65° in an open eppendorf, and resuspended in 50µL of water. 33ug of RNase A (SIGMA) were added to the 40uL of purified DNA, for 30min leave at room temperature, and then removed by "PCR purification kit" (QIAGEN, protocol supplied). DNA quality was assessed by electrophoresis on 0,8% agarose gel, and double stranded DNA was quantified on the SpectraMax® Fluorescence microplate reader with Quant-iT™ PicoGreen™ dsDNA Assay Kit (Thermo Fischer Scientific, protocole supplied).

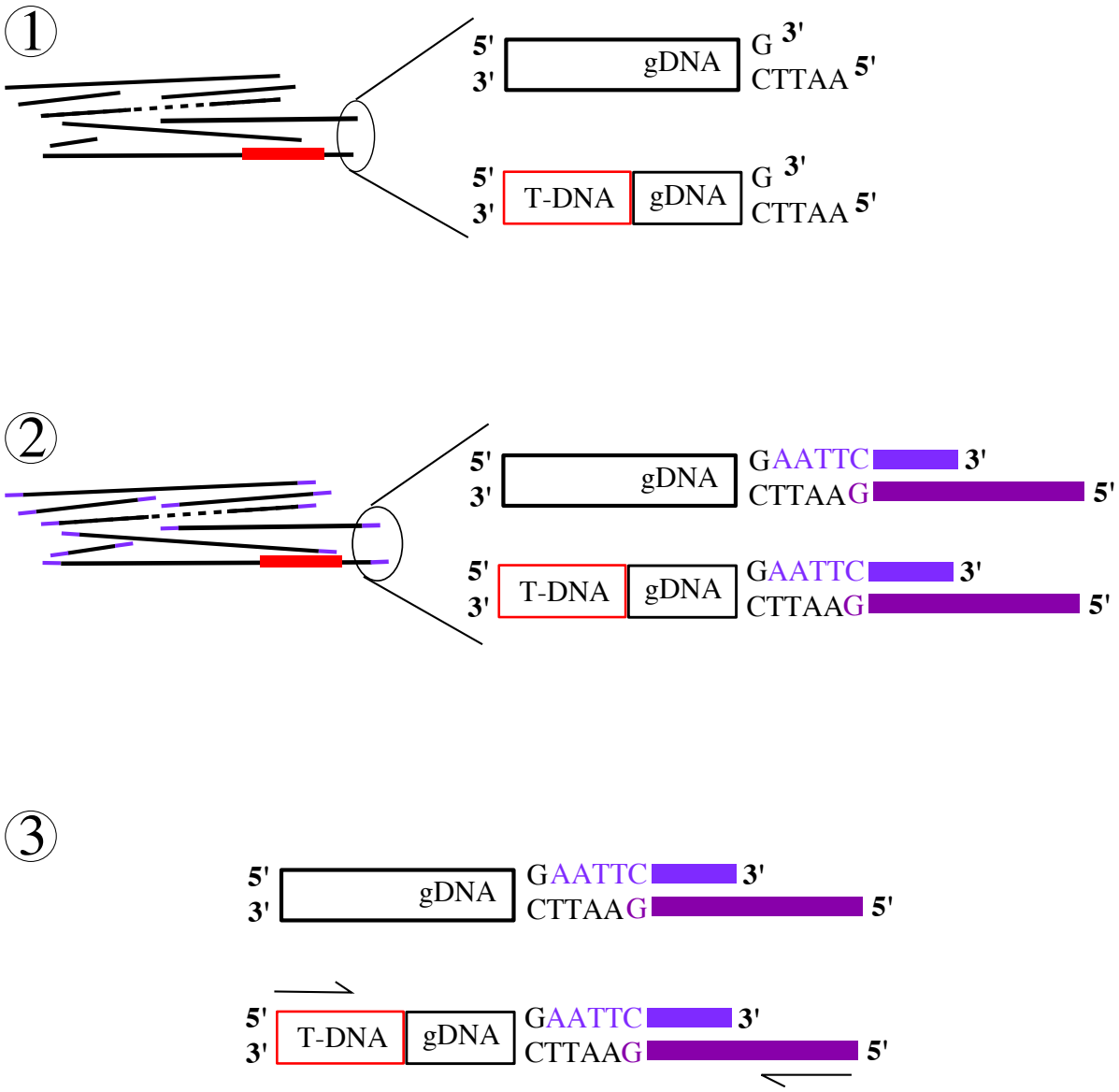

Figure M.2: Adaper-ligation-mediated PCR to find T-DNA insertion locus. 1) Genomic DNA (black lines) is enzymatically digested to generate fragments with specific borders (here EcoR1 sites) on both directions. 2) Asymetric adapters (purple) are ligated to the resulting borders to add hybridization sites for PCR. 3) Amplification between a T-DNA (red) border and adaptors allows isolation of a fragment containing the insertion locus sequence; the adapter primer does not have complementary strain to hybridate unless there is a first amplification cycle from the T-DNA primer.

IV.B – ADAPTER-LIGATION-MEDIATED PCR TO FIND T-DNA INSERTION LOCUS

The method used here was described by O'Malley *et al*. (2007), and is based on polymerase chain amplification reaction of chimeric sequence between a T-DNA border and the insertion locus (see Figure M.2). Whole genomic DNA extracts are enzymatically digested to generate fragments with equal border sequences, onto which adapters are ligated in order to have DNA fragments with known ends. PCR reaction is performed with one primer on the T-DNA border and another one on the adapter. Adapters are non-symmetrical in order to only allow amplification from fragments holding a T-DNA border (Figure M.2). The PCR is then performed with the adapter primer on the 3' sequence of the adapter B, so that it can only start if a first row of amplification has been performed on the complementary strain from the T-DNA border. Here we used HindIII and EcoR1 enzymes to generate cohesive borders, and two corresponding sets of adapters. The resulting fragments were purified from gel electrophoresis using the NucleoSpin® Gel and PCR Clean-up kit (Macherey-Nagel, protocol supplied), and sent to GATC Biotech (https://www.gatc-biotech.com/fr/index.html) for sequencing. The resulting chromatograms were analysed for quality purposes using ApE software (http://biologylabs.utah.edu/jorgensen/wayned/ape/), and sequences were aligned online against *Arabidopsis* sequence to identify the insertion locus using the NCBI Basic Local Alignment Search Tool (https://blast.ncbi.nlm.nih.gov/Blast.cgi). T-DNA border sequence should be visible as a signature of the insertion and true positive amplification of the T-DNA border, while the other part of the obtained sequence is matches an *Arabidopsis* genomic locus.

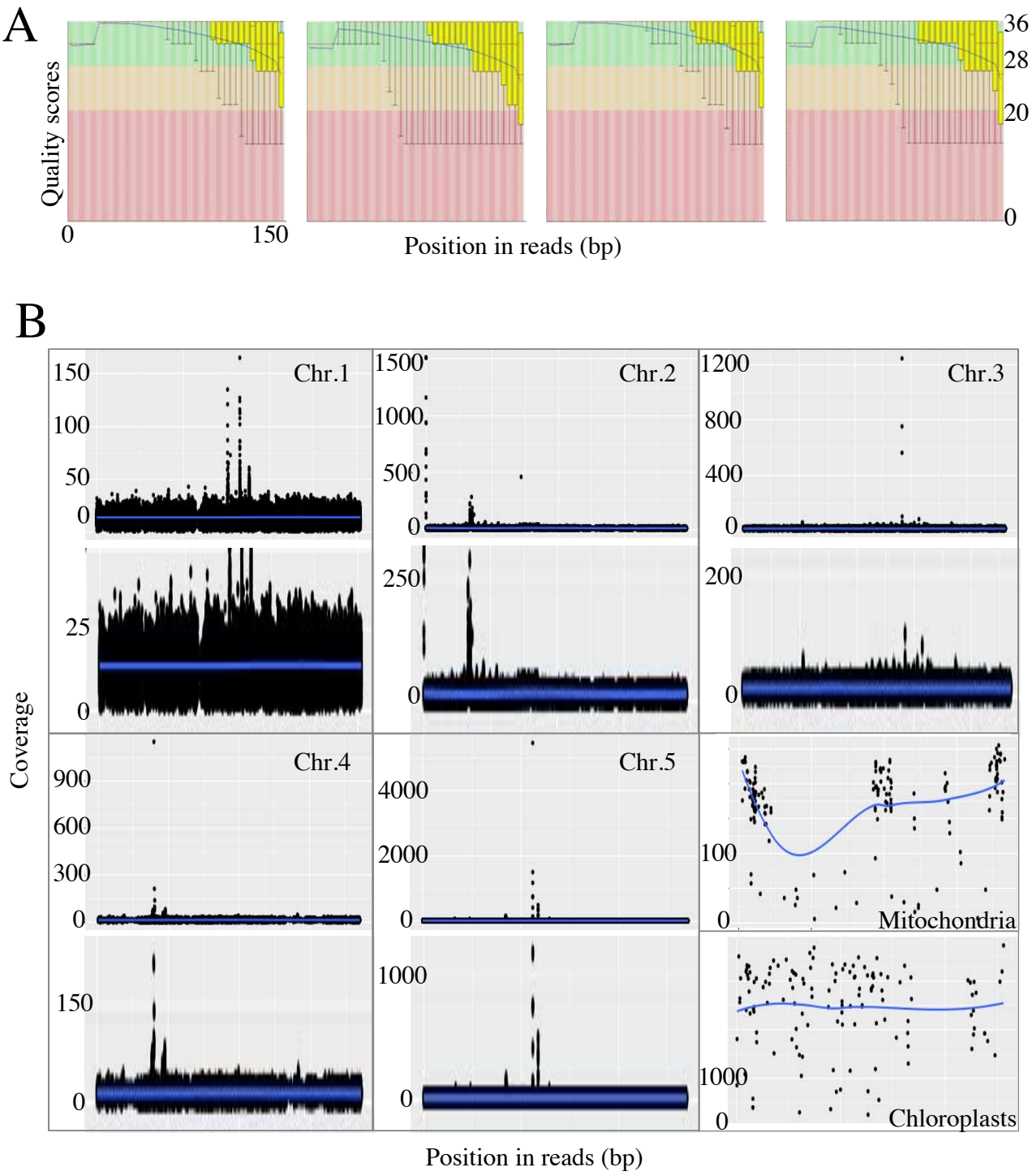

Figure M.3: Quality checks from whole genome re-sequencing. A) Phred average quality scores across all bases of forward and reverse reads of wild type, and forward and reverse reads of DRB27 from left to right. Good, average and low quality scores fall into the green, yellow and red domains respectively. B) Coverage (Y axis) on chromosomes 1 to 5, mitochondria and chloroplasts of the *Arabidopsis* genome. blue lines = mean coverage,

IV.C – WHOLE GENOME RE-SEQUENCING

DNA was purified as previously described from bulk aerial parts of a forest of 4-leaves *Ws-4* plants on one hand; and seven F2 homozygous plants from outcross of heterozygous DRB27 with *Col-0* and showing the whorled phenotype. Each sample was purified separately and pooled at equimolar quantities afterwards. A minimum of 2 µg of each samples of purified DNA was sent to the Helixio company (Hybrigenics), for whole genome sequencing.

Helixio performed the following procedure:
Quality controls of the genomic DNA were made with the fluorimetric Qubit® 2.0 kit (« Qubit® DNA BR assay », Thermo Fisher Scientific) for quantification, and the NanoDrop ND-1000 (Thermo Scientific) spectrophotometrer for purity assessment. DNA libraries were created from 2 µg of genomic DNA, with the «TruSeq DNA PCR-free Library Preparation » (Illumina) kit, and verified on the Bioanalyser 2100 with the « High Sensitivity DNA Assay » kit (Agilent Technologies). A Paired End Sequencing was performed with the « NextSeq500 » system (Illumina), and the « two-channel SBS » technology. Respectively 15 and 19 million reads were obtained for *Ws-4* and DRB27.

		WS-4		DRB27	
		*Ws-4*_forward	*Ws-4*_reverse	DRB27_forward	DRB27_reverse
DNA samples	Qubit concentration (ng/ul)	102		88	
	Ratio 260/280	1,85		1,88	
	fragments' size (bioanalyzer)	586 bp		561 bp	
Reads	total number of sequences	7998076	7998076	9899129	9899129
	sequences flagged as poor quality	0	0	0	0
	sequence length (bp)	35-151	35-151	35-151	35-151
	expected gap between mate reads (bp, bioanalyzer)	284-516	284-516	259-491	259-491
	% GC	37	36	36	36
	per base N content	0	0	0	0
	sequence duplication levels	<2%	<2%	<2%	<2%
	overrepresented sequences	G-stretch	G-stretch	G-stretch	G-stretch
	percentage of overrepresented sequences	0,23	0,85	0,17	0,35
	nb of reads	15 996 152		19 798 258	
	coverage after mapping				

Table M.C: Qualitative analysis of the Whole Genome Sequencing analysis. DNA samples meeting quality requirements were selected to proceed through Illumina sequencing. Quality controls for the resulting 4 FASTQ files (forward and reverse for each genotype) were satisfactory for sequence analysis.

IV.D – QUALITY CONTROLS OF THE SEQUENCING DATA

The reads were computed into 2 FastQ files, i.e. the forward and the reverse reads. The FastQ format is a Fasta-based format with additional information comprising the identity of each sequence and an error probability score (Phred) for each sequenced base.

Helixio sequencing report showed satisfactory sequence quality for analysis: good quality score was assessed according to the Phred quality score, across all bases but the last 30 that had an average mark; GC content was homogeneous with 36% and no unsequenced base (N); sequence lengths were measured with Bioanalyser and determined of 151 base pairs long which leaves an expected gap comprised between 259 and 516 base pairs in between the two mate-reads according to fragment size in the libraries between 561 and 586 bp; overall duplication levels were lower than 2%, and most overrepresented Kmers were located at the end of the reads, where the quality is lower. Most of these overrepresented sequences were stretches of G inherent to the "SBS two channels" technology. Indeed, the sequencer indicates the base read with a 2-color light code: red for C, green for T, both (yellow) for A, and no light for G. In these conditions, absence of base to read can be interpreted as a G.

All quality checks are summarized in Figure M.3 and Table M.C. Data cleanup and pre-processing was performed using GATK software (Genome analysis ToolKit, https://software.broadinstitute.org/gatk/) and real coverage was determined using the PICARD tool. Irregularities in the coverage data indicate that there are interruptions of represented nucleotides along the chromosomes. This may be a technical artefact due to mismatch of repeated sequences and G-stretches.

IV.E – SEQUENCE DATA ANALYSIS

This section was performed in collaboration with Fabrice Besnard, CR2 in the team. Three steps were followed to identify DRB27 candidate mutations:

1) Interval-mapping of the causative mutation: we used the HaplotypeCaller Genomic Variant Call Format (GVCF) tool from GATK software package in order to compare the *Col-0* reference (The *Arabidopsis* Information Resource, genome annotation version 10.31) and our re-sequenced *Ws-4* line, and define a set of polymorphic SNPs between them. The selected variants between *Col-0* and *Ws-4* were then called in the bulk DRB27 F2 sequencing reads aligned against the reference genome. Frequencies of *Ws-4* alleles versus *Col-0* alleles were computed for each polymorphic position along the whole genome. Regions of pure Ws-4 alleles indicate the mapping interval of the causing mutation(s) responsible for the recessive phenotype selected in the F2 population.

2) Variants found by GATK Haplotype Caller in DRB27 that were neither Col-0 nor Ws-4 alleles and fell within the mapping interval were also selected as a first set of candidate mutations. The potential impact of these variants was analysed with SnpEff (http://snpeff.sourceforge.net/), an effect prediction tool relying on genome annotation (Cingolani *et al*., 2012).

3) To detect specifically the *loci* of T-DNA insertions, we first mapped bulk DRB27 F2 reads on the pGKB5 T-DNA sequence in order to select reads mapping partially, or totally as singleton (http://www-ijpb.versailles.inra.fr/en/bc/equipes/cyto/ressources/pGKB5.html). Second we mapped paired reads corresponding to the selected singletons on *A. thaliana* genome to identify insertion *loci*. Junction sites were manually inspected using an alignment viewer (Tablet https://ics.hutton.ac.uk/tablet/), which allows discriminating possible heterozygous insertions or false positive insertion locus likely due to mapping errors. Since many insertions were present, we selected reads of each insertion and mapped them again on the T-DNA sequence to check whether their orientation and strand allow to reconstruct a coherent insertion. A tandem insertion could be deduced from this second mapping on the T-DNA sequence.

V – DRB27 COMPLEMENTATION AND GENERATION OF INDEPENDANT CRISPR-CAS9 MUTANT LINES

Constructions were made in order to: on the one hand complement DRB27 mutant by reinsertion of full sequences of *AUTOPHAGY-RELATED PROTEIN 8E (ATG8E), FILAMENTOUS FLOWER (FIL)* and *MIR166A* genes; on the other hand, independent mutant lines for the same three genes were generated using the Clustered Regularly Interspaced Short Palindromic Repeats (CRISPR) technology. All oligonucleotides used to amplify original sequences, and perform targeted mutagenesis, are listed in Table M.B.

V.A – COMPLEMENTATION CONSTRUCTIONS

ATG8E coding sequence was isolated from meristematic cDNA and cloned after the ubiquitous *RIBOSOMAL PROTEIN S5A (RPS5A)* promoter and a VENUS yellow fluorescent protein in 5' in the binary pH7m34GW vector, using the Gateway technology (Hartley *et al.*, 2000). Constructs for *FIL* and *MIRA66A* were made from amplification of the full wild type genomic sequence between the previous annotated gene and the end of the 3'UTR, and inserted in the binary pMDC99 plasmid, using Gateway technology. All constructs were inserted by heat shock in thermo competent *Escherichia coli* strain for selection.

V.B – CONSTRUCTION OF PLASMIDS REQUIRED FOR CRISPR-CAS9 GENOME EDITING

Plasmidic constructs for CRISPR-Cas9-mediated mutagenesis of *ATG8E* were made by insertion of the specific guides in the pDe-CAS9 vector, following the method described by Fauser *et al.* (2014). Golden Gate-mediated method for double-guided CRISPR described by Wang *et al.* (2015) was used for specific mutagenesis of *FIL* and *MIR166A*.

V.C – PLANT TRANSFORMATION

Plasmidic DNA was extracted from *E. coli* positive clones using the NucleoSpin® Plasmid kit (Macherey-Nagel), and transformed by electroporation into competent *Agrobacterium* strains for floral dipping plant transformation floral dipping technique (Clough & Bent, 1998). Inflorescences of freshly bolting plants (10cm tall in average) were dipped for 20 seconds in a solution containing the *Agrobacterium* strain carrying the wanted construction for T-DNA insertion. Plants were then left overnight in plastic bags to keep humidity and promote bacterial growth, prior to returning them to normal growth conditions. T1 seeds were grown on the adequate antibiotic and self-crossed.

VI – IMAGING

VI.A – SCANNING ELECTRON MICROSCOPY (SEM)

All *Arabidopsis* meristems were observed on bolting plants two weeks after transfer to long day culture conditions. Other species were observed immediately after sampling. All meristems were cleared out from lateral organs under a dissecting microscope, and observed immediately in a HIROX SH-3000 scanning electron microscope under vacuum, at 5 to 15kV beam, and a temperature of -10°C. Whorled sample collection was made in collaboration with the botanist Frederic Danet from the Botanical Garden of Lyon.

VI.B – CONFOCAL IMAGING

Meristems were sampled similarly as for SEM, but observed 24 hours after dissection, and cultured on *Arabidopsis* Apex Culture Medium (ACM). ACM is composed of 0,5X MS basal salt mixture, 1% sucrose, 0,8% agarose, at pH=5,8 with potassium hydroxide solution and complemented with vitamins ((0.01% myo-inositol, 0.0001% nicotinic acid, 0.0001% pyridoxine hydrochloride, 0.001% thiamine hydrochloride, 0.0002% glycine) and cytokinins (500 nM N6-benzyladenine).

All confocal images were taken under the LSM-ZEISS 700 laser scanning confocal microscope (Zeiss, Jena, Germany). In order to avoid bias induced by the observation of mutants with mixed genetic background, heterozygous plants from the same segregating population of DRB27 homozygous mutants were used as controls.

Single images were taken between 10am and 1pm, whereas time courses were composed of images covering all periods of the day for three days. In these cases, meristems were re-dissected after imaging once a day, and planted in a new plate of fresh and sterile ACM media.

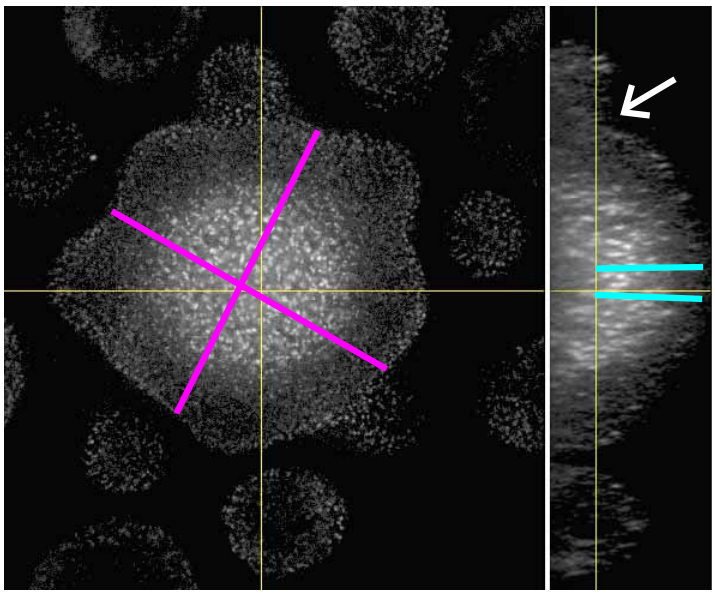

Figure M.4: Meristem measurements were made from z-section at the depth of the third furrow (white arrow). Two different measures were taken for diameter (pink lines) and height (blue lines) using orthogonal projections.

Images were processed using Fiji (is just ImageJ) software (http://rsbweb.nih.gov/ij/), for presentation purposes as well as meristem measurements. Meristem morphological measurements were made with the auto-fluorescence channel from all reporters used for expression domains studies, and at T0 in the case of time courses, following the same procedure (see Figure M.4): meristems were sampled in silico, from the top of the dome downward to the third furrow. To assess each meristem diameter, two independant measures were made at the base in two different directions and avoiding deformations due to primordia outgrowth, and averaged. Height measures were made similarly on orthogonal projections. Central zones were measured on the channels of the fluorescent reporters.

VI.C – ATOMIC FORCE MICROSCOPY

This technique allows mapping the surface stiffness of living tissues. It consists in a tip bound to a cantilever and a laser beam. When the tip is applied to the tissue surface, the cantilever bends accordingly to the surface stiffness, and the laser beam reflects this change of position.

Meristems were images in ACM plates similarly as for confocal microscopy experiments, but with a particular attention on their immobility by means of complete immersion of all lateral organs and primordia in 2% agarose gel. Imaging of cell wall stiffness at the meristem surface was performed using the AFM Bruker catalyst with a 42 N/m and spherical 400nm radius cantilever. The Quantitative Nanoscale Mapping (QNM) allows acquisition of 128x128 pixel images, each pixel represents a force curve.

VII – STATISTICAL ANALYSIS

Statistical analyses were all performed using R software. To compare samples, data distribution normality was assessed (Shapiro test), and variances were compared (Barlett test). Samples with similar variances and normal distribution of their values were compared using the parametric T-test, whereas all other cases were statistically analysed with the non-parametrical Wilcoxon test.

REFERENCE LIST

Besnard, Fabrice, Frédérique Rozier, and Teva Vernoux. 2014. "The AHP6 Cytokinin Signaling Inhibitor Mediates an Auxin-Cytokinin Crosstalk That Regulates the Timing of Organ Initiation at the Shoot Apical Meristem." *Plant Signaling & Behavior*: 4–7.

Bouchez D, Camilleri C, Caboche M (1993). A binary vector based on Basta resistance for *in planta* transformation of *Arabidopsis thaliana*. C R Acad Sci Paris, Life sciences **316** : 1188-1193.

Brunoud, Géraldine et al. 2012. "A Novel Sensor to Map Auxin Response and Distribution at High Spatio-Temporal Resolution." *Nature* 482(7383): 103–6. http://www.nature.com/doifinder/10.1038/nature10791.

Cingolani, Pablo et al. 2012. "A Program for Annotating and Predicting the Effects of Single Nucleotide Polymorphisms, SnpEff." *Landes Biosciences* 6(2): 80–92. http://www.tandfonline.com/doi/abs/10.4161/fly.19695.

Clough, Steven J., and Andrew F. Bent. 1998. "Floral Dip: A Simplified Method for Agrobacterium-Mediated Transformation of Arabidopsis Thaliana." *Plant Journal* 16(6): 735–43.

Contento, Anthony L., Yan Xiong, and Diane C. Bassham. 2005. "Visualization of Autophagy in Arabidopsis Using the Fluorescent Dye Monodansylcadaverine and a GFP-AtATG8e Fusion Protein." *Plant Journal* 42: 598–608.

Fauser, Friedrich, Simon Schiml, and Holger Puchta. 2014. "Both CRISPR / Cas-Based Nucleases and Nickases Can Be Used Efficiently for Genome Engineering in Arabidopsis Thaliana." *The Plant Journal*: 348–59.

Goldshmidt, Alexander, John Paul Alvarez, John L Bowman, and Yuval Eshed. 2008. "Signals Derived from YABBY Gene Activities in Organ Primordia Regulate Growth and Partitioning of Arabidopsis Shoot Apical Meristems." *The Plant cell* 20(5): 1217–

30.
http://www.pubmedcentral.nih.gov/articlerender.fcgi?artid=2438466&tool=pmcentrez&rendertype=abstract (December 19, 2013).

Hartley, James L., Gary F. Temple, and Michael a. Brasch. 2000. "DNA Cloning Using In Vitro Site-Specific Recombination." *Genome Research* 10(11): 1788–95.

Heisler, Marcus G. et al. 2005. "Patterns of Auxin Transport and Gene Expression during Primordium Development Revealed by Live Imaging of the Arabidopsis Inflorescence Meristem." *Current Biology* 15: 1899–1911.

Mähönen, Ari Pekka. 2006. "Cytokinin Signaling and Its Inhibitor." *Science* 94(2006): 94–98. http://www.ncbi.nlm.nih.gov/pubmed/16400151.

Murashige, Toshio, and Folke Skoog. 1962. "A Revised Medium for Rapid Growth and Bio Assays with Tobacco Tissue Cultures." *Physiologia Plantarum* 15(3): 473–97.

O'Malley, Ronan C et al. 2007. "An Adapter Ligation-Mediated PCR Method for High-Throughput Mapping of T-DNA Inserts in the Arabidopsis Genome." *Nature protocols* 2: 2910–17.

Ochando, Isabel et al. 2006. "Mutations in the microRNA Complementarity Site of the INCURVATA4 Gene Perturb Meristem Function and Adaxialize Lateral Organs in Arabidopsis." *Plant physiology* 141(2): 607–19. http://www.pubmedcentral.nih.gov/articlerender.fcgi?artid=1475466&tool=pmcentrez&rendertype=abstract.

Pfaffl, M W. 2001. "A New Mathematical Model for Relative Quantification in Real-Time RT-PCR." *Nucleic acids research* 29(9): e45. http://www.pubmedcentral.nih.gov/articlerender.fcgi?artid=55695&tool=pmcentrez&rendertype=abstract.

Pfeiffer, Anne et al. 2016. "Integration of Light and Metabolic Signals for Stem Cell Activation at the Shoot Apical Meristem." *eLife* 5(JULY): 1–21.

Vernoux, T. et al. 2014. “The Auxin Signalling Network Translates Dynamic Input into Robust Patterning at the Shoot Apex.” *Molecular Systems Biology* 7(1): 508–508. http://msb.embopress.org/cgi/doi/10.1038/msb.2011.39.

Wang, Zhi-Ping et al. 2015. “Egg Cell-Specific Promoter-Controlled CRISPR/Cas9 Efficiently Generates Homozygous Mutants for Multiple Target Genes in Arabidopsis in a Single Generation.” *Genome biology* 16(1): 144. http://genomebiology.biomedcentral.com/articles/10.1186/s13059-015-0715-0.

IMAGE SOURCES INVENTORY

INTRODUCTION

- Figure 0.2.A-D: adapted from Galvan-Ampudia, Chaumeret et al., 2015
- Figure 0.2.E: https://www.mnn.com/earth-matters/wilderness-resources/blogs/how-golden-ratio-manifests-nature
- Figure 0.2.G: https://keyserver.lucidcentral.org/weeds/data/media/Html/ocimum_basilicum.htm
- Figure 0.2.H: http://arcticplants.myspecies.info/category/classification/angiosperms/eudicots/plantaginaceae
- Figure 0.2.I, J & K: https://www.mathsisfun.com/numbers/nature-golden-ratio-fibonacci.html
- Figure 0.3: adapted from Galvan-Ampudia, Chaumeret et al., 2015
- Figure 0.5: adapted from Galvan-Ampudia, Chaumeret et al., 2015

RESULTS

- Preamble Figure A: https://floressilvestresdelmediterraneo.blogspot.fr/2013/04/rubiaceae-valantia-hispida.html
- Preamble Figure B: http://luirig.altervista.org/flora/taxa/floranam.php?genere=Cruciata
- Preamble Figure E: https://houseplantz.net/peperomia-rubella-radiator-plant/
- Preamble Figure G: https://www.aquaportail.com/fiche-plante-306-hippuris-vulgaris.html
- Preamble Figure I: http://keywordsuggest.org/gallery/403661.html
- Preamble Figure J: https://en.wikipedia.org/wiki/Elodea
- Figure I.5: Fabrice Besnard
- Figure I.12.A-C: Lugassi *et al.*, 2010
- Figure I.12.D-F: Sawa *et al.*, 1999
- Figure I.12.G-I: Chen *et al.*, 1999

- Figure II.1.D: eFP-Browser http://bar.utoronto.ca/efp/cgi-bin/efpWeb.cgi
- Figure II.3.B: http://www.uniprot.org/
- Figure II.5.C: Slavikova *et al*., 2005
- Figure II.5.D: Contento *et al*., 2005
- Figure II.6.G-H: Ochando *et al*., 2006
- Figure II.6.I: Ochando *et al*., 2008

MATERIALS AND METHODS

- Figure M.1: http://www-ijpb.versailles.inra.fr/en/bc/equipes/cyto/essources/pGKB5.html